

Effect of Interpopulation Spike-Timing-Dependent Plasticity on Synchronized Rhythms in Neuronal Networks with Inhibitory and Excitatory Populations

Sang-Yoon Kim* and Woosung Lim†

*Institute for Computational Neuroscience and Department of Science Education,
Daegu National University of Education, Daegu 42411, Korea*

We consider clustered small-world networks (SWNs) with two inhibitory (I) and excitatory (E) populations. This I-E neuronal network has adaptive dynamic I to E and E to I interpopulation synaptic strengths, governed by interpopulation spike-timing-dependent plasticity (STDP) [i.e., I to E inhibitory STDP (iSTDP) and E to I excitatory STDP (eSTDP)]. In previous works without STDPs, fast sparsely synchronized rhythms, related to diverse cognitive functions, were found to appear in a range of noise intensity D for static synaptic strengths. Here, by varying D , we investigate the effect of interpopulation STDPs on diverse population and individual properties of synchronized rhythms that emerge in the I- and the E-populations. Depending on values of D , long-term potentiation (LTP) and long-term depression (LTD) for population-averaged values of saturated interpopulation synaptic strengths are found to occur, and they make effects on the degree of population synchronization. In a broad region of intermediate D , the degree of good synchronization (with higher spiking measure) becomes decreased, while in a region of large D , the degree of bad synchronization (with lower spiking measure) gets increased. Consequently, in each I- or E-population, the synchronization degree becomes nearly the same in a wide range of D (including the intermediate and the large D regions). This kind of “equalization effect” is found to occur via cooperative interplay between the average occupation and pacing degrees of synchronized rhythms. Furthermore, such equalization effect is much more enhanced in the presence of combined I to E and E to I STDPs when compared with the case of individual I to E or E to I STDP. We note that the equalization effect in interpopulation synaptic plasticity is in contrast to the Matthew (bipolarization) effect in intrapopulation (I to I and E to E) synaptic plasticity where good (bad) synchronization gets better (worse). Moreover, emergences of LTP and LTD of interpopulation synaptic strengths are intensively investigated via a microscopic method based on the distributions of time delays between the pre- and the post-synaptic spike times.

PACS numbers: 87.19.lw, 87.19.lm, 87.19.lc

Keywords: Equalization Effect, Interpopulation Spike-Timing-Dependent Plasticity, Fast Sparsely Synchronized Rhythm, Inhibitory and Excitatory Populations

I. INTRODUCTION

Recently, much attention has been paid to brain rhythms that emerge via population synchronization between individual firings in neuronal networks [1–15]. In particular, we are concerned about fast sparsely synchronized rhythms, related to diverse cognitive functions (e.g., multisensory feature binding, selective attention, and memory formation) [16]. Fast sparsely synchronous oscillations [e.g., gamma rhythm (30–100 Hz) during awake behaving states and rapid eye movement sleep] have been observed in local field potential recordings, while at the cellular level individual neuronal recordings have been found to exhibit stochastic and intermittent spike discharges like Geiger counters at much lower rates than the population oscillation frequency [17–23]. Hence, single-cell firing activity differs distinctly from the population oscillatory behavior. We note that fast sparsely synchronized rhythms are in contrast to fully synchronized rhythms where individual neurons fire regularly at

the population oscillation frequency like clocks.

Fast sparse synchronization (FSS) was found to emerge under balance between strong external noise and strong recurrent inhibition in single-population networks of purely inhibitory interneurons and also in two-population networks of both inhibitory interneurons and excitatory pyramidal cells [24–29]. In neuronal networks, architecture of synaptic connections has been found to have complex topology which is neither regular nor completely random [30–37]. In recent works [38–40], we studied the effects of network architecture on emergence of FSS in small-world, scale-free, and clustered small-world complex networks, consisting of inhibitory interneurons. In these works on FSS, synaptic coupling strengths were static. However, in real brains synaptic strengths may vary for adjustment to the environment. Thus, synaptic strengths may be potentiated [41–43] or depressed [44–47]. These adaptations of synapses are called the synaptic plasticity which provides the basis for learning, memory, and development [48]. Here, we consider spike-timing-dependent plasticity (STDP) for the synaptic plasticity [49–56]. For the STDP, the synaptic strengths change through an update rule depending on the relative time difference between the pre- and the post-synaptic spike times. Recently, effects of STDP on

*Electronic address: sykim@icn.re.kr

†Electronic address: wclim@icn.re.kr

diverse types of synchronization in populations of coupled neurons were studied in various aspects [57–63]. Particularly, effects of inhibitory STDP (at inhibitory to inhibitory synapses) on FSS have been investigated in small-world networks of inhibitory fast spiking interneurons [64].

Synaptic plasticity at excitatory and inhibitory synapses is of great interest because it controls the efficacy of potential computational functions of excitation and inhibition. Studies of synaptic plasticity have been mainly focused on excitatory synapses between pyramidal cells, since excitatory-to-excitatory (E to E) synapses are most prevalent in the cortex and they form a relatively homogeneous population [65–71]. A Hebbian time window was used for the excitatory STDP (eSTDP) update rule [49–56]. When a pre-synaptic spike precedes (follows) a post-synaptic spike, long-term potentiation (LTP) [long-term depression (LTD)] occurs. In contrast, synaptic plasticity at inhibitory synapses has attracted less attention mainly due to experimental obstacles and diversity of interneurons [72–76]. With the advent of fluorescent labeling and optical manipulation of neurons according to their genetic types [77, 78], inhibitory synaptic plasticity has also begun to be focused. Particularly, studies on inhibitory STDP (iSTDP) at inhibitory-to-excitatory (I to E) synapses have been much made. Thus, iSTDP has been found to be diverse and cell-specific [72–76, 79–85].

In this paper, we consider clustered small-world networks (SWNs) with two inhibitory (I) and excitatory (E) populations. The I-SWN consists of fast spiking (FS) interneurons, the E-SWN is composed of regular spiking (RS) pyramidal cells, and random uniform connections are made between the two populations. By taking into consideration interpopulation STDPs between the I- and E-populations, we investigate their effects on diverse properties of population and individual behaviors of fast sparsely synchronized rhythms by varying the noise intensity D for the 3 cases of I to E iSTDP, E to I eSTDP, and combined I to E and E to I STDPs. A time-delayed Hebbian time window is employed for the I to E iSTDP update rule, while an anti-Hebbian time window is used for the E to I eSTDP update rule. We note that our present work is in contrast to previous works on FSS where STDPs were not considered in most cases [24–29] and only in one case [64], intrapopulation I to I iSTDP was considered in an inhibitory SWN of FS interneurons.

In the presence of interpopulation STDPs, interpopulation synaptic strengths $\{J_{ij}^{(XY)}\}$ between the source Y -population and the target X -population are evolved into saturated limit values $\{J_{ij}^{(XY)*}\}$ after a sufficiently long time. Depending on D , mean values $\langle J_{ij}^{(XY)*} \rangle$ of saturated limit values are potentiated [long-term potentiation (LTP)] or depressed [long-term depression (LTD)], in comparison with the initial mean value $J_0^{(XY)}$. These LTP and LTD make effects on the degree of FSS. In the case of I to E iSTDP, LTP (LTD) disfavors (favors) FSS

[i.e., LTP (LTD) tends to decrease (increase) the degree of FSS] due to increase (decrease) in the mean value of I to E synaptic inhibition. On the other hand, the roles of LTP and LTD are reversed in the case of E to I eSTDP, where LTP (LTD) favors (disfavors) FSS. Due to the effects of the mean (LTP or LTD), an “equalization effect” in interpopulation (I to E or E to I) synaptic plasticity is found to emerge in a wide range of D through cooperative interplay between the average occupation and pacing degrees between spikes in synchronized rhythms. In a broad region of intermediate D , the degree of good synchronization (with higher spiking measure) becomes decreased, while in a region of large D the degree of bad synchronization (with lower spiking measure) gets increased. Consequently, the degree of FSS becomes nearly the same in a wide range of D . Particularly, in the case of combined I to E and E to I STDPs, such equalization effect is much more enhanced in comparison with each case of individual I to E or E to I STDP. This equalization effect may be well visualized in the histograms for the spiking measures in the absence and in the presence of interpopulation STDPs. The standard deviation from the mean in the histogram in the case of interpopulation STDP is much smaller than that in the case without STDP, which clearly shows occurrence of the equalization effect. In addition, a dumbing-down effect in interpopulation synaptic plasticity also occurs, because the mean in the histogram in the presence of interpopulation STDP is smaller than that in the absence of STDP. Thus, equalization effect occurs together with dumbing-down effect. We also note that this kind of equalization effect in interpopulation synaptic plasticity is distinctly in contrast to the Matthew (bipolarization) effect in intrapopulation (I to I and E to E) synaptic plasticity where good (bad) synchronization gets better (worse) [61, 64].

Emergences of LTP and LTD of interpopulation synaptic strengths are also investigated through a microscopic method based on the distributions of time delays $\{\Delta t_{ij}^{(XY)}\}$ between the nearest spiking times of the post-synaptic neuron i in the (target) X -population and the pre-synaptic neuron j in the (source) Y -population. We follow time evolutions of normalized histograms $H(\Delta t_{ij}^{(XY)})$ in both cases of LTP and LTD. Because of the equalization effects, the two normalized histograms at the final (evolution) stage are nearly the same, which is in contrast to the case of intrapopulation STDPs where the two normalized histograms at the final stage are distinctly different due to the Matthew (bipolarization) effect.

This paper is organized as follows. In Sec. II, we describe clustered SWNs composed of FS interneurons (I-SWN) and RS pyramidal cells (E-SWN) with interpopulation STDPs. Then, in Sec. III the effects of interpopulation STDPs on FSS are investigated for the 3 cases of I to E iSTDP, E to I eSTDP, and combined I to E and E to I STDPs. Finally, we give summary and discussion in Sec. IV.

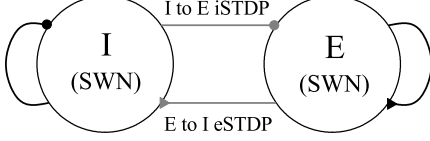


FIG. 1: Schematic representation of clustered SWNs of the inhibitory (I) and the excitatory (E) populations with random interpopulation connections. Black curves with circle and triangle represent the I to I and the E to E intrapopulation connections, respectively. Gray lines with circle and triangle denote the I to E and the E to I interpopulation connections, respectively.

II. CLUSTERED SMALL-WORLD NETWORKS COMPOSED OF TWO I- AND E-POPULATIONS WITH INTERPOPULATION SYNAPTIC PLASTICITY

A neural circuit in the brain cortex is composed of a few types of excitatory principal cells and diverse types of inhibitory interneurons. It is also known that interneurons make up about 20 percent of all cortical neurons, and exhibit diversity in their morphologies and functions [86]. Here, we consider clustered SWNs composed of two I- and E-populations. Each I(E)-population is modeled as a directed Watts-Strogatz SWN, consisting of N_I (N_E) FS interneurons (RS pyramidal cells) equidistantly placed on a one-dimensional ring of radius N_I (N_E)/ 2π ($N_E : N_I = 4 : 1$), and random uniform connections with the probability p_{inter} are made between the two I-SWN and E-SWN.

A schematic representation of the clustered SWNs is shown in Fig. 1. The Watts-Strogatz I-SWN (E-SWN) interpolates between a regular lattice with high clustering (corresponding to the case of $p_{wiring} = 0$) and a random graph with short average path length (corresponding to the case of $p_{wiring} = 1$) through random uniform rewiring with the probability p_{wiring} [87–89]. For

$p_{wiring} = 0$, we start with a directed regular ring lattice with N_I (N_E) nodes where each node is coupled to its first $M_{syn}^{(I)}$ ($M_{syn}^{(E)}$) neighbors [$M_{syn}^{(I)}/2$ ($M_{syn}^{(E)}/2$) on either side] through outward synapses, and rewire each outward connection uniformly at random over the whole ring with the probability p_{wiring} (without self-connections and duplicate connections). Throughout the paper, we consider the case of $p_{wiring} = 0.25$. This kind of Watts-Strogatz SWN model with predominantly local connections and rare long-range connections may be regarded as a cluster-friendly extension of the random network by reconciling the six degrees of separation (small-worldness) [90, 91] with the circle of friends (clustering).

As elements in the I-SWN (E-SWN), we choose the Izhikevich inhibitory FS interneuron (excitatory RS pyramidal cell) model which is not only biologically plausible, but also computationally efficient [92–95]. Unlike Hodgkin-Huxley-type conductance-based models, instead of matching neuronal electrophysiology, the Izhikevich model matches neuronal dynamics by tuning its parameters. The parameters k and b are related to the neuron's rheobase and input resistance, and a , c , and d are the recovery time constant, the after-spike reset value of v , and the after-spike jump value of u , respectively. Tuning these parameters, the Izhikevich neuron model may produce 20 of the most prominent neurocomputational features of biological neurons [92–95]. In particular, the Izhikevich model is employed to reproduce the six most fundamental classes of firing patterns observed in the mammalian neocortex; (i) excitatory RS pyramidal cells, (ii) inhibitory FS interneurons, (iii) intrinsic bursting neurons, (iv) chattering neurons, (v) low-threshold spiking neurons, and (vi) late spiking neurons [94]. Here, we use the parameter values for the FS interneurons and the RS pyramidal cells in the layer 5 rat visual cortex, which are listed in the 1st item of Table I (see the captions of Figs. 8.12 and 8.27 in [94]).

The following equations (1)-(11) govern population dynamics in the clustered SWNs with the I- and the E-populations:

$$C_I \frac{dv_i^{(I)}}{dt} = k_I(v_i^{(I)} - v_r^{(I)})(v_i^{(I)} - v_t^{(I)}) - u_i^{(I)} + \bar{I}_i^{(I)} + D_I \xi_i^{(I)} - I_{syn,i}^{(II)} - I_{syn,i}^{(IE)}, \quad (1)$$

$$\frac{du_i^{(I)}}{dt} = a_I \{U(v_i^{(I)}) - u_i^{(I)}\}, \quad i = 1, \dots, N_I, \quad (2)$$

$$C_E \frac{dv_i^{(E)}}{dt} = k_E(v_i^{(E)} - v_r^{(E)})(v_i^{(E)} - v_t^{(E)}) - u_i^{(E)} + \bar{I}_i^{(E)} + D_E \xi_i^{(E)} - I_{syn,i}^{(EE)} - I_{syn,i}^{(EI)}, \quad (3)$$

$$\frac{du_i^{(E)}}{dt} = a_E \{U(v_i^{(E)}) - u_i^{(E)}\}, \quad i = 1, \dots, N_E, \quad (4)$$

with the auxiliary after-spike resetting:

$$\text{if } v_i^{(X)} \geq v_p^{(X)}, \text{ then } v_i^{(X)} \leftarrow c_X \text{ and } u_i^{(X)} \leftarrow u_i^{(X)} + d_X, \quad (X = I \text{ or } E) \quad (5)$$

TABLE I: Parameter values used in our computations; units of the capacitance, the potential, the current, and the time are pF, mV, pA, and msec, respectively.

(1)	Single Izhikevich FS Interneurons [94]				
	$C_I = 20$	$v_r^{(I)} = -55$	$v_t^{(I)} = -40$	$v_p^{(I)} = 25$	$v_b^{(I)} = -55$
	$k_I = 1$	$a_I = 0.2$	$b_I = 0.025$	$c_I = -45$	$d_I = 0$
(2)	Single Izhikevich RS Pyramidal Cells [94]				
	$C_E = 100$	$v_r^{(E)} = -60$	$v_t^{(E)} = -40$	$v_p^{(E)} = 35$	
	$k_E = 0.7$	$a_E = 0.03$	$b_E = -2$	$c_E = -50$	$d_E = 100$
(3)	Random External Excitatory Input to Each Izhikevich FS Interneurons and RS Pyramidal Cells				
	$\bar{I}_i^{(I)} = \bar{I}_i^{(E)} = \bar{I}_i; \bar{I}_i \in [680, 720]$			$D_I = D_E = D$: Varying	
(4)	Inhibitory Synapse Mediated by The GABA _A Neurotransmitter [26]				
	I to I:	$\tau_l^{(II)} = 1.5$	$\tau_r^{(II)} = 1.5$	$\tau_d^{(II)} = 8$	$V_{syn}^{(I)} = -80$
	I to E:	$\tau_l^{(EI)} = 1.5$	$\tau_r^{(EI)} = 1.5$	$\tau_d^{(EI)} = 8$	
(5)	Excitatory Synapse Mediated by The AMPA Neurotransmitter [26]				
	E to E:	$\tau_l^{(EE)} = 1.5$	$\tau_r^{(EE)} = 0.4$	$\tau_d^{(EE)} = 2$	$V_{syn}^{(E)} = 0$
	E to I:	$\tau_l^{(IE)} = 1.5$	$\tau_r^{(IE)} = 0.2$	$\tau_d^{(IE)} = 1$	
(6)	Intra- and Inter-population Synaptic Connections between Neurons in The Clustered Watts-Strogatz SWNs with Inhibitory and Excitatory Populations				
	Intrapopulation Synaptic Connection:	$N_I = 600$	$M_{syn}^{(I)} = 40$	$N_E = 2400$	$M_{syn}^{(E)} = 160$ $p_{wiring} = 0.25$
	Interpopulation Synaptic Connection:	$p_{inter} = 1/15$			
	Synaptic Strengthes:	$J_0^{(II)} = 1300$	$J_0^{(EE)} = 300$	$J_0^{(EI)} = 800$	$J_0^{(IE)} = 487.5$ ($= J_0^{(II)} J_0^{(EE)} / J_0^{(IE)}$)
		$\sigma_0 = 5$	$J_{ij}^{(EI)} \in [0.0001, 2000]$ $J_{ij}^{(IE)} \in [0.0001, 2000]$		
(7)	Delayed Hebbian I to E iSTDP Rule				
	$\delta = 0.1$	$A_+ = 0.4$	$A_- = 0.35$	$\tau_+ = 2.6$	$\tau_- = 2.8$
(8)	Anti-Hebbian E to I eSTDP Rule				
	$\delta = 0.05$	$A_+ = 1.0$	$A_- = 0.9$	$\tau_+ = 15.0$	$\tau_- = 15.0$

where

$$U(v^{(I)}) = \begin{cases} 0 & \text{for } v^{(I)} < v_b^{(I)} \\ b_I(v^{(I)} - v_b^{(I)})^3 & \text{for } v^{(I)} \geq v_b^{(I)} \end{cases}, \quad (6)$$

$$U(v^{(E)}) = b_E(v^{(E)} - v_b^{(E)}), \quad (7)$$

$$I_{syn,i}^{(XX)}(t) = \frac{1}{d_{in,i}^{intra}} \sum_{j=1(j \neq i)}^{N_X} J_{ij}^{(XX)} w_{ij}^{(XX)} s_j^{(XX)}(t) (v_i^{(X)} - V_{syn}^{(X)}), \quad (8)$$

$$I_{syn,i}^{(XY)}(t) = \frac{1}{d_{in,i}^{inter}} \sum_{j=1}^{N_Y} J_{ij}^{(XY)} w_{ij}^{(XY)} s_j^{(XY)}(t) (v_i^{(X)} - V_{syn}^{(Y)}), \quad (9)$$

$$s_j^{(XY)}(t) = \sum_{f=1}^{F_j} E_{XY}(t - t_f^{(j)} - \tau_l^{(XY)}) \quad (X = Y \text{ or } X \neq Y); \quad (10)$$

$$E_{XY}(t) = \frac{1}{\tau_d^{(XY)} - \tau_r^{(XY)}} (e^{-t/\tau_d^{(XY)}} - e^{-t/\tau_r^{(XY)}}) \Theta(t). \quad (11)$$

Here, the state of the i th neuron in the X -population ($X = I$ or E) at a time t is characterized by two state variables: the membrane potential $v_i^{(X)}$ and the recovery current $u_i^{(X)}$. In Eq. (1), C_X is the membrane capaci-

tance, $v_r^{(X)}$ is the resting membrane potential, and $v_t^{(X)}$ is the instantaneous threshold potential. After the potential reaches its apex (i.e., spike cutoff value) $v_p^{(X)}$, the membrane potential and the recovery variable are reset according to Eq. (5). The units of the capacitance C_X ,

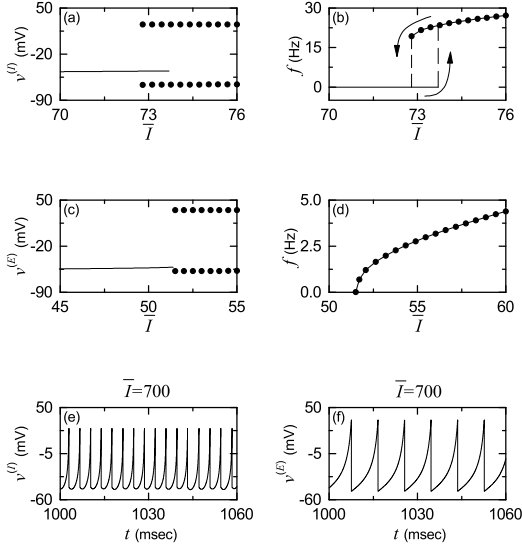


FIG. 2: Single Izhikevich FS interneuron for $D = 0$: (a) bifurcation diagram and (b) plot of the mean firing rate f versus the time-averaged constant \bar{I} of the external input I_{ext} . Single Izhikevich RS pyramidal cell for $D = 0$: (c) bifurcation diagram and (d) plot of f versus \bar{I} . In (a) and (c), solid lines denote stable equilibrium points, and solid circles represent maximum and minimum values of the membrane potential v for the spiking states. Time series of the membrane potential v of (e) the Izhikevich FS interneuron and (f) the Izhikevich RS pyramidal cell for $\bar{I} = 700$.

the potential $v^{(X)}$, the current $u^{(X)}$ and the time t are pF, mV, pA, and msec, respectively. All these parameter values used in our computations are listed in Table I. More details on the random external input, the synaptic currents and plasticity, and the numerical method for integration of the governing equations are given in the following subsections.

A. Random External Excitatory Input to Each Izhikevich FS Interneuron and RS Pyramidal Cell

Each neuron in the X -population ($X = I$ or E) receives stochastic external excitatory input $I_{ext,i}^{(X)}$ from other brain regions, not included in the network (i.e., corresponding to background excitatory input) [24–27]. Then, $I_{ext,i}^{(X)}$ may be modeled in terms of its time-averaged constant $\bar{I}_i^{(X)}$ and an independent Gaussian white noise $\xi_i^{(X)}$ (i.e., corresponding to fluctuation of $I_{ext,i}^{(X)}$ from its mean) [see the 3rd and the 4th terms in Eqs. (1) and (3)] satisfying $\langle \xi_i^{(X)}(t) \rangle = 0$ and $\langle \xi_i^{(X)}(t) \xi_j^{(X)}(t') \rangle = \delta_{ij} \delta(t - t')$, where $\langle \dots \rangle$ denotes the ensemble average. The intensity of the noise $\xi_i^{(X)}$ is controlled by using the parameter D_X . For simplicity, we consider the case of $\bar{I}_i^{(I)} = \bar{I}_i^{(E)} = \bar{I}_i$ and $D_I = D_E = D$.

Figure 2 shows spiking transitions for both the sin-

gle Izhikevich FS interneuron and RS pyramidal cell in the absence of noise (i.e., $D = 0$). The FS interneuron exhibits a jump from a resting state to a spiking state via subcritical Hopf bifurcation for $\bar{I}_h^* \simeq 73.7$ by absorbing an unstable limit cycle born via a fold limit cycle bifurcation for $\bar{I}_l^* \simeq 72.8$ [see Fig. 2(a)] [94]. Hence, the FS interneuron shows type-II excitability because it begins to fire with a non-zero frequency, as shown in Fig. 2(b) [96, 97]. Throughout this paper, we consider a suprathreshold case such that the value of \bar{I}_i is chosen via uniform random sampling in the range of [680, 720], as shown in the 3rd item of Table I. At the middle value of $\bar{I} = 700$, the membrane potential $v^{(I)}$ oscillates very fast with a mean firing rate (MFR) $f \simeq 271$ Hz [see Fig. 2(e)]. On the other hand, the RS pyramidal cell shows a continuous transition from a resting state to a spiking state through a saddle-node bifurcation on an invariant circle for $\bar{I}^* \simeq 51.5$, as shown in Fig. 2(c) [94]. Hence, the RS pyramidal cell exhibits type-I excitability because its frequency f increases continuously from 0 [see Fig. 2(d)]. For $\bar{I} = 700$, the membrane potential $v^{(E)}$ oscillates with $f \simeq 111$ Hz, as shown in Fig. 2(f). Hence, $v^{(I)}(t)$ (of the FS interneuron) oscillates about 2.4 times as fast as $v^{(E)}(t)$ (of the RS pyramidal cell) when $\bar{I} = 700$.

B. Synaptic Currents and Plasticity

The last two terms in Eq. (1) represent synaptic couplings of FS interneurons in the I-population with $N_I = 600$. $I_{syn,i}^{(II)}(t)$ and $I_{syn,i}^{(IE)}(t)$ in Eqs. (8) and (9) denote intrapopulation I to I synaptic current and interpopulation E to I synaptic current injected into the FS interneuron i , respectively, and $V_{syn}^{(I)}$ [$V_{syn}^{(E)}$] is the synaptic reversal potential for the inhibitory (excitatory) synapse. Similarly, RS pyramidal cells in the E-population with $N_E = 2400$ also have two types of synaptic couplings [see the last two terms in Eq. (3)]. In this case, $I_{syn,i}^{(EE)}(t)$ and $I_{syn,i}^{(EI)}(t)$ in Eqs. (8) and (9) represent intrapopulation E to E synaptic current and interpopulation I to E synaptic current injected into the RS pyramidal cell i , respectively.

The intrapopulation synaptic connectivity in the X -population ($X = I$ or E) is given by the connection weight matrix $W^{(XX)} (= \{w_{ij}^{(XX)}\})$ where $w_{ij}^{(XX)} = 1$ if the neuron j is pre-synaptic to the neuron i ; otherwise, $w_{ij}^{(XX)} = 0$. Here, the intrapopulation synaptic connection is modeled in terms of the Watts-Strogatz SWN. Then, the intrapopulation in-degree of the neuron i , $d_{in,i}^{intra}$ (i.e., the number of intrapopulation synaptic inputs to the neuron i) is given by $d_{in,i}^{intra} = \sum_{j=1(j \neq i)}^{N_X} w_{ij}^{(XX)}$. In this case, the average number of intrapopulation synaptic inputs per neuron is given by $M_{syn}^{(X)} = \frac{1}{N_X} \sum_{i=1}^{N_X} d_{in,i}^{intra}$. Throughout the paper, $M_{syn}^{(I)} = 40$ and $M_{syn}^{(E)} = 160$ (see the 6th item of Table I). Next, we consider interpopulation synaptic couplings. The interpopulation synaptic connectivity from the source Y -population to the target

X -population is given by the connection weight matrix $W^{(XY)} (= \{w_{ij}^{(XY)}\})$ where $w_{ij}^{(XY)} = 1$ if the neuron j in the source Y -population is pre-synaptic to the neuron i in the target X -population; otherwise, $w_{ij}^{(XY)} = 0$. Random uniform connections are made with the probability p_{inter} between the two I- and E-populations. Here, we consider the case of $p_{inter} = 1/15$. Then, the average number of E to I synaptic inputs per each FS interneuron and I to E synaptic inputs per each RS pyramidal cell are 160 and 40, respectively.

The fraction of open synaptic ion channels from the source Y -population to the target X -population at time t is denoted by $s^{(XY)}(t)$. The time course of $s_j^{(XY)}(t)$ of the neuron j in the source Y -population is given by a sum of delayed double-exponential functions $E_{XY}(t - t_f^{(j)} - \tau_l^{(XY)})$ [see Eq. (10)], where $\tau_l^{(XY)}$ is the synaptic delay for the Y to X synapse, and $t_f^{(j)}$ and F_j are the f th spiking time and the total number of spikes of the j th neuron in the Y -population at time t , respectively. Here, $E_{XY}(t)$ in Eq. (11) [which corresponds to contribution of a pre-synaptic spike occurring at time 0 to $s_j^{(XY)}(t)$ in the absence of synaptic delay] is controlled by the two synaptic time constants: synaptic rise time $\tau_r^{(XY)}$ and decay time $\tau_d^{(XY)}$, and $\Theta(t)$ is the Heaviside step function: $\Theta(t) = 1$ for $t \geq 0$ and 0 for $t < 0$. For the inhibitory GABAergic synapse (involving the GABA_A receptors), the values of $\tau_l^{(XI)}$, $\tau_r^{(XI)}$, $\tau_d^{(XI)}$, and $V_{syn}^{(I)}$ ($X = I$ or E) are listed in the 4th item of Table I [26]. For the excitatory AMPA synapse (involving the AMPA receptors), the values of $\tau_l^{(XE)}$, $\tau_r^{(XE)}$, $\tau_d^{(XE)}$, and $V_{syn}^{(E)}$ ($X = E$ or I) are given in the 5th item of Table I [26].

The coupling strength of the synapse from the pre-synaptic neuron j in the source Y -population to the post-synaptic neuron i in the target X -population is $J_{ij}^{(XY)}$; for the intrapopulation synaptic coupling $X = Y$, while for the interpopulation synaptic coupling, $X \neq Y$. Initial synaptic strengths are normally distributed with the mean $J_0^{(XY)}$ and the standard deviation $\sigma_0 (= 5)$. Here, $J_0^{(II)} = 1300$, $J_0^{(EE)} = 300$, $J_0^{(EI)} = 800$, $J_0^{(IE)} = 487.5$ ($= J_0^{(II)} J_0^{(EE)} / J_0^{(EI)}$) (see the 6th item of Table I). In this initial case, the E-I ratio (given by the ratio of average excitatory to inhibitory synaptic strengths) is the same in both FS interneurons and RS pyramidal cells (i.e., E-I ratio balance) [26, 27, 29]. Intrapopulation synaptic strengths are static because we do not take into consideration intrapopulation synaptic plasticity. For the interpopulation synaptic strengths $\{J_{ij}^{(XY)}\}$, we consider a multiplicative STDP (dependent on states) [58, 64, 98]. To avoid unbounded growth and elimination of synaptic connections, we set a range with the upper and the lower bounds: $J_{ij}^{(XY)} \in [J_l, J_h]$, where $J_l = 0.0001$ and $J_h = 2000$. With increasing time t , synaptic strength for each interpopulation synapse is updated with a nearest-

spike pair-based STDP rule [99]:

$$J_{ij}^{(XY)} \rightarrow J_{ij}^{(XY)} + \delta(J^* - J_{ij}^{(XY)}) |\Delta J_{ij}^{(XY)}(\Delta t_{ij}^{(XY)})|, \quad (12)$$

where $J^* = J_h$ (J_l) for the LTP (LTD) and $\Delta J_{ij}^{(XY)}(\Delta t_{ij}^{(XY)})$ is the synaptic modification depending on the relative time difference $\Delta t_{ij}^{(XY)} (= t_i^{(post,X)} - t_j^{(pre,Y)})$ between the nearest spike times of the post-synaptic neuron i in the target X -population and the pre-synaptic neuron j in the source Y -population. The values of the update rate δ for the I to E iSTDP and the E to I eSTDP are 0.1 and 0.05, respectively (see the 7th and the 8th items of Table I).

For the I to E iSTDP, we use a time-delayed Hebbian time window for the synaptic modification $\Delta J_{ij}^{(EI)}(\Delta t_{ij}^{(EI)})$ [60, 100, 101]:

$$\Delta J_{ij}^{(EI)}(\Delta t_{ij}^{(EI)}) = \begin{cases} E_+(\Delta t_{ij}^{(EI)}) \Delta t_{ij}^{(EI)\beta} & \text{for } \Delta t_{ij}^{(EI)} \geq 0 \\ E_-(\Delta t_{ij}^{(EI)}) \Delta t_{ij}^{(EI)\beta} & \text{for } \Delta t_{ij}^{(EI)} < 0 \end{cases}. \quad (13)$$

Here, $E_+(\Delta t_{ij}^{(EI)})$ and $E_-(\Delta t_{ij}^{(EI)})$ are Hebbian exponential functions used in the case of E to E eSTDP [49, 61]:

$$\begin{aligned} E_+(\Delta t_{ij}^{(EI)}) &= A_+ N_+ e^{-\Delta t_{ij}^{(EI)}/\tau_+} \text{ and} \\ E_-(\Delta t_{ij}^{(EI)}) &= A_- N_- e^{\Delta t_{ij}^{(EI)}/\tau_-}, \end{aligned} \quad (14)$$

where $N_+ = \frac{e^\beta}{\beta^\beta \tau_+^\beta}$, $N_- = \frac{e^\beta}{\beta^\beta \tau_-^\beta}$, $\beta = 10$, $A_+ = 0.4$, $A_- = 0.35$, $\tau_+ = 2.6$ msec, and $\tau_- = 2.8$ msec (these values are also given in the 7th item of Table I). We note that the synaptic modification $\Delta J_{ij}^{(EI)}$ in Eq. (13) is given by the products of Hebbian exponential functions in Eq. (14) and the power function $\Delta t_{ij}^{(EI)\beta}$. As in the E to E Hebbian time window, LTP occurs for $\Delta t_{ij}^{(EI)} > 0$, while LTD takes place for $\Delta t_{ij}^{(EI)} < 0$. However, due to the effect of the power function, $\Delta J_{ij}^{(EI)} \sim 0$ near $\Delta t_{ij}^{(EI)} \sim 0$, and delayed maximum and minimum for $\Delta J_{ij}^{(EI)}$ appear at $\Delta t_{ij}^{(EI)} = \beta\tau_+$ and $-\beta\tau_-$, respectively. Thus, Eq. (13) is called a time-delayed Hebbian time window, in contrast to the E to E Hebbian time window.

For the E to I eSTDP, we employ an anti-Hebbian time window for the synaptic modification $\Delta J_{ij}^{(IE)}(\Delta t_{ij}^{(IE)})$ [48, 102, 103]:

$$\Delta J_{ij}^{(IE)}(\Delta t_{ij}^{(IE)}) = \begin{cases} -A_+ e^{-\Delta t_{ij}^{(IE)}/\tau_+} & \text{for } \Delta t_{ij}^{(IE)} > 0 \\ A_- e^{\Delta t_{ij}^{(IE)}/\tau_-} & \text{for } \Delta t_{ij}^{(IE)} < 0 \end{cases}, \quad (15)$$

where $A_+ = 1.0$, $A_- = 0.9$, $\tau_+ = 15$ msec, $\tau_- = 15$ msec (these values are also given in the 8th item of Table I), and $\Delta J_{ij}^{(IE)}(0) = 0$. For $\Delta t_{ij}^{(IE)} > 0$, LTD occurs, while LTP takes place for $\Delta t_{ij}^{(IE)} < 0$, in contrast to the Hebbian time window for the E to E eSTDP [49, 61].

C. Numerical Method for Integration

Numerical integration of stochastic differential Eqs. (1)-(11) with a multiplicative STDP update rule of Eqs. (12) is done by employing the Heun method [104] with the time step $\Delta t = 0.01$ msec. For each realization of the stochastic process, we choose random initial points $[v_i^{(X)}(0), u_i^{(X)}(0)]$ for the neuron i ($i = 1, \dots, N_X$) in the X -population ($X = I$ or E) with uniform probability in the range of $v_i^{(X)}(0) \in (-50, -45)$ and $u_i^{(X)}(0) \in (10, 15)$.

III. EFFECTS OF INTERPOPULATION STDP ON FAST SPARSELY SYNCHRONIZED RHYTHMS

We consider clustered SWNs with the two I- and E-populations in Fig. 1. Each Watts-Strogatz SWN with the rewiring probability $p_{\text{wiring}} = 0.25$ has high clustering and short path length due to presence of predominantly local connections and rare long-range connections. The I-SWN consists of N_I FS interneurons, and the E-SWN is composed of N_E RS pyramidal cells. Random and uniform interconnections between the two I- and E-SWNs are made with the probability $p_{\text{inter}} = 1/15$. Throughout the paper, $N_I = 600$ and $N_E = 2400$, except for the cases in Figs. 4(a1)-4(a3). For more details on the values of parameters, refer to Table I. We first study emergence of FSS and its properties in the absence of interpopulation STDP. Then, we investigate the effects of interpopulation STDPs on diverse properties of population and individual behaviors of FSS in the 3 cases of the I to E iSTDP, E to I eSTDP, and the combined I to E and E to I STDPs.

A. Emergence of FSS and Its Properties in The Absence of STDP

Here, we are concerned about emergence of FSS and its properties in the I- and the E-populations in the absence of STDP. We also consider an interesting case of the E-I ratio balance where the ratio of average excitatory to inhibitory synaptic strengths is the same in both FS interneurons and RS pyramidal cells [26, 27, 29]. Initial synaptic strengths are chosen from the Gaussian distribution with the mean $J_0^{(XY)}$ and the standard deviation σ_0 ($= 5$). The I to I synaptic strength $J_0^{(II)} (= 1300)$ is strong, and hence FSS may appear in the I-population under the balance between strong inhibition and strong external noise. This I-population is a dominant one in our coupled two-population system because $J_0^{(II)}$ is much stronger in comparison with the E to E synaptic strength $J_0^{(EE)} (= 300)$. Moreover, the I to E synaptic strength $J_0^{(EI)} = 800$ is so strong that FSS may also appear in the E-population when the noise intensity D passes a threshold. In this state of FSS, RS pyramidal cells in

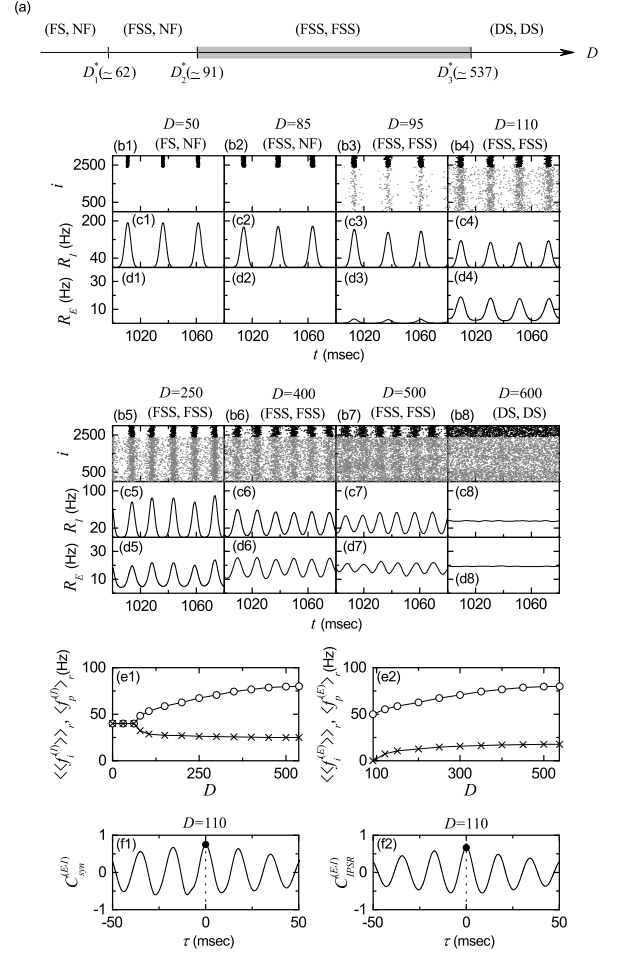


FIG. 3: Synchronized rhythms in the two I- and E-populations in the absence of STDP. (a) Bar diagram for the population states (I, E) in the I- and the E-populations. FS, FSS, NF, and DS denote full synchronization, fast sparse synchronization, non-firing, and desynchronization, respectively. (b1)-(b8) Raster plots of spikes; Lower gray dots and upper black dots denote spikes in the E- and I-populations, respectively. (c1)-(c8) IPSRs $R_I(t)$ of the I population. (d1)-(d8) IPSRs $R_E(t)$ of the E population. Plots of the population frequency $\langle f_p^{(X)} \rangle_r$ (represented by open circles) and the population-averaged MFR of individual neurons $\langle f_i^{(X)} \rangle_r$ (denoted by crosses) versus D ; (e1) $X = I$ (I-population) and (e2) $X = E$ (E-population). (f1) Cross-correlation function between total synaptic input currents $I_{\text{syn}}^{(E)}(t)$ and $I_{\text{syn}}^{(I)}(t)$ for $D = 110$. (f2) Cross-correlation function between IPSRs $R_E(t)$ and $R_I(t)$ for $D = 110$. In (f1) and (f2), solid circles represent the maxima of the cross-correlation functions.

the E-population make firings at much lower rates than FS interneurons in the I-population. Finally, the E to I synaptic strength $J_0^{(IE)} (= 487.5)$ is given by the E-I ratio balance (i.e., $J_0^{(IE)}/J_0^{(II)} = J_0^{(EE)}/J_0^{(EI)}$). In this subsection, all these synaptic strengths are static because we do not consider any synaptic plasticity.

By varying the noise intensity D , we investigate emer-

gence of diverse population states in both the I- and the E-populations. Figure 3(a) shows a bar diagram for the population states (I, E) in the two I- and E-populations, where FS, FSS, NF, and DS represents full synchronization, fast sparse synchronization, non-firing, and desynchronization. Population synchronization may be well visualized in the raster plot of neural spikes which is a collection of spike trains of individual neurons. Such raster plots of spikes are fundamental data in experimental neuroscience. As a population quantity showing collective behaviors, we use an instantaneous population spike rate (IPSR) which may be obtained from the raster plots of spikes [16, 24–29, 105]. For a synchronous case, “stripes” (consisting of spikes and indicating population synchronization) are found to be formed in the raster plot, while in a desynchronized case spikes are completely scattered without forming any stripes.

Such raster plots of spikes are well shown for various values of D in Figs. 3(b1)-3(b8). In each raster plot, spikes of N_I ($= 600$) FS interneurons are shown with black dots in the upper part, while spikes of N_E ($= 2400$) RS pyramidal cells are shown with gray dots in the lower part. Hence, in a synchronous case, an oscillating IPSR $R_X(t)$ ($X = I$ or E) appears, while in a desynchronized case $R_X(t)$ is nearly stationary. To obtain a smooth IPSR, we employ the kernel density estimation (kernel smoother) [106]. Each spike in the raster plot is convoluted (or blurred) with a kernel function $K_h(t)$ to obtain a smooth estimate of IPSR $R_X(t)$:

$$R_X(t) = \frac{1}{N_X} \sum_{i=1}^{N_X} \sum_{s=1}^{n_i^{(X)}} K_h(t - t_s^{(i,X)}), \quad (X = I \text{ or } E) \quad (16)$$

where $t_s^{(i,X)}$ is the s th spiking time of the i th neuron in the X -population, $n_i^{(X)}$ is the total number of spikes for the i th neuron, and we use a Gaussian kernel function of band width h :

$$K_h(t) = \frac{1}{\sqrt{2\pi}h} e^{-t^2/2h^2}, \quad -\infty < t < \infty. \quad (17)$$

Throughout the paper, the band width h of $K_h(t)$ is 1 msec. The IPSRs $R_I(t)$ [$R_E(t)$] for the I-(E-)population are shown for various values of D in Figs. 3(c1)-3(c8) [Figs. 3(d1)-3(d8)].

For sufficiently small D , individual FS interneurons in the I-population fire regularly with the population-averaged MFR $\langle\langle f_i^{(I)} \rangle\rangle_r$ which is the same as the population frequency $\langle f_p^{(I)} \rangle_r$ of the IPSR $R_I(t)$. Throughout the paper, $\langle \dots \rangle$ denotes a population average and $\langle \dots \rangle_r$ represents an average over 20 realizations. In this case, all FS interneurons make spikings in each spiking stripe in the raster plot, and hence each stripe is fully occupied by spikes of all FS interneurons. As a result, full synchronization with $\langle f_p^{(I)} \rangle_r = \langle\langle f_i^{(I)} \rangle\rangle_r$ occurs. As an example of full synchronization in the I-population, we consider the case of $D = 50$. Figure 3(b1) shows the

raster plot of spikes where black spiking stripes for the I-population appear successively, and the corresponding IPSR $R_I(t)$ with a large amplitude oscillates regularly with $\langle f_p^{(I)} \rangle_r \simeq 40$ Hz [see Fig. 3(c1)]. In contrast, for $D = 50$, RS pyramidal cells in the E-population do not make firings (i.e., the E-population is in the non-firing state) due to strong I to E synaptic strength $J_0^{(EI)} = 800$. In the isolated E-population (without synaptic coupling with the I-population), RS pyramidal cells make firings with $\langle\langle f_i^{(E)} \rangle\rangle_r \simeq 189.9$ Hz in a complete incoherent way, and hence population state becomes desynchronized (i.e., in this case, spikes of RS pyramidal cells are completely scattered without forming any stripes in the raster plot). However, in the presence of strong I to E synaptic current, the population state for the E-population is transformed into a non-firing state. Thus, for $D = 50$ there are no spikes of RS pyramidal cells in the raster plot and no IPSR $R_E(t)$ appears.

The full synchronization in the I-population persists until $D = D_1^*$ ($\simeq 62$). For $D > D_1^*$, full synchronization is developed into FSS with $\langle f_p^{(I)} \rangle_r > \langle\langle f_i^{(I)} \rangle\rangle_r$ through a pitchfork bifurcation, as shown in Fig. 3(e1). In the case of FSS for $D > D_1^*$, $\langle f_p^{(I)} \rangle_r$ ($\langle\langle f_i^{(I)} \rangle\rangle_r$) increases (decreases) monotonically from 40 Hz with increasing D . In each realization, we get the population frequency $f_p^{(X)}$ ($X = I$ or E) from the reciprocal of the ensemble average of 10^4 time intervals between successive maxima of $R_X(t)$, and obtain the MFR $f_i^{(X)}$ for each neuron in the X -population via averaging for 2×10^4 msec; $\langle f_i^{(X)} \rangle$ denotes a population-average of $f_i^{(X)}$ over all neurons in the X -population. Due to the noise effect, individual FS interneurons fire irregularly and intermittently at lower rates than the population frequency $\langle f_p^{(I)} \rangle_r$. Hence, only a smaller fraction of FS interneurons fire in each spiking stripe in the raster plot (i.e., each spiking stripe is sparsely occupied by spikes of a smaller fraction of FS interneurons). Figures 3(b2), 3(c2), and 3(d2) show an example of FSS in the I-population for $D = 85$. In this case, the IPSR $R_I(t)$ of the I-population rhythm makes fast oscillations with the population frequency $\langle f_p^{(I)} \rangle_r$ ($\simeq 48.3$ Hz), while FS interneurons make spikings intermittently with lower population-averaged MFR $\langle\langle f_i^{(I)} \rangle\rangle_r$ ($\simeq 32.2$ Hz) than the population frequency $\langle f_p^{(I)} \rangle_r$. Then, the I-stripes in the raster plot become a little sparse and smeared, in comparison to the case of full synchronization for $D = 50$, and hence the amplitude of the corresponding IPSR $R_I(t)$ (which oscillates with increased $\langle f_p^{(I)} \rangle_r$) also has a little decreased amplitude. Thus, fast sparsely synchronized rhythm appears in the I-population. In contrast, for $D = 85$ the E-population is still in a non-firing state [see Figs. 3(b2) and 3(d2)].

However, as D passes a 2nd threshold D_2^* ($\simeq 91$), a transition from a non-firing to a firing state occurs in the E-population (i.e., RS pyramidal cells begin to make noise-induced intermittent spikings). [Details on this

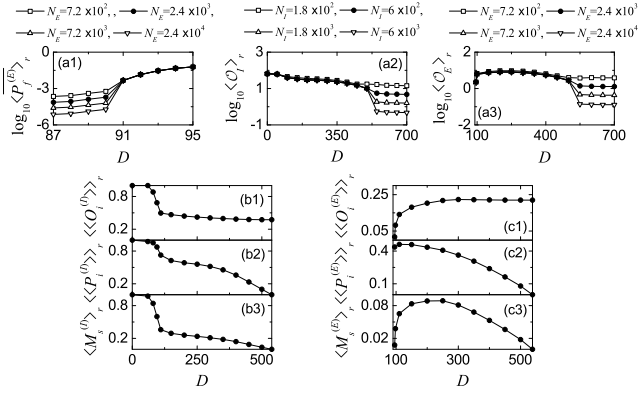


FIG. 4: Characterization of population synchronization in the absence of STDP. (a1) Plot of the average firing probability $\langle P_f^{(E)} \rangle_r$ versus D in the E-population. (a2) Plot of the thermodynamic order parameter $\langle O_I \rangle_r$ versus D in the I-population. (a3) Plot of the thermodynamic order parameter $\langle O_E \rangle_r$ versus D in the E-population. Plots of (b1) the average occupation degree $\langle \langle O_i^{(I)} \rangle \rangle_r$, (b2) the average pacing degree $\langle \langle P_i^{(I)} \rangle \rangle_r$, and (b3) the statistical-mechanical spiking measure $\langle M_s^{(I)} \rangle_r$ versus D in the I-population. Plots of (c1) the average occupation degree $\langle \langle O_i^{(E)} \rangle \rangle_r$, (c2) the average pacing degree $\langle \langle P_i^{(E)} \rangle \rangle_r$, and (c3) the statistical-mechanical spiking measure $\langle M_s^{(E)} \rangle_r$ versus D in the E-population.

kind of firing transition will be given below in Fig. 4(a1)]. Then, FSS also appears in the E-population due to strong coherent I to E synaptic current to stimulate coherence between noise-induced spikings. Thus, FSS occurs together in both the (stimulating) I- and the (stimulated) E-populations, as shown in the raster plot of spikes in Fig. 3(b3) for $D = 95$. The IPSRs $R_I(t)$ and $R_E(t)$ for the sparsely synchronized rhythms in the I- and the E-populations oscillate fast with the same population frequency $\langle f_p^{(I)} \rangle_r = \langle f_p^{(E)} \rangle_r (\simeq 51.3 \text{ Hz})$. Here, we note that the population frequency of fast sparsely synchronized rhythms is determined by the dominant stimulating I-population, and hence $\langle f_p^{(E)} \rangle_r$ for the E-population is just as the same as $\langle f_p^{(I)} \rangle_r$ for the I-population. However, RS pyramidal cells fire intermittent spikings with much lower population-averaged MFR $\langle \langle f_i^{(E)} \rangle \rangle_r (\simeq 2.7 \text{ Hz})$ than $\langle \langle f_i^{(I)} \rangle \rangle_r (\simeq 30 \text{ Hz})$ of FS interneurons. Hence, the gray E-stripes (i.e., gray spiking stripes for the E-population) in the raster plot of spikes are much more sparse than the black I-stripes, and the amplitudes of $R_E(t)$ are much smaller than those of $R_I(t)$.

With further increasing D , we study evolutions of (FSS, FSS) in both the I- and the E-populations for various values of D ($D = 110, 250, 400$, and 500). For these cases, raster plots of spikes are shown in Figs. 3(b4)-3(b7), and IPSRs $R_I(t)$ and $R_E(t)$ are given in Figs. 3(c4)-3(c7) and Figs. 3(d4)-3(d7), respectively. In the I-population, as D is increased, more number of black I-stripes appear successively in the raster

plots, which implies increase in the population frequency $\langle f_p^{(I)} \rangle_r$ [see Fig. 3(e1)]. Furthermore, these black I-stripes become more sparse (i.e., density of spikes in the black I-stripes decreases) due to decrease in $\langle \langle f_i^{(I)} \rangle \rangle_r$ [see Fig. 3(e1)], and they also are more and more smeared. Hence, with increasing D monotonic decrease in amplitudes of the corresponding IPSR $R_I(t)$ occurs (i.e. the degree of FSS in the I-population is decreased). Eventually, when passing the 3rd threshold $D_3^* (\simeq 537)$, a transition from FSS to desynchronization occurs because of complete overlap between black I-stripes in the raster plot. Then, spikes of FS interneurons are completely scattered in the raster plot, and the IPSR $R_I(t)$ is nearly stationary, as shown in Figs. 3(b8) and 3(c8) for $D = 600$.

In the E-population, the IPSR $R_E(t)$ for the sparsely synchronized rhythm oscillates fast with the population frequency $\langle f_p^{(E)} \rangle_r$ which is the same as $\langle f_p^{(I)} \rangle_r$ for the I-population; $\langle f_p^{(E)} \rangle_r$ increases with D [see Fig. 3(e2)]. As D is increased, population-averaged MFR $\langle \langle f_i^{(E)} \rangle \rangle_r$ also increases due to decrease in the I to E synaptic current (which results from decrease in the degree of FSS in the I-population) [see Fig. 3(e2)], in contrast to the case of $\langle \langle f_i^{(I)} \rangle \rangle_r$ in the I-population (which decreases with D). Hence, as D is increased, density of spikes in gray E-stripes in the raster plot increases (i.e., gray E-stripes become less sparse), unlike the case of I-population. On the other hand, with increasing D for $D > 110$ E-stripes are more and more smeared, as in the case of I-population. The degree of FSS is given by considering both the density of spikes [denoting the average occupation degree (corresponding to average fraction of spiking RS pyramidal cells in each E-stripe)] and the pacing degree of spikes (representing the degree of phase coherence between spikes) in the E-stripes, the details of which will be given in Fig. 4. Through competition between the (increasing) occupation degree and the (decreasing) pacing degree, it is found that the E-population has the maximum degree of FSS for $D \sim 250$; details on the degree of FSS will be given below in Fig. 4. Thus, the amplitude of $R_E(t)$ (representing the overall degree of FSS) increases until $D \sim 250$, and then it decreases monotonically. Like the case of I-population, due to complete overlap between the gray E-stripes in the raster plot, a transition to desynchronization occurs at the same 3rd threshold D_3^* . Then, spikes of RS pyramidal cells are completely scattered in the raster plot and the IPSR $R_E(t)$ is nearly stationary [see Figs. 3(b8) and 3(d8) for $D = 600$].

The E-I ratios, α_I and α_E , in the I- and the E-populations are given by the ratios of average excitatory to inhibitory synaptic strengths in the FS interneurons and the RS pyramidal cells, respectively [26, 27, 29]:

$$\alpha_I = \frac{\langle J_{ij}^{(IE)} \rangle}{\langle J_{ij}^{(II)} \rangle} \quad \text{and} \quad \alpha_E = \frac{\langle J_{ij}^{(EE)} \rangle}{\langle J_{ij}^{(EI)} \rangle}. \quad (18)$$

In the absence of STDP, we consider the case of E-I ratio balance [i.e., $\alpha_I (= J_0^{(IE)}/J_0^{(II)}) = \alpha_E (=$

$J_0^{(EE)}/J_0^{(EI)} = 0.375$] where the ratio of average excitatory to inhibitory synaptic strengths is the same in both FS interneurons and RS pyramidal cells. In this case, we study the phase shift between fast sparsely synchronized rhythms in the I- and the E-populations. We note that the black I-stripes and the gray E-stripes in the raster plot of spikes are in-phase, as shown in Figs. 3(b3)-3(b7). Hence, both $R_I(t)$ and $R_E(t)$ make in-phase oscillations with the same population frequency [compare Figs. 3(c3)-3(c7) with Figs. 3(d3)-3(d7)].

As an example for quantitative analysis of the phase shift, we consider a case of $D = 110$. Figure 3(f1) shows the cross-correlation function $C_{syn}^{(E,I)}(\tau)$ between the population-averaged total synaptic input currents $I_{syn}^{(E)}(t)$ and $I_{syn}^{(I)}(t)$ into the E- and the I-populations:

$$C_{syn}^{(E,I)}(\tau) = \frac{\overline{\Delta I_{syn}^{(E)}(t+\tau) \Delta I_{syn}^{(I)}(t)}}{\sqrt{\overline{\Delta I_{syn}^{(E)}(t)^2}} \sqrt{\overline{\Delta I_{syn}^{(I)}(t)^2}}}, \quad (19)$$

where $\Delta I_{syn}^{(X)}(t) = I_{syn}^{(X)}(t) - \overline{I_{syn}^{(X)}(t)}$ ($X = I$ or E), and throughout the paper, the overbar represents the time average. Here, $I_{syn}^{(E)}(t)$ [$I_{syn}^{(I)}(t)$] represents a population average of the total (inhibitory + excitatory) synaptic input currents into the RS pyramidal cells (FS interneurons) over the E-(I-)population:

$$\begin{aligned} I_{syn}^{(E)}(t) &= \frac{1}{N_E} \sum_{i=1}^{N_E} [I_{syn,i}^{(EE)}(t) + I_{syn,i}^{(EI)}(t)] \quad \text{and} \\ I_{syn}^{(I)}(t) &= \frac{1}{N_I} \sum_{i=1}^{N_I} [I_{syn,i}^{(II)}(t) + I_{syn,i}^{(IE)}(t)], \end{aligned} \quad (20)$$

where the intrapopulation and the interpopulation synaptic currents $I_{syn,i}^{(XX)}(t)$ and $I_{syn,i}^{(XY)}(t)$ are given in Eqs. (8) and (9), respectively. Throughout the paper, a cross-correlation function is numerically calculated with 2^{16} data points. We note that the main peak of the cross-correlation function $C_{syn}^{(E,I)}(\tau)$ in Fig. 3(f1) appears at $\tau = 0$, which implies that population-averaged total synaptic inputs $I_{syn}^{(E)}(t)$ and $I_{syn}^{(I)}(t)$ are in-phase. As a result, IPSR outputs $R_E(t)$ and $R_I(t)$ of the E- and the I-populations are also in-phase, which may be well seen in the cross-correlation function $C_{IPSR}^{(E,I)}(\tau)$ between $R_E(t)$ and $R_I(t)$ which also has the main peak at $\tau = 0$ [see Fig. 3(f2)], where

$$C_{IPSR}^{(E,I)}(\tau) = \frac{\overline{\Delta R_E(t+\tau) \Delta R_I(t)}}{\sqrt{\overline{\Delta R_E(t)^2}} \sqrt{\overline{\Delta R_I(t)^2}}}. \quad (21)$$

For characterization of population synchronization (shown in Fig. 3), we first determine the 2nd and 3rd thresholds D_2^* ($\simeq 91$) and D_3^* ($\simeq 537$). When passing the 2nd threshold D_2^* , a firing transition (i.e., transition from a non-firing to a firing state) occurs in the E-population. We quantitatively characterize this firing transition in

terms of the average firing probability $\overline{P_f^{(E)}}$ [107]. In each raster plot of spikes in the E-population, we divide a long-time interval into bins of width δ ($= 5$ msec) and calculate the firing probability in each i th bin (i.e., the fraction of firing RS pyramidal cells in the i th bin):

$$P_f^{(E)}(i) = \frac{N_f^{(E)}(i)}{N_E}, \quad i = 1, 2, \dots, \quad (22)$$

where $N_f^{(E)}(i)$ is the number of firing RS pyramidal cells in the i th bin. Then, we get the average firing probability $\overline{P_f^{(E)}}$ via time average of $P_f^{(E)}(i)$ over sufficiently many bins:

$$\overline{P_f^{(E)}} = \frac{1}{N_b} \sum_{i=1}^{N_b} P_f^{(E)}(i), \quad (23)$$

where N_b is the number of bins for averaging. In each realization, the averaging is done for sufficiently large number of bins ($N_b = 4000$). For a firing (non-firing) state, the average firing probability $\overline{P_f^{(E)}}$ approaches a non-zero (zero) limit value in the thermodynamic limit of $N_E \rightarrow \infty$. Figure 4(a1) shows a plot of $\log_{10} \langle \overline{P_f^{(E)}} \rangle_r$ versus the noise intensity D . For $D > D_2^*$, firing states appear in the E-population (i.e., RS pyramidal cells make noise-induced intermittent spikings) because $\langle \overline{P_f^{(E)}} \rangle_r$ tends to converge toward non-zero limit values. Then, strong coherent I to E synaptic input current stimulates FSS between these noise-induced intermittent spikes in the E-population. Thus, when passing D_2^* ($\simeq 91$), (FSS, FSS) occurs in both the I- and the E-populations.

However, as D is further increased, the degree of (FSS, FSS) decreases, and eventually when passing the 3rd threshold D_3^* , a transition to desynchronization occurs in both the I- and the E-populations, due to a destructive role of noise to spoil FSS. We characterize this kind of synchronization-desynchronization transition in the X -population ($X = I$ or E) in terms of the order parameter \mathcal{O}_X , corresponding to the mean square deviation of the IPSR $R_X(t)$ [105]:

$$\mathcal{O}_X = \overline{(R_X(t) - \overline{R_X(t)})^2}. \quad (24)$$

This order parameter may be regarded as a thermodynamic measure because it concerns just the macroscopic IPSR $R_X(t)$ without any consideration between $R_X(t)$ and microscopic individual spikes. For a synchronized state, $R_X(t)$ exhibits an oscillatory behavior, while for a desynchronized state it is nearly stationary. Hence, the order parameter \mathcal{O}_X approaches a non-zero (zero) limit value in the synchronized (desynchronized) case in the thermodynamic limit of $N_X \rightarrow \infty$. In each realization, we obtain \mathcal{O}_X by following a stochastic trajectory for 3×10^4 msec. Figures 4(a2) and 4(a3) show plots of $\log_{10} \langle \mathcal{O}_I \rangle_r$ and $\log_{10} \langle \mathcal{O}_E \rangle_r$ versus D , respectively. For $D < D_3^*$ ($\simeq 537$), (FSS, FSS) occurs in both the I- and

the E-populations because the order parameters $\langle \mathcal{O}_I \rangle_r$ and $\langle \mathcal{O}_E \rangle_r$ tend to converge toward non-zero limit values. In contrast, for $D > D_3^*$, with increasing N_I and N_E both the order parameters $\langle \mathcal{O}_I \rangle_r$ and $\langle \mathcal{O}_E \rangle_r$ tend to approach zero, and hence a transition to desynchronization occurs together in both the I- and the E-populations.

We now measure the degree of population synchronization in the I- and the E-populations by employing the statistical-mechanical spiking measure $M_s^{(X)}$ ($X = I$ or E) [105]. For a synchronous case, spiking I-(E-)stripes appear successively in the raster plot of spikes of FS interneurons (RS pyramidal cells). The spiking measure $M_i^{(X)}$ of the i th X -stripe is defined by the product of the occupation degree $O_i^{(X)}$ of spikes (denoting the density of the i th X -stripe) and the pacing degree $P_i^{(X)}$ of spikes (representing the degree of phase coherence between spikes in the i th X -stripe):

$$M_i^{(X)} = O_i^{(X)} \cdot P_i^{(X)}. \quad (25)$$

The occupation degree $O_i^{(X)}$ of spikes in the X -stripe is given by the fraction of spiking neurons:

$$O_i^{(X)} = \frac{N_i^{(s,X)}}{N_X}, \quad (26)$$

where $N_i^{(s,X)}$ is the number of spiking neurons in the i th X -stripe. In the case of sparse synchronization, $O_i^{(X)} < 1$, in contrast to the case of full synchronization with $O_i^{(X)} = 1$.

The pacing degree $P_i^{(X)}$ of spikes in the i th X -stripe can be determined in a statistical-mechanical way by considering their contributions to the macroscopic IPSR $R_X(t)$. Central maxima of $R_X(t)$ between neighboring left and right minima of $R_X(t)$ coincide with centers of X -stripes in the raster plot. A global cycle begins from a left minimum of $R_X(t)$, passes a maximum, and ends at a right minimum. An instantaneous global phase $\Phi^{(X)}(t)$ of $R_X(t)$ was introduced via linear interpolation in the region forming a global cycle [for details, refer to Eqs. (16) and (17) in [105]]. Then, the contribution of the k th microscopic spike in the i th X -stripe occurring at the time $t_k^{(s,X)}$ to $R_X(t)$ is given by $\cos \Phi_k^{(X)}$, where $\Phi_k^{(X)}$ is the global phase at the k th spiking time [i.e., $\Phi_k^{(X)} \equiv \Phi^{(X)}(t_k^{(s,X)})$]. A microscopic spike makes the most constructive (in-phase) contribution to $R_X(t)$ when the corresponding global phase $\Phi_k^{(X)}$ is $2\pi n$ ($n = 0, 1, 2, \dots$). In contrast, it makes the most destructive (anti-phase) contribution to $R_X(t)$ when $\Phi_k^{(X)}$ is $2\pi(n - 1/2)$. By averaging the contributions of all microscopic spikes in the i th X -stripe to $R_X(t)$, we get the pacing degree of spikes in the i th X -stripe [refer to Eq. (18) in [105]]:

$$P_i^{(X)} = \frac{1}{S_i^{(X)}} \sum_{k=1}^{S_i^{(X)}} \cos \Phi_k^{(X)}, \quad (27)$$

where $S_i^{(X)}$ is the total number of microscopic spikes in the i th X -stripe. Then, via averaging $M_i^{(X)}$ of Eq. (25) over a sufficiently large number $N_s^{(X)}$ of X -stripes, we obtain the statistical-mechanical spiking measure $M_s^{(X)}$, based on the IPSR $R_X(t)$ [refer to Eq. (19) in [105]]:

$$M_s^{(X)} = \frac{1}{N_s^{(X)}} \sum_{i=1}^{N_s^{(X)}} M_i^{(X)}. \quad (28)$$

In each realization, we obtain $\langle O_i^{(X)} \rangle$, $\langle P_i^{(X)} \rangle$, and $M_s^{(X)}$ by following 6×10^3 X -stripes.

We first consider the case of I-population (i.e., $X = I$) which is a dominant one in our coupled two-population network. Figures 4(b1)-4(b3) show the average occupation degree $\langle \langle O_i^{(I)} \rangle \rangle_r$, the average pacing degree $\langle \langle P_i^{(I)} \rangle \rangle_r$, and the statistical-mechanical spiking measure $\langle M_s^{(I)} \rangle_r$ in the range of $0 < D < D_3^*$, respectively. With increasing D from 0 to D_1^* ($\simeq 62$), full synchronization persists, and hence $\langle \langle O_i^{(I)} \rangle \rangle_r = 1$. In this range of D , $\langle \langle P_i^{(I)} \rangle \rangle_r$ decreases very slowly from 1.0 to 0.98. In the case of full synchronization, the statistical-mechanical spiking measure is equal to the average pacing degree (i.e., $\langle M_s^{(I)} \rangle_r = \langle \langle P_i^{(I)} \rangle \rangle_r$). However, as D is increased from D_1^* , full synchronization is developed into FSS. In the case of FSS, at first $\langle \langle O_i^{(I)} \rangle \rangle_r$ (representing the density of spikes in the I-stripes) decreases rapidly due to break-up of full synchronization, and then it slowly decreases toward a limit value of $\langle \langle O_i^{(I)} \rangle \rangle_r \simeq 0.37$ for $D = D_3^*$, like the behavior of population-averaged MFR $\langle \langle f_i^{(I)} \rangle \rangle_r$ in Fig. 3(e1). The average pacing degree $\langle \langle P_i^{(I)} \rangle \rangle_r$ denotes well the average degree of phase coherence between spikes in the I-stripes; as the I-stripes become more smeared, their pacing degree gets decreased. With increasing D , $\langle \langle P_i^{(I)} \rangle \rangle_r$ decreases due to intensified smearing, and for large D near D_3^* it converges to zero due to complete overlap between sparse spiking I-stripes. The statistical-mechanical spiking measure $\langle M_s^{(I)} \rangle_r$ is obtained via product of the occupation and the pacing degrees of spikes. Due to the rapid decrease in $\langle \langle O_i^{(I)} \rangle \rangle_r$, at first $\langle M_s^{(I)} \rangle_r$ also decreases rapidly, and then it makes a slow convergence to zero for $D = D_3^*$, like the case of $\langle \langle P_i^{(I)} \rangle \rangle_r$. Thus, three kinds of downhill-shaped curves (composed of solid circles) for $\langle \langle O_i^{(I)} \rangle \rangle_r$, $\langle \langle P_i^{(I)} \rangle \rangle_r$ and $\langle M_s^{(I)} \rangle_r$ are formed [see Figs. 4(b1)-4(b3)].

Figures 4(c1)-4(c3) show $\langle \langle O_i^{(E)} \rangle \rangle_r$, $\langle \langle P_i^{(E)} \rangle \rangle_r$, and $\langle M_s^{(E)} \rangle_r$ in the E-population for $D_2^* < D < D_3^*$, respectively. When passing the 2nd threshold D_2^* , FSS appears in the E-population because strong I to E synaptic input current stimulates coherence between noise-induced intermittent spikes [i.e., sparsely synchronized E-population rhythms are locked to (stimulating) sparsely synchronized I-population rhythms]. In this case, at first, the average occupation degree $\langle \langle O_i^{(E)} \rangle \rangle_r$ begins to make

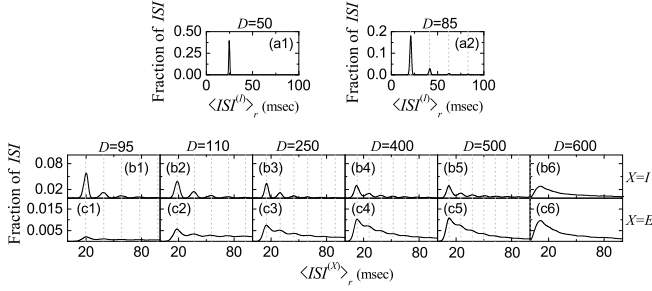


FIG. 5: Characterization of individual spiking behaviors in the absence of STDP. ISI histograms for $D = (a1) 50$ and $(a2) 85$ in the I-population. ISI histograms for various values of D in the I-population [(b1)-(b6)] and the E-population [(c1)-(c6)]. Vertical dotted lines in (a2), (b1)-(b5), and (c1)-(c5) represent multiples of the global period $T_G^{(X)}$ of the IPSR $R_X(t)$ ($X = I$ and E).

a rapid increase from 0, and then it increases slowly to a saturated limit value of $\langle\langle O_i^{(E)} \rangle\rangle_r \simeq 0.22$. Thus, an uphill-shaped curve for $\langle\langle O_i^{(E)} \rangle\rangle_r$ is formed, similar to the case of population-averaged MFR $\langle\langle f_i^{(E)} \rangle\rangle_r$ in Fig. 3(e2). In contrast, just after $D = D_2^*$, the average pacing degree $\langle\langle P_i^{(E)} \rangle\rangle_r$ starts from a non-zero value (e.g., $\langle\langle P_i^{(E)} \rangle\rangle_r \simeq 0.409$ for $D = 92$), it increases to a maximum value ($\simeq 0.465$) for $D \sim 150$, and then it decreases monotonically to zero at the 3rd threshold D_3^* because of complete overlap between sparse E-strips. Thus, for $D > 150$ the graph for $\langle\langle P_i^{(E)} \rangle\rangle_r$ is a downhill-shaped curve. Through the product of the occupation (uphill curve) and the pacing (downhill curve) degrees, the spiking measure $\langle M_s^{(E)} \rangle_r$ forms a bell-shaped curve with a maximum ($\simeq 0.089$) at $D \sim 250$; the values of $\langle M_s^{(E)} \rangle_r$ are zero at both ends (D_2^* and D_3^*). This spiking measure $\langle M_s^{(E)} \rangle_r$ of the E-population rhythms is much less than that $\langle M_s^{(I)} \rangle_r$ of the dominant I-population rhythms.

In addition to characterization of population synchronization in Fig. 4, we also characterize individual spiking behaviors of FS interneurons and RS pyramidal cells in terms of interspike intervals (ISIs) in Fig. 5. In each realization, we obtain one ISI histogram which is composed of 10^5 ISIs obtained from all individual neurons, and then we get an averaged ISI histogram for $\langle ISI^{(X)} \rangle_r$ ($X = I$ or E) via 20 realizations.

We first consider the case of (stimulating) dominant I-population. In the case of full synchronization for $D = 50$, the ISI histogram is shown in Fig. 5(a1). It has a sharp single peak at $\langle ISI^{(I)} \rangle_r = 25$ msec. In this case, all FS interneurons exhibit regular spikings like clocks with $\langle\langle f_i^{(I)} \rangle\rangle_r \simeq 40$ Hz, which leads to emergence of fully synchronized rhythm with the same population frequency $\langle f_p^{(I)} \rangle_r \simeq 40$ Hz. However, when passing the 1st threshold D_1^* ($\simeq 62$), FSS emerges via break-up of full synchronization due to a destructive role of noise. Due

to the noise effect, individual FS interneurons exhibit intermittent spikings phase-locked to the IPSR $R_I(t)$ at random multiples of the global period $T_G^{(I)}$ of $R_I(t)$, unlike the case of full synchronization. This “stochastic phase locking,” resulting in “stochastic spike skipping,” is well shown in the ISI histogram with multiple peaks appearing at integer multiples of $T_G^{(I)}$, as shown in Fig. 5(a2) for $D = 85$, which is in contrast to the case of full synchronization with a single-peaked ISI histogram. In this case, the 1st-order main peak at $T_G^{(I)}$ ($\simeq 20.7$ msec) is a dominant one, and smaller 2nd- and 3rd-order peaks (appearing at $2 T_G^{(I)}$ and $3 T_G^{(I)}$) may also be seen. Thus, the average ISI $\langle\langle ISI^{(I)} \rangle\rangle_r$ ($\simeq 31.0$ msec) is increased, in comparison with that in the case of full synchronization. Thus, FS interneurons make intermittent spikings at lower population-averaged MFR $\langle\langle f_i^{(I)} \rangle\rangle_r$ ($\simeq 32.3$ Hz) than the population frequency $\langle f_p^{(I)} \rangle_r$ ($\simeq 48.3$ Hz), in contrast to the case of full synchronization with $\langle\langle f_i^{(I)} \rangle\rangle_r = \langle f_p^{(I)} \rangle_r$ ($\simeq 40$ Hz).

This kind of spike-skipping phenomena (characterized with multi-peaked ISI histograms) have also been found in networks of coupled inhibitory neurons where noise-induced hoppings from one cluster to another one occur [108], in single noisy neuron models exhibiting stochastic resonance due to a weak periodic external force [109, 110], and in inhibitory networks of coupled subthreshold neurons showing stochastic spiking coherence [111–113]. Because of this stochastic spike skipping, the population-averaged MFR of individual neurons becomes less than the population frequency, which leads to occurrence of sparse synchronization (i.e., sparse occupation occurs in spiking stripes in the raster plot).

As D passes the 2nd threshold D_2^* ($\simeq 91$), FSS emerges in the E-population because of strong coherent I to E synaptic input current stimulating coherence between noise-induced intermittent spikes. Thus, for $D > D_2^*$ FSS occurs together in both the I- and the E-populations. However, when passing the large 3rd threshold D_3^* ($\simeq 537$), a transition from FSS to desynchronization occurs due to a destructive role of noise to spoil FSS. Hence, for $D > D_3^*$ desynchronized states exist in both the I- and the E-populations. With increasing D from D_2^* , we investigate individual spiking behaviors in terms of ISIs in both the I- and the E-populations.

Figures 5(b1)-5(b5) show ISI histograms for various values of D in the case of FSS in the (stimulating) dominant I-population. Due to the stochastic spike skipplings, multiple peaks appear at integer multiples of the global period $T_G^{(I)}$ of $R_I(t)$. As D is increased, the 1st-order main peak becomes lowered and broadened, higher-order peaks also become wider, and thus mergings between multiple peaks occur. Hence, with increasing D , the average ISI $\langle\langle ISI^{(I)} \rangle\rangle_r$ increases due to developed tail part, and spiking I-strips in the raster plot in Fig. 3 become more and more smeared [i.e., the average pacing degree $\langle\langle P_i^{(I)} \rangle\rangle_r$ of spikes in the I-strips decreases, as shown in

Fig. 4(b2)], because of merging between multiple peaks. We note that the population-averaged MFR $\langle\langle f_i^{(I)} \rangle\rangle_r$ corresponds to the reciprocal of the average ISI $\langle\langle ISI^{(I)} \rangle\rangle_r$. Hence, with increasing D in the case of FSS, $\langle\langle f_i^{(I)} \rangle\rangle_r$ decreases [see Fig. 3(e1)]. Due to decrease in $\langle\langle f_i^{(I)} \rangle\rangle_r$, I-strips in the raster plot becomes more and more sparse [i.e., the average occupation degree $\langle\langle O_i^{(I)} \rangle\rangle_r$ of spikes in the I-strips decreases, as shown in Fig. 4(b1)]

In the case of desynchronization, multiple peaks overlap completely, and hence spikes in the raster plot are completely scattered. Thus, a single-peaked ISI histogram with a long tail appears, as shown in Fig. 5(b6) for $D = 600$. In this case of $D = 600$, the average ISI $\langle\langle ISI^{(I)} \rangle\rangle_r$ ($\simeq 39.7$ msec) is a little shorter than that ($\simeq 40$ msec) for $D = 500$, in contrast to the increasing tendency in the case of FSS. In the desynchronized state for $D > D_3^*$, the I to I synaptic current is incoherent (i.e., the IPSR $R_I(t)$ is nearly stationary), and hence noise no longer causes stochastic phase lockings. In this case, noise just makes FS interneurons fire more frequently, along with the incoherent synaptic input currents. Thus, with increasing D in the desynchronized case, the average ISI $\langle\langle ISI^{(I)} \rangle\rangle_r$ tends to decrease, in contrast to the case of FSS. The corresponding population-averaged MFR $\langle\langle f_i^{(I)} \rangle\rangle_r$ in the desynchronized case also tends to increase, in contrast to the decreasing tendency in the case of FSS.

We now consider the case of (stimulated) E-population for $D > D_2^*$. Figures 5(c1)-5(c5) show ISI histograms for various values of D in the case of FSS. Due to the stochastic spike skipings, multiple peaks appear, as in the case of I-population. Just after appearance of FSS (appearing due to coherent I to E synaptic current), a long tail is developed so much in the ISI histogram [e.g., see Fig. 5(c1) for $D = 95$], and hence multiple peaks are less developed. As D is a little more increased, multiple peaks begin to be clearly developed due to a constructive role of coherent I to E synaptic input, as shown in Fig. 5(c2) for $D = 110$. Thus, the average pacing degree $\langle\langle P_i^{(E)} \rangle\rangle_r$ of spikes in the E-strips for $D = 110$ increases a little in comparison with that for $D = 95$, as shown in Fig. 4(c2). However, as D is further increased for $D > 150$, mergings between multiple peaks begin to occur due to a destructive role of noise, along with increase in the height of the 1st-order main peak [see Figs. 5(c3)-5(c5)], in contrast to the case of I-population where the main peak is lowered. Because of the merging of peaks, the average pacing degree $\langle\langle P_i^{(E)} \rangle\rangle_r$ of spikes in the E-strips begins to decrease [see Fig. 4(c2)]. With increasing D in the case of FSS the average ISI $\langle\langle ISI^{(E)} \rangle\rangle_r$ decreases, in contrast to the increasing tendency of I-population. This decreasing tendency continues even in the case of desynchronization. Figure 5(c6) shows a single-peaked ISI histogram with a long tail (that appears through complete merging between multiple peaks) for $D = 600$. In this case, the average ISI $\langle\langle ISI^{(E)} \rangle\rangle_r$ ($\simeq 54.9$ msec) is shorter than that (56.8 msec) in the case of FSS for $D = 500$. We

also note that for each value of D (in the case of FSS and desynchronization), $\langle\langle ISI^{(E)} \rangle\rangle_r$ is longer than that in the case of I-population, due to much more developed tail part.

As a result of decrease in the average ISI $\langle\langle ISI^{(E)} \rangle\rangle_r$, the population-averaged MFR $\langle\langle f_i^{(E)} \rangle\rangle_r$ (corresponding to the reciprocal of $\langle\langle ISI^{(E)} \rangle\rangle_r$) increases with D [see Fig. 3(e2)]. We also note that these population-averaged MFRs $\langle\langle f_i^{(E)} \rangle\rangle_r$ are much lower than $\langle\langle f_i^{(I)} \rangle\rangle_r$ in the (stimulated) I-population, although the population frequencies in both populations are the same. In the case of FSS, due to increase in $\langle\langle f_i^{(E)} \rangle\rangle_r$, E-strips in the raster plot become less sparse [i.e., the average occupation degree $\langle\langle O_i^{(E)} \rangle\rangle_r$ of spikes in the E-strips increases, as shown in Fig. 4(c1)]. The increasing tendency for $\langle\langle f_i^{(E)} \rangle\rangle_r$ continues even in the case of desynchronization. For example, the population-averaged MFR $\langle\langle f_i^{(E)} \rangle\rangle_r$ ($\simeq 18.2$ Hz) for $D = 600$ is increased in comparison with that ($\simeq 17.6$ Hz) for $D = 500$.

B. Effect of I to E iSTDP on Population States in the I- and the E-populations

In this subsection, we study the effect of I to E iSTDP on population states in the I- and the E-populations, and make comparison with the case without STDP. A main finding is occurrence of an equalization effect in the spiking measure $\langle M_s^{(X)} \rangle_r$ ($X = I$ or E) (denoting the overall synchronization degree). In a wide region of intermediate D , the degree of good synchronization (with higher spiking measure) gets decreased, while in a region of large D the degree of bad synchronization (with lower spiking measure) becomes increased. Thus, the degree of population synchronization becomes nearly the same in a broad region of D (i.e., the standard deviation in the distribution of spiking measures is much decreased in comparison with that in the absence of STDP). This kind of equalization effect with much smaller standard deviation is in contrast to the Matthew (bipolarization) effect in the case of intrapopulation (I to I and E to E) STDP where good (bad) synchronization becomes better (worse) [61, 64]. In addition, the population frequency $\langle f_p^{(X)} \rangle_r$ also exhibits a weak equalization effect with a decreased standard deviation, while the population-averaged MFR $\langle\langle f_i^{(X)} \rangle\rangle_r$ shows a non-equalization effect with an increased standard deviation. It is also found that the E-population has high dynamical susceptibility with respect to variations in I to E synaptic inputs, while the dominant I-population has low dynamical susceptibility with respect to variations in E to I synaptic inputs. In contrast to the case without STDP, the E-I ratio balance is broken up, and thus a phase shift between the fast sparsely synchronized rhythms in the I- and the E-populations occurs.

Here, we are concerned about population states (I, E)

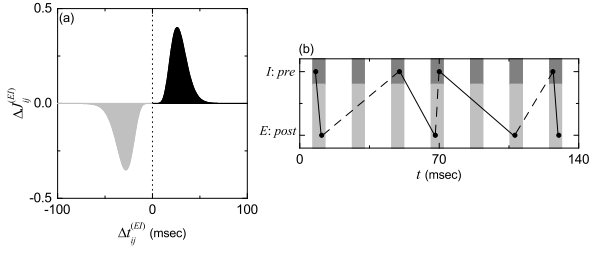


FIG. 6: (a) Time window for the delayed Hebbian I to E iSTDP. Plot of synaptic modification $\Delta J_{ij}^{(EI)}$ versus $\Delta t_{ij}^{(EI)}$ ($= t_i^{(post,E)} - t_j^{(pre,I)}$) for $A_+ = 0.4$, $A_- = 0.35$, $\tau_+ = 2.6$ msec, and $\tau_- = 2.8$ msec. $t_i^{(post,E)}$ and $t_j^{(pre,I)}$ are spiking times of the post-synaptic RS pyramidal cell i in the target E-population and the pre-synaptic FS interneuron j in the source I-population, respectively. (b) Schematic diagram for the nearest-spike pair-based STDP rule. $I : Pre$ and $E : Post$ correspond to a pre-synaptic FS interneuron and a post-synaptic RS pyramidal cell, respectively. Gray and light gray boxes represent I- and E-strips in the raster plot of spikes, respectively, and spikes in the stripes are represented by solid circles. Solid and dashed lines denote iLTP (inhibitory LTP) and iLTD (inhibitory LTD), respectively.

in the I- and the E-populations for $D > D_2^*$ ($\simeq 91$). In the absence of STDP, (FSS, FSS) appears for $D_2^* < D < D_3^*$, while for $D > D_3^*$ ($\simeq 537$) desynchronization occurs together in both the I- and the E-populations [see Fig. 3(a)]. By increasing D from D_2^* , we investigate the effect of I to E iSTDP on population states (I, E) in the I- and the E-populations. The initial synaptic strengths are chosen from the Gaussian distribution with the mean $J_0^{(XY)}$ and the standard deviation σ_0 ($= 5$), where $J_0^{(II)} = 1300$, $J_0^{(EE)} = 300$, $J_0^{(EI)} = 800$, and $J_0^{(IE)} = 487.5$ ($= J_0^{(II)} J_0^{(EE)} / J_0^{(EI)}$). In this initial case, we consider the E-I ratio balance (i.e., the ratio of average excitatory to inhibitory synaptic strengths is the same in both FS interneurons and RS pyramidal cells). Here, we consider just the interpopulation I to E iSTDP. Hence, intrapopulation (I to I and E to E) synaptic strengths and interpopulation E to I synaptic strengths are static. Just synaptic strength $J_{ij}^{(EI)}$ for each interpopulation I to E synapse is updated according to a nearest-spike pair-based STDP rule in Eq. (12).

Figure 6(a) shows a time-delayed Hebbian time window for the synaptic modification $\Delta J_{ij}^{(EI)}(\Delta t_{ij}^{(EI)})$ of Eq. (13) [60, 100, 101]. As in the E to E Hebbian time window [49–56], LTP occurs in the black region for $\Delta t_{ij}^{(EI)} > 0$, while LTD takes place in the gray region for $\Delta t_{ij}^{(EI)} < 0$. However, unlike the E to E Hebbian time window, $\Delta J_{ij}^{(EI)} \sim 0$ near $\Delta t_{ij}^{(EI)} \sim 0$, and delayed maximum and minimum for $\Delta J_{ij}^{(EI)}$ appear at $\Delta t_{ij}^{(EI)} = \beta\tau_+$ and $-\beta\tau_-$, respectively.

$\Delta J_{ij}^{(EI)}(\Delta t_{ij}^{(EI)})$ varies depending on the relative time difference $\Delta t_{ij}^{(EI)}$ ($= t_i^{(post,E)} - t_j^{(pre,I)}$) between the near-

est spike times of the post-synaptic RS pyramidal cell i and the pre-synaptic FS interneuron j . When a post-synaptic spike follows a pre-synaptic spike (i.e., $\Delta t_{ij}^{(EI)}$ is positive), inhibitory LTP (iLTP) of I to E synaptic strength appears; otherwise (i.e., $\Delta t_{ij}^{(EI)}$ is negative), inhibitory LTD (iLTD) occurs. A schematic diagram for the nearest-spike pair-based STDP rule is given in Fig. 6(b), where $I : Pre$ and $E : Post$ correspond to a pre-synaptic FS interneuron and a post-synaptic RS pyramidal cell, respectively. Here, gray and light gray boxes represent I- and E-strips in the raster plot of spikes, respectively, and spikes in the stripes are denoted by solid circles.

When the post-synaptic RS pyramidal cell ($E : Post$) fires a spike, iLTP (represented by solid lines) occurs via I to E iSTDP between the post-synaptic spike and the previous nearest pre-synaptic spike of the FS interneuron ($I : Pre$). In contrast, when the pre-synaptic FS interneuron ($I : Pre$) fires a spike, iLTD (denoted by dashed lines) occurs through I to E iSTDP between the pre-synaptic spike and the previous nearest post-synaptic spike of the RS pyramidal cell ($E : Post$). In the case of FSS, individual neurons make stochastic phase lockings (i.e., they make intermittent spikings phase-locked to the IPSR at random multiples of its global period). As a result of stochastic phase lockings (leading to stochastic spike skippings), nearest-neighboring pre- and post-synaptic spikes may appear in any two separate stripes (e.g., nearest-neighboring, next-nearest-neighboring or farther-separated stripes), as well as in the same stripe, in contrast to the case of full synchronization where they appear in the same or just in the nearest-neighboring stripes [compare Fig. 6(b) with Fig. 4(b) (corresponding to the case of full synchronization) in [61]]. For simplicity, only the cases, corresponding to the same, the nearest-neighboring, and the next-nearest-neighboring stripes, are shown in Fig. 6(b).

Figure 7(a) shows time-evolutions of population-averaged (I to E) synaptic strengths $\langle J_{ij}^{(EI)} \rangle$ for various values of D ; $\langle \dots \rangle$ denotes an average over all synapses. In each case of intermediate values of $D = 110, 250$, and 400 , $\langle J_{ij}^{(EI)} \rangle$ increases monotonically above its initial value $J_0^{(EI)}$ ($= 800$), and eventually it approaches a saturated limit value $\langle J_{ij}^{(EI)*} \rangle$ nearly at $t = 1500$ sec. As a result, iLTP occurs for these values of D . In contrast, for small and large values of $D = 95, 500$, and 600 , $\langle J_{ij}^{(EI)} \rangle$ decreases monotonically below $J_0^{(EI)}$, and approaches a saturated limit value $\langle J_{ij}^{(EI)*} \rangle$. Consequently, iLTD occurs in the cases of $D = 95, 500$ and 600 . Figure 7(b1) shows a bell-shaped plot of population-averaged limit values $\langle \langle J_{ij}^{(EI)*} \rangle \rangle_r$ of (I to E) synaptic strengths (open circles) versus D , where $J_{ij}^{(EI)*}$ are saturated limit values of $J_{ij}^{(EI)}$. Here, the horizontal dotted line denotes the initial average value of (I to E)

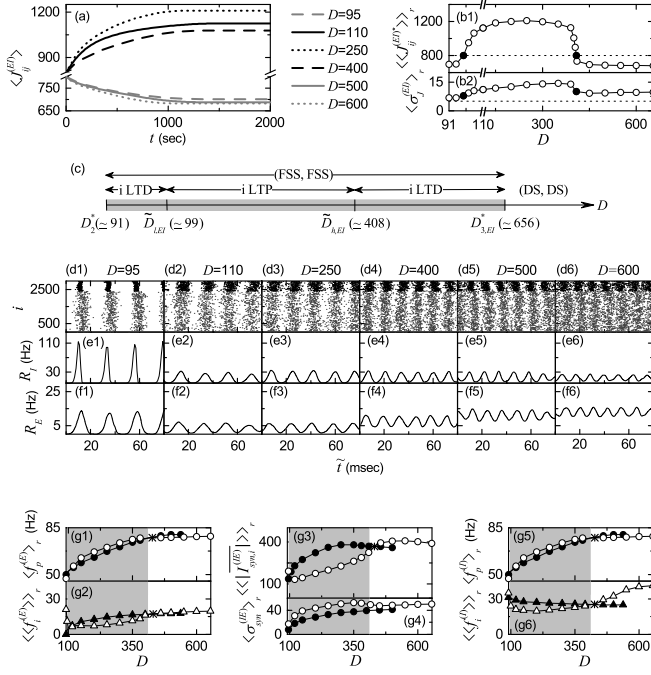


FIG. 7: Effects of I to E iSTDP on population states. (a) Time-evolutions of population-averaged synaptic strengths $\langle J_{ij}^{(EI)} \rangle$ for various values of D . (b1) Plot of population-averaged limit values $\langle \langle J_{ij}^{(EI)*} \rangle \rangle_r$ of synaptic strengths versus D . (b2) Plot of standard deviations $\langle \sigma_J^{(EI)} \rangle_r$ versus D . (c) Bar diagram for the population states (I, E) in the I- and E-populations. Raster plots of spikes in (d1)-(d6) and IPSRs $R_I(t)$ in (e1)-(e6) and $R_E(t)$ in (f1)-(f6) for various values of D after the saturation time t^* , where $t = t^* + \tilde{t}$ (saturation time = 1500 sec). Plots of (g1) the population frequency $\langle f_p^{(E)} \rangle$ (open circles) and (g2) the population-averaged MFR of RS pyramidal cells $\langle \langle f_i^{(E)} \rangle \rangle_r$ (open triangles) versus D in the E-populations; those in the absence of STDP are denoted by solid circles and triangles, respectively. Plots of (g3) population average $\langle \langle |I_{syn,i}^{(IE)}| \rangle \rangle_r$ (open circles) and (g4) standard deviation $\langle \sigma_{syn}^{(IE)} \rangle_r$ (open circles) for time-averaged strengths $\{I_{syn,i}^{(IE)}\}$ of individual E to I synaptic currents; those in the absence of STDP are represented by solid circles. Plots of (g5) the population frequency $\langle f_p^{(I)} \rangle$ (open circles) and (g6) the population-averaged MFR of FS interneurons $\langle \langle f_i^{(I)} \rangle \rangle_r$ (open triangles) versus D in the I-populations; those in the absence of STDP are denoted by solid circles and triangles.

synaptic strengths $J_0^{(EI)}$ ($= 800$), and the lower and the higher thresholds, $\tilde{D}_{l,EI}$ ($\simeq 99$) and $\tilde{D}_{h,EI}$ ($\simeq 408$), for iLTP/iLTD (where $\langle \langle J_{ij}^{(EI)*} \rangle \rangle_r = J_0^{(EI)}$) are denoted by solid circles. Thus, in a broad region of intermediate D ($\tilde{D}_{l,EI} < D < \tilde{D}_{h,EI}$), iLTP occurs, while iLTD takes place in the other two (separate) regions of small and large D ($D < \tilde{D}_{l,EI}$ and $D > \tilde{D}_{h,EI}$). Figure 7(b2) also shows a plot of standard deviations $\langle \sigma_J^{(EI)} \rangle_r$ (from the population-averaged limit values) versus D . All the values of $\langle \sigma_J^{(EI)} \rangle_r$ are larger than the initial value σ_0 ($= 5$),

independently of D .

A bar diagram for the population states (I, E) in the I- and the E-populations is shown in Fig. 7(c). We note that (FSS, FSS) appears in a widened range of D [$D_2^* (\simeq 91) < D < D_{3,EI}^* (\simeq 656)$], in comparison with the case without STDP where (FSS, FSS) occurs for $D_2^* < D < D_3^* (\simeq 537)$ [see Fig. 3(a)]. Desynchronized states for $D_3^* < D < D_{3,EI}^*$ in the absence of STDP are transformed into (FSS, FSS) via iLTD in the presence of I to E iSTDP, and thus the region of (FSS, FSS) is widened.

The effects of iLTP and iLTD on population states after the saturation time ($t^* = 1500$ sec) may be well seen in the raster plot of spikes and the corresponding IPSRs $R_I(t)$ and $R_E(t)$. Figures 7(d1)-7(d6), Figures 7(e1)-7(e6), and Figures 7(f1)-7(f6) show raster plots of spikes, the IPSRs $R_I(t)$, and the IPSRs $R_E(t)$ for various values of D , respectively. When compared with Figs. 3(b4)-3(b6), Figs. 3(c4)-3(c6), and Figs. 3(d4)-3(d6) in the absence of STDP, the degrees of (FSS, FSS) in the case of iLTP ($D = 110, 250$, and 400) are decreased (i.e., the amplitudes of $R_I(t)$ and $R_E(t)$ are decreased) due to increased I to E synaptic inhibition. On the other hand, in the case of iLTD for $D = 95$ and 500 , the degrees of (FSS, FSS) are increased (i.e., the amplitudes of $R_I(t)$ and $R_E(t)$ are increased) due to decreased I to E synaptic inhibition [compare the corresponding raster plots, $R_I(t)$, and $R_E(t)$ for $D = 95$ and 500 in Figs. 3 and 7]. Particularly, the desynchronized state for $D = 600$ in the absence of STDP [see Figs. 3(b8), 3(c8), and 3(d8)] is transformed into (FSS, FSS) [see Figs. 7(d6), 7(e6), and 7(f6)] via iLTD. Here, we note that the degree of FSS in the I-(E-)population tends to be nearly the same (i.e., the amplitudes of $R_I(t)$ [$R_E(t)$] for $D = 110, 250, 400, 500$, and 600 are nearly the same) in a wide range of $\tilde{D}_{l,EI} < D < \tilde{D}_{3,EI}^*$, except for the narrow small- D region ($D_2^* < D < \tilde{D}_{l,EI}$). In such a sense, an equalization effect in the synchronization degree occurs in a wide range of D (including the regions of both intermediate and large D). Quantitative analysis for the synchronization degree and the equalization effect will be made intensively in Fig. 9.

We also study the effect of iLTP and iLTD on population-averaged MFR $\langle \langle f_i^{(E)} \rangle \rangle_r$ and the population frequency $\langle f_p^{(E)} \rangle_r$ in the (target) E-population. Figures 7(g1) and 7(g2) show plots of $\langle f_p^{(E)} \rangle_r$ and $\langle \langle f_i^{(E)} \rangle \rangle_r$ versus D , respectively. In the gray region of iLTP ($\tilde{D}_{l,EI} < D < \tilde{D}_{h,EI}$), the population-averaged MFR $\langle \langle f_i^{(E)} \rangle \rangle_r$ (open triangles) are lower than those (solid triangles) in the absence of STDP, due to increased synaptic inhibition $\langle \langle J_{ij}^{(EI)*} \rangle \rangle_r$. As a result of decreased $\langle \langle f_i^{(E)} \rangle \rangle_r$, the population frequency $\langle f_p^{(E)} \rangle_r$ (open circles) becomes higher than that (solid circles) in the absence of STDP. In contrast, in most cases of iLTD (except for a narrow region near the higher threshold $\tilde{D}_{h,EI}$), the population-averaged MFRs $\langle \langle f_i^{(E)} \rangle \rangle_r$ (open triangles) are higher

than those (solid triangles) in the absence of STDP, because of decreased synaptic inhibition $\langle\langle J_{ij}^{(EI)*} \rangle\rangle_r$. Due to increased $\langle\langle f_i^{(E)} \rangle\rangle_r$, the population frequency $\langle f_p^{(E)} \rangle_r$ (open circles) becomes lower than that (solid circles) in the absence of STDP. In the (exceptional) narrow region of iLTD near the higher threshold $[\tilde{D}_{h,EI} \leq D < D_{cr}^* (\simeq 430) (D_{cr}^*: \text{denoted by stars})]$, the overall effect of standard deviation $\langle\sigma_J^{(EI)} \rangle_r$ (decreasing $\langle\langle f_i^{(E)} \rangle\rangle_r$) is found to be dominant in comparison with the effect of iLTD (increasing $\langle\langle f_i^{(E)} \rangle\rangle_r$), and hence $\langle\langle f_i^{(E)} \rangle\rangle_r$ (open triangles) are lower than those (solid triangles) in the absence of STDP, like the case of iLTP (in the gray region of intermediate D). In this way, the E-population seems to have high dynamical susceptibility against variations (i.e., $\langle\sigma_J^{(EI)} \rangle_r$) in I to E synaptic strengths $\{J_{ij}^{(EI)*}\}$. As a result of decrease in $\langle\langle f_i^{(E)} \rangle\rangle_r$, in this region of D , the population frequency $\langle f_p^{(E)} \rangle_r$ (open circle) becomes higher than that (solid circles) in the absence of STDP. After passing the crossing point D_{cr}^* (denoted by a star), the effect of iLTD (increasing $\langle\langle f_i^{(E)} \rangle\rangle_r$) becomes dominant, as in the usual case of iLTD.

In a wide range of $\tilde{D}_{l,EI} < D < D_{3,EI}^*$ (including the regions of both intermediate and large D), a weak equalization effect is found to occur in the population frequency $\langle f_p^{(E)} \rangle_r$. In the absence of STDP, $\langle f_p^{(E)} \rangle_r$ (solid circles) increases monotonically with increasing D . The lower population frequencies $\langle f_p^{(E)} \rangle_r$ (solid circles) in the absence of STDP are increased to higher values (open circles) in the gray region of iLTP ($\tilde{D}_{l,EI} < D < \tilde{D}_{h,EI}$), while in most cases of iLTD for large D , the higher population frequencies (solid circles) $\langle f_p^{(E)} \rangle_r$ in the absence of STDP are decreased to lower values (open circles). Thus, the standard deviation in the distribution of $\langle f_p^{(E)} \rangle_r$ in the presence of I to E iSTDP becomes decreased, in comparison to that in the absence of STDP [see Fig. 7(g1)]. Such decrease in the standard deviation may be regarded as occurrence of a weak equalization effect in $\langle f_p^{(E)} \rangle_r$, which is in contrast to the case of strong equalization effect in the synchronization degree where amplitudes of $R_I(t)$ [$R_E(t)$] are nearly the same in a wide range of D in the I-(E-)population. Particularly, the values of $\langle f_p^{(E)} \rangle_r$ for $D > 350$ seem to be nearly the same.

In contrast to weak equalization effect in $\langle f_p^{(E)} \rangle_r$, a non-equalization effect is found to occur in the population-averaged MFR $\langle\langle f_i^{(E)} \rangle\rangle_r$ in the wide region of $\tilde{D}_{l,EI} < D < D_{3,EI}^*$. In the absence of STDP, $\langle\langle f_i^{(E)} \rangle\rangle_r$ (solid triangles) increases monotonically with increasing D , as in the case of $\langle f_p^{(E)} \rangle_r$. However, behaviors of $\langle\langle f_i^{(E)} \rangle\rangle_r$ (open triangles) in the presence of I to E iSTDP are different from those of $\langle f_p^{(E)} \rangle_r$ (open circles). In the gray region of iLTP ($\tilde{D}_{l,EI} < D < \tilde{D}_{h,EI}$), the lower population-averaged MFRs $\langle\langle f_i^{(E)} \rangle\rangle_r$ (solid triangles) in the absence of STDP are decreased to lower values (open

triangles), while for most cases of iLTD for large D , the higher population-averaged MFRs $\langle\langle f_i^{(E)} \rangle\rangle_r$ (solid triangles) in the absence of STDP are increased to higher values (open triangles). Thus, the standard deviation in the distribution of $\langle\langle f_i^{(E)} \rangle\rangle_r$ in the presence of I to E iSTDP becomes increased, in comparison to that in the absence of STDP [see Fig. 7(g2)]. Such increase in the standard deviation may be regarded as occurrence of a non-equalization effect in $\langle\langle f_i^{(E)} \rangle\rangle_r$.

Figures 7(g3) and 7(g4) show plots of population average $\langle\langle |I_{syn,i}^{(IE)}| \rangle\rangle_r$ (open circles) and standard deviation $\langle\sigma_{syn}^{(IE)} \rangle_r$ (from the population average) (open circles) for time-averaged strengths $\{|I_{syn,i}^{(IE)}|\}$ of individual E to I synaptic currents, respectively. Here, the excitatory synaptic current $I_{syn,i}^{(IE)}$ is negative, and then the excitatory synaptic input $(-I_{syn,i}^{(IE)})$ in the last term of Eq. (1) becomes positive. We take the absolute value of $I_{syn,i}^{(IE)}$ as its magnitude (i.e., strength). For comparison, $\langle\langle |I_{syn,i}^{(IE)}| \rangle\rangle_r$ and $\langle\sigma_{syn}^{(IE)} \rangle_r$ in the absence of STDP are also represented by solid circles. We note that MFRs of RS pyramidal cells in the E-population affect individual E to I synaptic currents $I_{syn,i}^{(IE)}$ so much [see Eqs. (9) and (10)]. Hence, the population average $\langle\langle |I_{syn,i}^{(IE)}| \rangle\rangle_r$ has a strong correlation with the population-averaged MFR $\langle\langle f_i^{(E)} \rangle\rangle_r$ of RS pyramidal cells [i.e., their Pearson's correlation coefficient r is so large; $r \simeq 0.92$ (0.94) in the presence (absence) of I to E iSTDP]. Here, the Pearson's correlation coefficient r is a measure of the strength and direction of the linear relationship between two variables that is defined as the covariance of the two variables divided by the product of their standard deviations [114]. Thus, in the gray region of iLTP ($\tilde{D}_{l,EI} < D < \tilde{D}_{h,EI}$), the population-average values of $\langle\langle |I_{syn,i}^{(IE)}| \rangle\rangle_r$ (open circles) are lower than those (solid circles) in the absence of STDP, mainly due to decrease in $\langle\langle f_i^{(E)} \rangle\rangle_r$. On the other hand, in most cases of iLTD (except for a narrow region near the higher threshold $\tilde{D}_{h,EI}$), the population averages $\langle\langle |I_{syn,i}^{(IE)}| \rangle\rangle_r$ (open circles) are higher than those (solid circles) in the absence of STDP, mainly because of increase in $\langle\langle f_i^{(E)} \rangle\rangle_r$. In the (exceptional) narrow region of iLTD near the higher threshold $[\tilde{D}_{h,EI} \leq D < D_{cr}^* (\simeq 430) (D_{cr}^*: \text{denoted by a star})]$, the population-average values of $\langle\langle |I_{syn,i}^{(IE)}| \rangle\rangle_r$ (open circles) are lower than those (solid circles) in the absence of STDP, mainly due to decrease in $\langle\langle f_i^{(E)} \rangle\rangle_r$, as in the gray region of iLTP ($\tilde{D}_{l,EI} < D < \tilde{D}_{h,EI}$). Like the case of $\langle\langle f_i^{(E)} \rangle\rangle_r$, the standard deviation in the distribution of $\langle\langle |I_{syn,i}^{(IE)}| \rangle\rangle_r$ (open circles) in the presence of I to E iSTDP is increased, in comparison to that (solid circles) in the absence of STDP [see Fig. 7(g3)]. Hence,

a non-equalization effect occurs in $\langle \langle |I_{syn,i}^{(IE)}| \rangle \rangle_r$. In addition to $\langle \langle |I_{syn,i}^{(IE)}| \rangle \rangle_r$, Fig. 7(g4) shows a plot of standard deviations $\langle \sigma_{syn}^{(IE)} \rangle_r$ (from the population-average values) versus D . All the values of $\langle \sigma_{syn}^{(IE)} \rangle_r$ are larger than the initial values, independently of D .

We now study the effect of population average $\langle \langle |I_{syn,i}^{(IE)}| \rangle \rangle_r$ for time-averaged strengths of individual E to I synaptic currents on population-averaged MFR $\langle \langle f_i^{(I)} \rangle \rangle_r$ and the population frequency $\langle f_p^{(I)} \rangle_r$ in the I-population. Figures 7(g5) and 7(g6) show plots of $\langle f_p^{(I)} \rangle_r$ and $\langle \langle f_i^{(I)} \rangle \rangle_r$ versus D , respectively. In the gray region of iLTP ($\tilde{D}_{l,EI} < D < \tilde{D}_{h,EI}$), the population-averaged MFR $\langle \langle f_i^{(I)} \rangle \rangle_r$ (open triangles) are lower than those (solid triangles) in the absence of STDP, due to decrease in E to I synaptic excitation $\langle \langle |I_{syn,i}^{(IE)}| \rangle \rangle_r$. As a result of decreased $\langle \langle f_i^{(I)} \rangle \rangle_r$, the population frequency $\langle f_p^{(I)} \rangle_r$ (open circle) becomes higher than that (solid circles) in the absence of STDP. On the other hand, in most cases of iLTD for large D (except for a narrow region near the higher threshold $\tilde{D}_{h,EI}$), the population-averaged MFRs $\langle \langle f_i^{(I)} \rangle \rangle_r$ (open triangles) become higher than those (solid triangles) in the absence of STDP, due to increase in E to I synaptic excitation $\langle \langle |I_{syn,i}^{(IE)}| \rangle \rangle_r$. Because of increase in $\langle \langle f_i^{(I)} \rangle \rangle_r$, the population frequency $\langle f_p^{(I)} \rangle_r$ (open circle) becomes lower than that (solid circles) in the absence of STDP. In the (exceptional) narrow region of iLTD near the higher threshold [$\tilde{D}_{h,EI} \leq D < D_{cr}^*$ ($\simeq 430$) (D_{cr}^* : denoted by a star), population-averaged MFRs $\langle \langle f_i^{(I)} \rangle \rangle_r$ (open triangles) are lower than those (solid triangles) in the absence of STDP, due to decrease in E to I synaptic excitation $\langle \langle |I_{syn,i}^{(IE)}| \rangle \rangle_r$, as in the case of iLTP (in the gray region of intermediate D). As a result, in this region of D , the population frequency $\langle f_p^{(I)} \rangle_r$ (open circle) becomes higher than that (solid circles) in the absence of STDP.

As mentioned in the above subsection, the population frequency in our coupled two-population system is determined by the dominant I-population, and hence the population frequencies $\langle f_p^{(I)} \rangle_r$ and $\langle f_p^{(E)} \rangle_r$ are the same. Consequently, like the case of $\langle f_p^{(E)} \rangle_r$, a weak equalization effect in $\langle f_p^{(I)} \rangle_r$ occurs due to decrease in the standard deviation in the distribution of population frequencies $\langle f_p^{(I)} \rangle_r$. On the other hand, a non-equalization effect takes place in population-averaged MFR $\langle \langle f_i^{(I)} \rangle \rangle_r$ because of increase in the standard deviation in the distribution of population-averaged MFRs $\langle \langle f_i^{(I)} \rangle \rangle_r$ [see Fig. 7(g6)]. Although non-equalization effects occur in both $\langle \langle f_i^{(I)} \rangle \rangle_r$ and $\langle \langle f_i^{(E)} \rangle \rangle_r$, the ways for increase in the standard deviations in their distributions are different. In the I-population, $\langle \langle f_i^{(I)} \rangle \rangle_r$ decreases with increasing D in the absence of STDP, unlike the case of $\langle \langle f_i^{(E)} \rangle \rangle_r$ (which

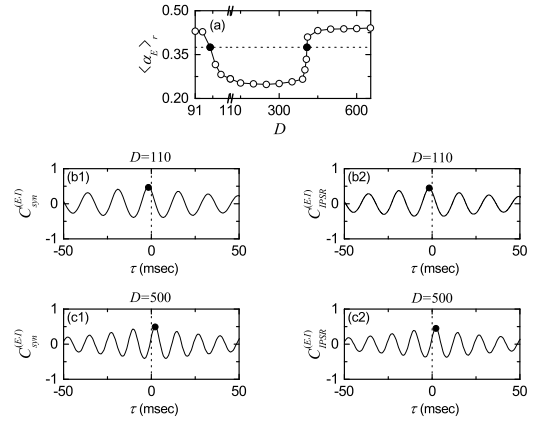


FIG. 8: Break-up of E-I ratio balance in the presence of I to E iSTDP. (a) Plot of the E-I ratio $\langle \alpha_E \rangle_r$ ($= J_0^{(EE)} / \langle \langle J_{ij}^{(EI)} \rangle \rangle_r$) versus D . Horizontal dotted line denotes the E-I ratio α_E ($= 0.375$) in the absence of I to E iSTDP. Cross-correlation functions between total synaptic input currents $I_{syn}^{(E)}(t)$ and $I_{syn}^{(I)}(t)$ for $D =$ (b1) 110 (iLTP) and (c1) 500 (iLTD). Cross-correlation functions between IPSRs $R_E(t)$ and $R_I(t)$ for $D =$ (b2) 110 (iLTP) and (c2) 500 (iLTD). Solid circles represent the maxima of the cross-correlation functions.

is an increasing function of D). In this case, in the gray region of iLTP ($\tilde{D}_{l,EI} < D < \tilde{D}_{h,EI}$), higher population-averaged MFRs $\langle \langle f_i^{(I)} \rangle \rangle_r$ (solid triangles) in the absence of STDP are decreased much, while in most cases of iLTD for large D lower population-averaged MFRs $\langle \langle f_i^{(I)} \rangle \rangle_r$ (solid triangles) in the absence of STDP are increased so much. In this way, higher (lower) population-averaged MFRs $\langle \langle f_i^{(I)} \rangle \rangle_r$ in the absence of STDP are transformed into lower (higher) ones in the presence of I to E iSTDP. Thus, the standard deviation in distribution of $\langle \langle f_i^{(I)} \rangle \rangle_r$ becomes increased in a different way for the case of E-population. We also note that effects of time-averaged strengths of individual E to I synaptic input currents on the I-population are given mainly by their population average $\langle \langle |I_{syn,i}^{(IE)}| \rangle \rangle_r$ in Fig. 7(g3); effects of standard deviation $\langle \sigma_{syn}^{(IE)} \rangle_r$ in Fig. 7(g4) may be neglected in comparison with those of $\langle \langle |I_{syn,i}^{(IE)}| \rangle \rangle_r$. Hence, the I-population seems to have low dynamical susceptibility against variations ($\langle \sigma_{syn}^{(IE)} \rangle_r$) in time-averaged strengths in the E to I synaptic currents.

We study the effect of I to E iSTDP on the E-I ratio and the phase shift between fast synchronized rhythms in the I- and the E-populations. In the absence of STDP, there exists an E-I ratio balance between the E- and the I-populations such that $\alpha_E (= \langle J_{ij}^{(EE)} \rangle / \langle J_{ij}^{(EI)} \rangle) = \alpha_I (= \langle J_{ij}^{(IE)} \rangle / \langle J_{ij}^{(II)} \rangle) = 0.375$, where the two fast sparsely synchronized rhythms in both the E- and the I-populations are in-phase, as shown in Fig. 3. In the presence of I to E iSTDP, α_E in the (target) E-population changes, while no change in α_I in the (source)

I-population occurs. Thus, break-up of the E-I ratio balance occurs, in contrast to the case without STDP. Figure 8(a) shows a well-shaped plot of the E-I ratio $\langle \alpha_E \rangle_r$ ($= J_0^{(EE)} / \langle J_{ij}^{(EI)} \rangle_r$; $J_0^{(EE)} = 300$) versus D in the presence of I to E iSTDP. In the region of intermediate D [$\tilde{D}_{l,EI} (\simeq 99) < D < \tilde{D}_{h,EI} (\simeq 408)$] where iLTP occurs, $\langle \alpha_E \rangle_r$ is decreased below the value ($=0.375$) in the absence of STDP, denoted by the horizontal dotted line, due to increase in I to E synaptic inhibition. Hence, in this region, the values of $\langle \alpha_E \rangle_r$ become smaller than those of $\langle \alpha_I \rangle_r$. On the other hand, in the other two separate regions of small and large D [$D_2^* (\simeq 91) < D < \tilde{D}_{l,EI}$ and $\tilde{D}_{h,EI} < D < D_{3,EI}^* (\simeq 656)$] where iLTD takes place, $\langle \alpha_E \rangle_r$ is increased above the value ($=0.375$) in the absence of STDP, because of decrease in I to E synaptic inhibition. In these two regions, the values of $\langle \alpha_E \rangle_r$ are larger than those of $\langle \alpha_I \rangle_r$.

Due to break-up of the E-I ratio balance, phase shifts between fast sparsely synchronized rhythms in the E- and the I-populations occur. As an example of iLTP, we consider the case of $D = 110$ with $\langle \alpha_E \rangle_r = 0.267$. Figure 8(b1) shows the cross-correlation function $C_{syn}^{(E,I)}(\tau)$ of Eq. (19) between the population-averaged total synaptic input currents $I_{syn}^{(E)}(t)$ and $I_{syn}^{(I)}(t)$ into the E- and the I-populations. The main peak appears at $\tau^* = -1.7$ msec, in contrast to the case without STDP where $\tau^* = 0$ [see Fig. 3(f1)]. Thus, $I_{syn}^{(E)}(t)$ shows a phase advance of 36.6° ahead of $I_{syn}^{(I)}(t)$. Consequently, the cross-correlation function $C_{IPSR}^{(E,I)}(\tau)$ of Eq. (21) between the IPSR outputs $R_E(t)$ and $R_I(t)$ also has the main peak at $\tau = -1.7$ msec, as shown in Fig. 8(b2). This phase advance of the E-population rhythm may be well seen in Figs. 7(d2), 7(e2), and 7(f2). The gray E-stripes in the raster plot of spikes are phase-advanced with respect to the black I-stripes, and $R_E(t)$ also makes phase-advanced oscillations with respect to $R_I(t)$. These phase-advanced behaviors for $\langle \alpha_E \rangle_r < \langle \alpha_I \rangle_r$ in the case of iLTP are in contrast to the in-phase behaviors in the absence of STDP where $\langle \alpha_E \rangle_r = \langle \alpha_I \rangle_r$.

We also consider another case of $D = 500$ where iLTD occurs. In this case, $\langle \alpha_E \rangle_r = 0.437$. Figure 8(c1) shows the cross-correlation function $C_{syn}^{(E,I)}(\tau)$ between $I_{syn}^{(E)}(t)$ and $I_{syn}^{(I)}(t)$. The main peak appears at $\tau^* = 2.1$ msec, in contrast to the above case of iLTP. Hence, $I_{syn}^{(E)}(t)$ shows a phase lag of -58.2° behind $I_{syn}^{(I)}(t)$. As a result, the cross-correlation function $C_{IPSR}^{(E,I)}(\tau)$ between $R_E(t)$ and $R_I(t)$ also has the main peak at $\tau = 2.1$ msec [see Fig. 8(c2)]. This phase lag of the E-population rhythm may be well seen in Figs. 7(d5), 7(e5), and 7(f5). The gray E-stripes in the raster plot of spikes are phase-delayed with respect to the black I-stripes, and $R_E(t)$ also makes phase-delayed oscillations with respect to $R_I(t)$. These phase-delayed behaviors for $\langle \alpha_E \rangle_r > \langle \alpha_I \rangle_r$ in the case of iLTD are in contrast to the phase-advanced behaviors for $\langle \alpha_E \rangle_r < \langle \alpha_I \rangle_r$ in the case of iLTP.

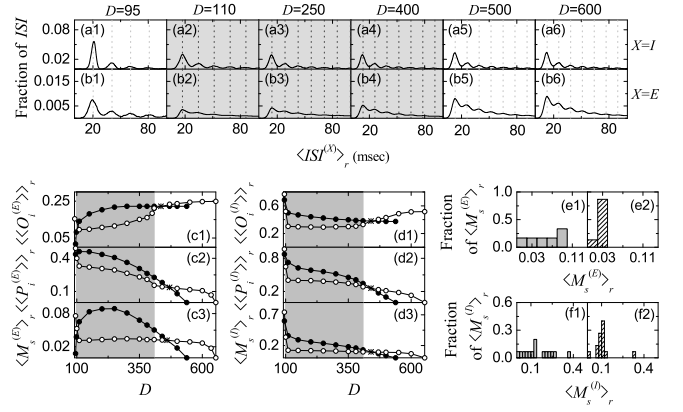


FIG. 9: Characterization of individual and population behaviors for (FSS, FSS) after the saturation time ($t^* = 1500$ sec) in the presence of I to E iSTDP. ISI histograms for various values of D in the (a1)-(a6) I- and (b1)-(b6) E-populations. Vertical dotted lines represent multiples of the global period $T_G^{(X)}$ of the IPSR $R_X(t)$ ($X = I$ and E). Plots of (c1) the average occupation degree $\langle \langle O_i^{(E)} \rangle \rangle_r$ (open circles), (c2) the average pacing degree $\langle \langle P_i^{(E)} \rangle \rangle_r$ (open circles), and (c3) the statistical-mechanical spiking measure $\langle M_s^{(E)} \rangle_r$ (open circles) versus D in the E-population. Plots of (d1) the average occupation degree $\langle \langle O_i^{(I)} \rangle \rangle_r$ (open circles), (d2) the average pacing degree $\langle \langle P_i^{(I)} \rangle \rangle_r$ (open circles), and (d3) the statistical-mechanical spiking measure $\langle M_s^{(I)} \rangle_r$ (open circles) versus D in the I-population. For comparison, $\langle \langle O_i^{(X)} \rangle \rangle_r$, $\langle \langle P_i^{(X)} \rangle \rangle_r$, and $\langle M_s^{(X)} \rangle_r$ ($X = E$ and I) in the absence of STDP are also denoted by solid circles. In (a2)-(a4), (b2)-(b4), (c1)-(c3) and (d1)-(d3), iLTP occurs in the intermediate gray-shaded regions. Histograms for distribution of statistical-mechanical spiking measures $\langle M_s^{(E)} \rangle_r$ in the E-population in the (e1) absence and the (e2) presence of I to E iSTDP. Histograms for distribution of statistical-mechanical spiking measures $\langle M_s^{(I)} \rangle_r$ in the I-population in the (f1) absence and the (f2) presence of I to E iSTDP.

In the range of $D_2^* (\simeq 91) < D < D_{3,EI}^* (\simeq 656)$, we characterize individual and population behaviors for (FSS, FSS) in both the I- and the E-populations. We first characterize individual spiking behaviors of FS interneurons and RS pyramidal cells in terms of ISIs. Figures 9(a1)-9(a6) [Figures 9(b1)-9(b6)] show ISI histograms for various values of D in the case of FSS in the I-(E)-population. Because of stochastic spike skipings, multiple peaks appear at integer multiples of the global period $T_G^{(X)}$ of $R_X(t)$ ($X = I$ or E), as in the case of FSS in the absence of STDP (see Fig. 5). For $D = 110, 250$, and 400 in the case of iLTP, ISI histograms are shaded in gray color. In these gray-shaded histograms, when compared with those in the absence of STDP (see the corresponding figures in Fig. 5), the 1st-order main peaks become lowered and broadened, higher-order peaks also become wider, and thus tendencies for merging between multiple peaks are more enhanced. Hence, in comparison with those in the case without STDP, the aver-

age ISIs $\langle\langle ISI^{(X)} \rangle\rangle_r$ ($X = I$ or E) are increased [i.e., $\langle\langle f_i^{(X)} \rangle\rangle_r$ is decreased, as shown in Figs. 7(g2) and 7(g6)] because of the developed tail part, and spiking stripes in the raster plots in Fig. 7 become more smeared (i.e., the average pacing degrees $\langle\langle P_i^{(X)} \rangle\rangle_r$ of spikes in the stripes are decreased [see Figs. 9(c2) and 9(d2)]) due to enhanced merging between peaks. In contrast to the case of iLTP, ISI histograms in the case of iLTD for $D = 95, 500$, and 600 have much more clear peaks in comparison with those in the absence of STDP. Particularly, for $D = 600$, the single-peaked ISI histograms in the absence of STDP are transformed into the multiple-peaked histograms because desynchronization in the case without STDP is developed into FSS in the presence of I to E iSTDP. Thus, in comparison with those in the absence of STDP, the average ISI $\langle\langle ISI^{(X)} \rangle\rangle_r$ ($X = I$ or E) are decreased [i.e., $\langle\langle f_i^{(X)} \rangle\rangle_r$ is increased, as shown in Figs. 7(g2) and 7(g6)], due to enhanced lower-order peaks, and spiking stripes in the raster plots in Fig. 7 become less smeared (i.e., the average pacing degrees $\langle\langle P_i^{(X)} \rangle\rangle_r$ of spikes in the stripes are increased [see Figs. 9(c2) and 9(d2)]) due to appearance of clear peaks.

We also characterize population behaviors for (FSS, FSS) in both the E- and the I-populations by employing the average occupation degree $\langle\langle O_i^{(X)} \rangle\rangle_r$, the average pacing degrees $\langle\langle P_i^{(X)} \rangle\rangle_r$, and the statistical-mechanical spiking measure $\langle M_s^{(X)} \rangle_r$ ($X = E$ or I). As shown in Eqs. (26), (27), and (28), $\langle\langle O_i^{(X)} \rangle\rangle_r$ represents average density of spikes in the stripes in the raster plot, $\langle\langle P_i^{(X)} \rangle\rangle_r$ denotes average phase coherence of spikes in the stripes, and $\langle M_s^{(X)} \rangle_r$ (given by a product of occupation and pacing degrees) represents overall degree of population synchronization. In the case of $\langle\langle O_i^{(X)} \rangle\rangle_r$, the average occupation degree is mainly determined by population-averaged MFRs $\langle\langle f_i^{(X)} \rangle\rangle_r$, and hence they have strong correlations with the Pearson's correlation coefficients $r \simeq 1.0$.

We first consider the case of the (target) E-population for the I to E iSTDP. Figures 9(c1)-9(c3) show plots of $\langle\langle O_i^{(E)} \rangle\rangle_r$, $\langle\langle P_i^{(E)} \rangle\rangle_r$, and $\langle M_s^{(E)} \rangle_r$ in the E-population, respectively. In the gray region of iLTP ($\tilde{D}_{l,EI} < D < \tilde{D}_{h,EI}$), the average occupation degrees $\langle\langle O_i^{(E)} \rangle\rangle_r$ and the average pacing degrees $\langle\langle P_i^{(E)} \rangle\rangle_r$ (open circles) are lower than those (solid circles) in the absence of STDP, mainly due to increased I to E synaptic inhibition $\langle\langle J_{ij}^{(EI)*} \rangle\rangle_r$. On the other hand, in most cases of iLTD (except for a narrow region near the higher threshold $\tilde{D}_{h,EI}$), $\langle\langle O_i^{(E)} \rangle\rangle_r$ and $\langle\langle P_i^{(E)} \rangle\rangle_r$ (open circles) are higher than those (solid circles) in the absence of STDP, mainly because of decreased I to E synaptic inhibition $\langle\langle J_{ij}^{(EI)*} \rangle\rangle_r$. In the (exceptional) narrow region of iLTD near the higher threshold [$\tilde{D}_{h,EI} \leq D < D_{cr}^*$] [D_{cr}^* (denoted by stars) $\simeq 430$ (470) in the case of $\langle\langle O_i^{(E)} \rangle\rangle_r$

($\langle\langle P_i^{(E)} \rangle\rangle_r$), the overall effect of (increased) standard deviation $\langle\sigma_J^{(EI)} \rangle_r$ (decreasing $\langle\langle O_i^{(E)} \rangle\rangle_r$ and $\langle\langle P_i^{(E)} \rangle\rangle_r$) is found to be dominant in comparison with the effect of iLTD (increasing $\langle\langle O_i^{(E)} \rangle\rangle_r$ and $\langle\langle P_i^{(E)} \rangle\rangle_r$), and hence $\langle\langle O_i^{(E)} \rangle\rangle_r$ and $\langle\langle P_i^{(E)} \rangle\rangle_r$ (open circles) are lower than those (solid circles) in the absence of STDP, as in the case of iLTP (in the gray region of intermediate D). We also note that the effect of standard deviation $\langle\sigma_J^{(EI)} \rangle_r$ on $\langle\langle P_i^{(E)} \rangle\rangle_r$ is stronger than that on $\langle\langle O_i^{(E)} \rangle\rangle_r$ (i.e., the value of D_{cr}^* in the case of $\langle\langle P_i^{(E)} \rangle\rangle_r$ is larger than that for the case of $\langle\langle O_i^{(E)} \rangle\rangle_r$), because the increased standard deviation $\langle\sigma_f^{(E)} \rangle_r$ (resulting from increase in $\langle\sigma_J^{(EI)} \rangle_r$) for the distributions of MFRs of RS pyramidal cells has a strong tendency to decrease $\langle\langle P_i^{(E)} \rangle\rangle_r$. Thus, $\langle\sigma_J^{(EI)} \rangle_r$ have much effects on $\langle\langle O_i^{(E)} \rangle\rangle_r$ and $\langle\langle P_i^{(E)} \rangle\rangle_r$, as well as $\langle\langle f_i^{(E)} \rangle\rangle_r$, because the E-population has a high dynamical susceptibility in response to variations in I to E synaptic strengths.

In a wide region of $\tilde{D}_{l,EI} (\simeq 99) < D < D_{3,EI}^* (\simeq 656)$ (including the regions of both intermediate and large D), $\langle\langle O_i^{(E)} \rangle\rangle_r$ increases with D in a relatively fast way, and exhibits a non-equalization effect, as in the case of $\langle\langle f_i^{(E)} \rangle\rangle_r$, because the standard deviation in the distribution of $\langle\langle O_i^{(E)} \rangle\rangle_r$ (open circles) is increased in comparison with that (solid circles) in the absence of STDP [see Fig. 9(c1)]. On the other hand, $\langle\langle P_i^{(E)} \rangle\rangle_r$ is a relatively slowly-decreasing function of D and shows a weak equalization effect, like the case of $\langle\langle f_p^{(E)} \rangle\rangle_r$, because the standard deviation in the distribution of $\langle\langle P_i^{(E)} \rangle\rangle_r$ (open circles) is decreased in comparison with that (solid circles) in the absence of STDP [see Fig. 9(c2)].

We note that the statistical-mechanical spiking measure $M_s^{(E)}$ is given by a product of the occupation and the pacing degrees which exhibit increasing and decreasing behaviors with increasing D , respectively. In the region of intermediate D (iLTP), the degrees of good synchronization (solid circles) in the absence of STDP become decreased to lower ones (open circles), while in most cases of large D (iLTD) the degrees of bad synchronization (solid circles) in the absence of STDP get increased to higher values (open circles). Through the effects of iLTD, even desynchronized states in the absence of STDP become transformed into sparsely synchronized states in the range of $D_3^* (\simeq 537) < D < D_{3,EI}^* (\simeq 656)$, and hence the region of FSS is so much extended in the presence of I to E iSTDP. In this way, via cooperative interplay between the weak equalization effect in (decreasing) $\langle\langle P_i^{(E)} \rangle\rangle_r$ and the non-equalization effect in (increasing) $\langle\langle O_i^{(E)} \rangle\rangle_r$, strong equalization effect in the spiking measure $\langle M_s^{(E)} \rangle_r$ with much smaller standard deviation is found to occur [i.e., the values of $\langle M_s^{(E)} \rangle_r$ in Fig. 9(c3) are nearly the same in a wide range of D], which is distinctly in contrast to the Matthew (bipolarization) effect

in the intrapopulation (I to I and E to E) STDPs where good (bad) synchronization gets better (worse) [61, 64]. Thus, a bell-shaped curve (composed of solid circles) for $\langle M_s^{(E)} \rangle_r$ in the absence of STDP is transformed into a nearly flat curve in the presence of I to E iSTDP.

This kind of equalization effect may be well seen in the histograms for the distribution of $\langle M_s^{(E)} \rangle_r$. The gray histogram in the absence of STDP is shown in Fig. 9(e1) and the hatched histogram in the presence of I to E iSTDP is given in Fig. 9(e2). The standard deviation ($\simeq 0.009$) from the mean in the hatched histogram is much smaller than that ($\simeq 0.028$) in the gray histogram, and hence strong equalization emerges. Moreover, a dumbing-down effect also occurs because the mean value ($\simeq 0.029$) in the hatched histogram is smaller than that ($\simeq 0.056$) in the gray histogram.

We also characterize population behaviors of FSS in the (source) I-population for the I to E iSTDP. Figures 9(d1)-9(d3) show plots of $\langle \langle O_i^{(I)} \rangle \rangle_r$, $\langle \langle P_i^{(I)} \rangle \rangle_r$, and $\langle M_s^{(I)} \rangle_r$ in the I-population, respectively. In the gray region of iLTP ($\tilde{D}_{l,EI} < D < \tilde{D}_{h,EI}$), the average occupation degrees $\langle \langle O_i^{(I)} \rangle \rangle_r$ and the average pacing degrees $\langle \langle P_i^{(I)} \rangle \rangle_r$ (open circles) become decreased in comparison with those (solid circles) in the absence of STDP, mainly because of decreased E to I synaptic excitation $\langle \langle |I_{syn,i}^{(IE)}| \rangle \rangle_r$ (corresponding to population average for time-averaged strengths of individual E to I synaptic currents) [see Fig. 7(g3)]. On the other hand, in most cases of iLTD (except for a narrow region near the higher threshold $\tilde{D}_{h,EI}$), $\langle \langle O_i^{(I)} \rangle \rangle_r$ and $\langle \langle P_i^{(I)} \rangle \rangle_r$ (open circles) get increased when compared with those (solid circles) in the absence of STDP, mainly due to increased E to I synaptic excitation $\langle \langle |I_{syn,i}^{(IE)}| \rangle \rangle_r$.

In the narrow region of iLTD near the higher threshold ($\tilde{D}_{h,EI} \leq D < D_{cr}^*$) [D_{cr}^* (denoted by open circles) $\simeq 430$], the values of $\langle \langle |I_{syn,i}^{(IE)}| \rangle \rangle_r$ are lower than those in the absence of STDP, due to decrease in $\langle \langle f_i^{(E)} \rangle \rangle_r$, as shown in Figs. 7(g2) and 7(g3). Hence, both $\langle \langle O_i^{(I)} \rangle \rangle_r$ and $\langle \langle P_i^{(I)} \rangle \rangle_r$ (open circles) are also lower than those (solid circles) in the absence of STDP. Like the case of $\langle \langle f_i^{(I)} \rangle \rangle_r$, effects of the standard deviation $\langle \sigma_{syn}^{(IE)} \rangle_r$ in Fig. 7(g4) on $\langle \langle O_i^{(I)} \rangle \rangle_r$ and $\langle \langle P_i^{(I)} \rangle \rangle_r$ are negligibly small, in comparison with effects of the population average $\langle \langle |I_{syn,i}^{(IE)}| \rangle \rangle_r$ in Fig. 7(g3), because the I-population has low dynamical susceptibility in response to variations in time-averaged strengths of E to I synaptic currents.

As in the case of E-population, we are particularly concerned about population behaviors in a wide region of $\tilde{D}_{l,EI} < D < D_{3,EI}^*$. $\langle \langle O_i^{(I)} \rangle \rangle_r$ is an increasing function of D (composed of open circles) with increased standard deviation, in contrast to a slowly-decreasing function (consisting of solid circles) in the absence of STDP [see Fig. 9(d1)]. Hence, as in the case of $\langle \langle O_i^{(E)} \rangle \rangle_r$, $\langle \langle O_i^{(I)} \rangle \rangle_r$

also exhibits a non-equalization effect with larger standard deviation. On the other hand, $\langle \langle P_i^{(I)} \rangle \rangle_r$ is a relatively slowly-decreasing function of D with decreased standard deviation, in comparison with the case without STDP [see Fig. 9(d2)], and shows a weak equalization effect with smaller standard deviation, similar to the case of $\langle \langle P_i^{(E)} \rangle \rangle_r$. Through cooperative interplay between the weak equalization effect in (decreasing) $\langle \langle P_i^{(I)} \rangle \rangle_r$ and the non-equalization effect in (increasing) $\langle \langle O_i^{(I)} \rangle \rangle_r$, strong equalization effect in the spiking measure $\langle M_s^{(I)} \rangle_r$ with much smaller standard deviation is found to emerge, like the case of $\langle M_s^{(E)} \rangle_r$. Thus, the values of $\langle M_s^{(I)} \rangle_r$ in Fig. 9(d3) are nearly the same in a broad range of D (i.e., nearly flat curve), which is also markedly in contrast to the Matthew (bipolarization) effect in the intrapopulation (I to I and E to E) STDPs where good (bad) synchronization gets better (worse) [61, 64].

This kind of equalization effect (occurring in a wide range of intermediate and large D) in the I-population may also be well seen in the histograms for the distribution of $\langle M_s^{(I)} \rangle_r$. The gray histogram in the absence of STDP is given in Fig. 9(f1), and the hatched histogram in the presence of I to E iSTDP is shown in Fig. 9(f2). The standard deviation ($\simeq 0.067$) in the hatched histogram is decreased in comparison with that ($\simeq 0.112$) in the gray histogram, and thus strong equalization effect occurs, as in the case of the E-population. Furthermore, the mean value ($\simeq 0.111$) in the hatched histogram is also decreased in comparison with that ($\simeq 0.162$) in the gray histogram, and hence a dumbing-down effect also occurs.

From now on, we make an intensive investigation on emergences of iLTP and iLTD of I to E synaptic strengths through a microscopic method based on the distributions of time delays $\{\Delta t_{ij}^{(EI)}\}$ ($= t_i^{(post,E)} - t_j^{(pre,I)}$) between the nearest spike times of the post-synaptic RS pyramidal cell i and the pre-synaptic FS interneuron j . Figures 10(a1)-10(a5) and 10(b1)-10(b5) show time-evolutions of normalized histograms $H(\Delta t_{ij}^{(EI)})$ for the distributions of time delays $\{\Delta t_{ij}^{(EI)}\}$ for $D = 110$ and 500 , respectively; the bin size in each histogram is 0.5 msec. Here, we consider 5 stages, represented by I (starting from 0 sec), II (starting from 100 sec), III (starting from 400 sec), IV (starting from 800 sec), and V (starting from 1300 sec). At each stage, we obtain the distribution of $\{\Delta t_{ij}^{(EI)}\}$ for all synaptic pairs during 0.2 sec and get the normalized histogram by dividing the distribution with the total average number of synapses ($= 96000$).

In a case of iLTP for $D = 110$ (iLTP), multiple peaks appear in each histogram, in contrast to the case of full synchronization [61]. As explained in Fig. 6(b), due to stochastic spike skipings, nearest-neighboring pre- and post-synaptic spikes appear in any two separate stripes (e.g., nearest-neighboring, next-nearest-neighboring or farther-separated stripes), as well as in the same stripe, which is similar to the multi-peaked ISI histogram. In

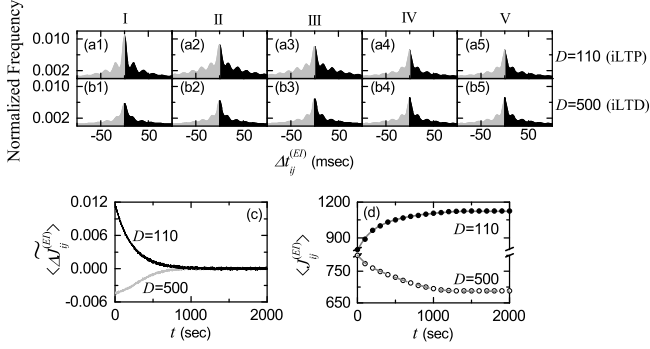


FIG. 10: Microscopic investigations on emergences of iLTP and iLTD in the presence of I to E iSTDP. Time-evolutions of the normalized histogram $H(\Delta t_{ij}^{(EI)})$ for distributions of time delays $\{\Delta t_{ij}^{(EI)}\}$ between the pre- and the post-synaptic spike times for $D = 110$ in (a1)-(a5) and for $D = 500$ in (b1)-(b5); 5 stages are shown in I (starting from 0 sec), II (starting from 100 sec), III (starting from 400 sec), IV (starting from 800 sec), and V (starting from 1300 sec). (c) Time-evolutions of multiplicative synaptic modification $\langle \Delta J_{ij}^{(EI)} \rangle$ for $D = 110$ (black line) and $D = 500$ (gray line). (d) Time-evolutions of population-averaged synaptic strength $\langle J_{ij}^{(EI)} \rangle$ (obtained by an approximate method) for $D = 110$ (solid circle) and $D = 500$ (open circle); gray solid and dashed lines represent ones (obtained by direct calculations) for $D = 110$ and 500 in Fig. 7(a), respectively

the stage I, in addition to the sharp main central (1st-order) peak, higher k th-order ($k = 2, \dots, 5$) left and right minor peaks also are well seen. Here, iLTP and iLTD occur in the black ($\Delta t^{(EI)} > 0$) and the gray ($\Delta t^{(EI)} < 0$) parts, respectively. As the time t is increased (i.e., with increase in the level of stage), the 1st-order main peak becomes lowered and widened, higher-order peaks also become broadened, and thus mergings between multiple peaks occur. Thus, at the final stage V, the histogram is composed of lowered and broadened 1st-order peak and merged higher-order minor peaks. In the stage I, the effect in the right black part (iLTP) is dominant, in comparison with the effect in the left gray part (iLTD), and hence the overall net iLTP begins to emerge. As the level of stage is increased, the effect of iLTP in the black part tends to nearly cancel out the effect of iLTD in the gray part at the stage V.

In a case of iLTD for $D = 500$, in the initial stage I, the histogram consists of much lowered and widened 1st-order main peak and higher-order merged peaks, in

contrast to the case of $D = 110$. For this initial stage, the effect in the left gray part (iLTD) is dominant, in comparison with the effect in the right black part (iLTP), and hence the overall net iLTD begins to occur. However, with increasing the level of stage, the heights of peaks become increased, their widths tend to be narrowed, and thus peaks (particularly, main peak) become more clear, which is in contrast to the progress in the case of $D = 110$. Moreover, the effect of iLTD in the gray part tends to nearly cancel out the effect of iLTP in the black part at the stage V. We also note that the two initially-different histograms for both $D = 110$ (iLTP) and 500 (iLTD) are evolved into similar ones at the final stage V [see Figs. 10(a5) and 10(b5)], which shows the equalization effect occurring in I to E synaptic plasticity.

We consider successive time intervals $I_k \equiv (t_k, t_{k+1})$, where $t_k = 0.2 \cdot (k-1)$ sec ($k = 1, 2, 3, \dots$). With increasing the time t , in each k th time interval I_k , we get the k th normalized histogram $H_k(\Delta t_{ij}^{(EI)})$ ($k = 1, 2, 3, \dots$) via the distribution of $\{\Delta t_{ij}^{(EI)}\}$ for all synaptic pairs during 0.2 sec. Then, from Eq. (12), we get the population-averaged synaptic strength $\langle J_{ij}^{(XY)} \rangle_k$ recursively:

$$\langle J_{ij}^{(XY)} \rangle_k = \langle J_{ij}^{(XY)} \rangle_{k-1} + \delta \cdot \langle \widetilde{\Delta J_{ij}^{(XY)}}(\Delta t_{ij}^{(XY)}) \rangle_k. \quad (29)$$

Here, $X = E$ (post-synaptic population), $Y = I$ (pre-synaptic population), $\langle J_{ij}^{(EI)} \rangle_0 = J_0^{(EI)}$ ($=800$: initial mean value), $\langle \dots \rangle_k$ in the 2nd term means the average over the distribution of time delays $\{\Delta t_{ij}^{(XY)}\}$ for all synaptic pairs in the k th time interval, and the multiplicative synaptic modification $\widetilde{\Delta J_{ij}^{(XY)}}(\Delta t_{ij}^{(XY)})$ is given by the product of the multiplicative factor $(J^* - J_{ij}^{(XY)})$ [$J_{ij}^{(XY)}$: synaptic coupling strength at the $(k-1)$ th stage] and the absolute value of synaptic modification $|\Delta J_{ij}^{(XY)}(\Delta t_{ij}^{(XY)})|$:

$$\widetilde{\Delta J_{ij}^{(XY)}}(\Delta t_{ij}^{(XY)}) = (J^* - J_{ij}^{(XY)}) |\Delta J_{ij}^{(XY)}(\Delta t_{ij}^{(XY)})|. \quad (30)$$

Here, we obtain the population-averaged multiplicative synaptic modification $\langle \widetilde{\Delta J_{ij}^{(XY)}}(\Delta t_{ij}^{(XY)}) \rangle_k$ for the k th stage through a population-average approximation where $J_{ij}^{(XY)}$ is replaced by its population average $\langle J_{ij}^{(XY)} \rangle_{k-1}$ at the $(k-1)$ th stage:

$$\langle \widetilde{\Delta J_{ij}^{(XY)}}(\Delta t_{ij}^{(XY)}) \rangle_k \simeq (J^* - \langle J_{ij}^{(XY)} \rangle_{k-1}) \langle |\Delta J_{ij}^{(XY)}(\Delta t_{ij}^{(XY)})| \rangle_k. \quad (31)$$

Here, $\langle |\Delta J_{ij}^{(XY)}(\Delta t_{ij}^{(XY)})| \rangle_k$ may be easily got from the k th normalized histogram $H_k(\Delta t_{ij}^{(XY)})$:

$$\langle |\Delta J_{ij}^{(XY)}(\Delta t_{ij}^{(XY)})| \rangle_k \simeq \sum_{\text{bins}} H_k(\Delta t_{ij}^{(XY)}) \cdot |\Delta J_{ij}^{(XY)}(\Delta t_{ij}^{(XY)})|. \quad (32)$$

Using Eqs. (29), (31), and (32), we get approximate values of $\langle \Delta J_{ij}^{(XY)} \rangle_k$ and $\langle J_{ij}^{(XY)} \rangle_k$ in a recursive way.

Figure 10(c) shows time-evolutions of $\langle \Delta J_{ij}^{(EI)} \rangle$ for $D = 110$ (black curve) and $D = 500$ (gray curve). $\langle \Delta J_{ij}^{(EI)} \rangle$ for $D = 110$ is positive, while $\langle \Delta J_{ij}^{(EI)} \rangle$ for $D = 500$ is negative. For both cases they converge toward nearly zero at the stage V (starting from 1300 sec) because the effects of iLTP and iLTD in the normalized histograms are nearly cancelled out. The time-evolutions of $\langle J_{ij}^{(EI)} \rangle$ for $D = 110$ (solid circles) and $D = 500$ (open circles) are also shown in Fig. 10(d). We note that the approximately-obtained values for $\langle J_{ij}^{(EI)} \rangle$ agree well with directly-obtained ones [denoted by the gray solid (dashed) line for $D = 110$ (500)] in Fig. 7(a). As a result, iLTP (iLTD) emerges for $D = 110$ (500).

C. Effect of E to I eSTDP on Populations States in The I- and The E-populations

In this subsection, we study the effect of E to I eSTDP on population states in the I- and the E-populations, and make comparison with those in both the case without STDP and the case of I to E iSTDP. As in the case of I to E iSTDP, an equalization effect in the spiking measure $\langle M_s^{(X)} \rangle_r$ ($X = I$ or E) is thus found to occur in a wide range of D . However, the equalization effect in the E to I eSTDP is weaker than that in I to E iSTDP, because the I-population is a dominant one in our coupled two-population system. Thus, the region for (FSS, FSS) in the case of E to I eSTDP becomes narrower than that in the case of I to E iSTDP, although both of them are much wider than that in the absence of STDP. Also, behaviors of both the population frequency $\langle f_p^{(X)} \rangle_r$ and the population-averaged MFR $\langle \langle f_i^{(X)} \rangle \rangle_r$ are similar to those in the case of I to E iSTDP. Hence, $\langle f_p^{(X)} \rangle_r$ shows a weak equalization effect with a decreased standard deviation, while $\langle \langle f_i^{(X)} \rangle \rangle_r$ exhibits a non-equalization effect with an increased standard deviation. The weak equalization effect in $\langle f_p^{(X)} \rangle_r$ is nearly the same in both cases of E to I eSTDP and I to E iSTDP. On the other hand, the non-equalization effect in $\langle \langle f_i^{(X)} \rangle \rangle_r$ in the case of E to I eSTDP is weaker than that in the case of I to E iSTDP. Like the case of I to E iSTDP, E-I ratio balance is also broken up, and hence a phase shift between the fast sparsely synchronized rhythms in the I- and the E-populations occurs. However, the phase shift in the case of E to I eSTDP is opposite to that in the case of I to E iSTDP.

In the absence of STDP, (FSS, FSS) appears for $D_2^* (\simeq 91) < D < D_3^* (\simeq 537)$, while for $D > D_3^*$ desynchronized states appear in both the I- and the E-populations [see Fig. 3(a)]. In addition to the I to E iSTDP (in Subsec. IIIB), we consider another interpopulation E to I eSTDP. As in Subsec. IIIB, the

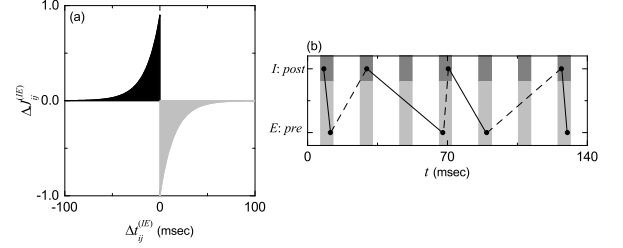


FIG. 11: (a) Time window for the anti-Hebbian E to I eSTDP. Plot of synaptic modification $\Delta J_{ij}^{(IE)}$ versus $\Delta t_{ij}^{(IE)}$ ($= t_i^{(post,I)} - t_j^{(pre,E)}$) for $A_+ = 1.0$, $A_- = 0.9$, $\tau_+ = 15$ msec, and $\tau_- = 15$ msec. $t_i^{(post,I)}$ and $t_j^{(pre,E)}$ are spiking times of the post-synaptic FS interneuron i in the target I-population and the pre-synaptic RS pyramidal cell j in the source E-population, respectively. (b) Schematic diagram for the nearest-spike pair-based STDP rule. $E: Pre$ and $I: Post$ correspond to a pre-synaptic RS pyramidal cell and a post-synaptic FS interneuron, respectively. Gray and light gray boxes represent I- and E-strips in the raster plot, respectively, and spikes in the stripes are denoted by solid circles. Solid and dashed lines represent eLTP (excitatory LTP) and eLTD (excitatory LTD), respectively.

initial synaptic strengths are normally distributed with the mean $J_0^{(XY)}$ and the standard deviation $\sigma_0 (= 5)$, where $J_0^{(II)} = 1300$, $J_0^{(EE)} = 300$, $J_0^{(EI)} = 800$, and $J_0^{(IE)} = 487.5 (= J_0^{(II)} J_0^{(EE)} / J_0^{(EI)})$. In this initial case, the E-I ratio balance occurs (i.e., the ratio of average excitatory to inhibitory synaptic strengths is the same in both FS interneurons and RS pyramidal cells). Here, we consider just the interpopulation E to I eSTDP. Thus, intrapopulation (I to I and E to E) synaptic strengths and interpopulation I to E synaptic strengths are static. Only synaptic strength $J_{ij}^{(IE)}$ for each interpopulation E to I synapse is updated according to the nearest-spike pair-based STDP rule in Eq. (12). By increasing D from D_2^* , we investigate the effect of E to I eSTDP on population states (I, E) in the I- and the E-populations, and make comparison with that of I to E iSTDP. The overall effects of E to I eSTDP on population states are thus found to be similar to those of I to E iSTDP, but the effects in the case of E to I eSTDP are weaker than those for the case of I to E iSTDP because the I-population is a dominant one in our coupled two-population system.

Figure 11(a) shows an anti-Hebbian time window for the synaptic modification $\Delta J_{ij}^{(IE)}(\Delta t_{ij}^{(IE)})$ of Eq. (15) [48, 102, 103]. Unlike the case of the I to E time-delayed Hebbian time window [60, 100, 101], LTD occurs in the gray region for $\Delta t_{ij}^{(IE)} > 0$, while LTP takes place in the black region for $\Delta t_{ij}^{(IE)} < 0$. Furthermore, the anti-Hebbian time window for E to I eSTDP is in contrast to the Hebbian time window for the E to E eSTDP [49–56], although both cases correspond to the same excitatory synapses (i.e., the type of time window may vary depending on the type of target neurons of excitatory synapses).

The synaptic modification $\Delta J_{ij}^{(IE)}(\Delta t_{ij}^{(IE)})$ changes depending on the relative time difference $\Delta t_{ij}^{(IE)} (= t_i^{(post,I)} - t_j^{(pre,E)})$ between the nearest spike times of the post-synaptic FS interneurons i and the pre-synaptic RS pyramidal cell j . When a post-synaptic spike follows a pre-synaptic spike (i.e., $\Delta t_{ij}^{(IE)}$ is positive), excitatory LTD (eLTD) of E to I synaptic strength occurs; otherwise (i.e., $\Delta t_{ij}^{(IE)}$ is negative), excitatory LTP (eLTP) appears. A schematic diagram for the nearest-spike pair-based STDP rule is given in Fig. 11(b), where $E: Pre$ and $I: Post$ correspond to a pre-synaptic RS pyramidal cell and a post-synaptic FS interneuron, respectively. Here, gray and light gray boxes denote I- and E-stripes in the raster plot, respectively, and spikes in the stripes are denoted by solid circles. When the post-synaptic FS interneuron ($I: Post$) fires a spike, eLTD (represented by dashed lines) occurs via E to I eSTDP between the post-synaptic spike and the previous nearest pre-synaptic spike of the RS pyramidal cell ($E: Pre$). On the other hand, when the pre-synaptic RS pyramidal cell ($E: Pre$) fires a spike, eLTP (denoted by solid lines) occurs through E to I eSTDP between the pre-synaptic spike and the previous nearest post-synaptic spike of the FS interneuron ($I: Post$). In the case of FSS, individual neurons make stochastic phase lockings (i.e., they make intermittent spikings phase-locked to the IPSR at random multiples of its global period). As a result of stochastic phase lockings (resulting in stochastic spike skippings), nearest-neighboring pre- and post-synaptic spikes may appear in any two separate stripes (e.g., nearest-neighboring, next-nearest-neighboring or farther-separated stripes), as well as in the same stripe, which is in contrast to the case of full synchronization where they appear in the same or just in the nearest-neighboring stripes [compare Fig. 11(b) with Fig. 4(b) (corresponding to the case of full synchronization) in [61]]. For simplicity, only the cases, corresponding to the same, the nearest-neighboring, and the next-nearest-neighboring stripes, are shown in Fig. 11(b).

Figure 12(a) shows time-evolutions of population-averaged (E to I) synaptic strengths $\langle J_{ij}^{(IE)} \rangle$ for various values of D . In each case of intermediate values of $D = 110, 250$, and 400 , $\langle J_{ij}^{(IE)} \rangle$ decreases monotonically below its initial value $J_0^{(IE)} (= 487.5)$, and eventually it converges to a saturated limit value $\langle J_{ij}^{(IE)*} \rangle$ nearly at $t = 1500$ sec. Consequently, eLTD occurs for these values of D . On the other hand, for small and large values of $D = 95, 500$, and 600 , $\langle J_{ij} \rangle$ increases monotonically above $J_0^{(IE)}$, and converges to a saturated limit value $\langle J_{ij}^{(IE)*} \rangle$. As a result, eLTP occurs in the cases of $D = 95, 500$ and 600 . These tendencies for time-evolutions of $\langle J_{ij}^{(IE)} \rangle$ are opposite to those in the case of I to E iSTDP [see Fig. 7(a)] where in the region of intermediate D , iLTP occurs, while iLTD takes place in the other two separate regions of small and large D . Figure

12(b1) shows a well-shaped plot of population-averaged limit values $\langle \langle J_{ij}^{(IE)*} \rangle \rangle_r$ (open circles) of (E to I) synaptic strengths versus D , where $J_{ij}^{(IE)*}$ are saturated limit values of $J_{ij}^{(IE)}$ at $t = 1500$ sec. This well-shaped graph for $\langle \langle J_{ij}^{(IE)*} \rangle \rangle_r$ is in contrast to the bell-shaped one in the case of I to E iSTDP [see Fig. 7(b1)]. Here, the horizontal dotted line denotes the initial average value of (E to I) synaptic strengths $J_0^{(IE)}$ ($\simeq 487.5$), and the lower and the higher thresholds, $\tilde{D}_{l,IE}$ ($\simeq 99$) and $\tilde{D}_{h,IE}$ ($\simeq 406$), for eLTP/eLTD (where $\langle \langle J_{ij}^{(IE)*} \rangle \rangle_r = J_0^{(IE)}$) are denoted by solid circles; in comparison with those in the case of I to E iSTDP, $\tilde{D}_{l,IE}$ is the same as $\tilde{D}_{l,EI}$, and $\tilde{D}_{h,IE}$ is a little smaller than $\tilde{D}_{h,EI}$ ($\simeq 408$). Thus, in a broad region of intermediate D ($\tilde{D}_{l,IE} < D < \tilde{D}_{h,IE}$), eLTD takes place, while eLTP occurs in the other two (separate) regions of small and large D ($D < \tilde{D}_{l,IE}$ and $D > \tilde{D}_{h,IE}$). Figure 12(b2) also shows a plot of standard deviations $\langle \sigma_J^{(IE)} \rangle_r$ (from the population-averaged limit values) versus D . As in the case of I to E iSTDP [see Fig. 7(b2)], all the values of $\langle \sigma_J^{(IE)} \rangle_r$ are larger than the initial value $\sigma_0 (= 5)$, independently of D .

A bar diagram for the population states (I, E) in the I- and the E-populations is shown in Fig. 12(c). We note that (FSS, FSS) occurs in a broadened range of D [$D_2^* (\simeq 91) < D < D_{3,IE}^* (\simeq 632)$], in comparison with the case without STDP where (FSS, FSS) appears for $D_2^* < D < D_3^* (\simeq 537)$ [see Fig. 3(a)]. Desynchronized states for $D_3^* < D < D_{3,IE}^*$ in the absence of STDP are transformed into (FSS, FSS) via eLTP in the presence of E to I eSTDP, and thus the region of (FSS, FSS) is broadened. However, the effect of E to I eSTDP is weaker than that of I to E iSTDP, because the I-population is a dominant one in our coupled two-population system. Hence, the region of (FSS, FSS) in the presence of E to I eSTDP is narrower than that in the case of I to E iSTDP where (FSS, FSS) appears for $D_2^* < D < D_{3,EI}^* (\simeq 656)$ [see Fig. 7(c)].

The effects of eLTD and eLTP on population states after the saturation time ($t^* = 1500$ sec) may be well seen in the raster plot of spikes and the corresponding IPSRs $R_I(t)$ and $R_E(t)$. Figures 12(d1)-12(d6), Figures 12(e1)-12(e6), and Figures 12(f1)-12(f6) show raster plots of spikes, the IPSRs $R_I(t)$, and the IPSRs $R_E(t)$ for various values of D , respectively. When compared with the case without STDP [see Figs. 3(b4)-3(b6), Figs. 3(c4)-3(c6), and Figs. 3(d4)-3(d6)], the degrees of (FSS, FSS) in the case of eLTD ($D = 110, 250$, and 400) are decreased (i.e., the amplitudes of $R_I(t)$ and $R_E(t)$ are decreased) because of decreased E to I synaptic excitation. In contrast, in the case of eLTP for $D = 95$ and 500 , the degrees of (FSS, FSS) are increased (i.e., the amplitudes of $R_I(t)$ and $R_E(t)$ are increased) because of increased E to I synaptic excitation [compare the corresponding raster plots, $R_I(t)$, and $R_E(t)$ for $D = 95$ and 500 in

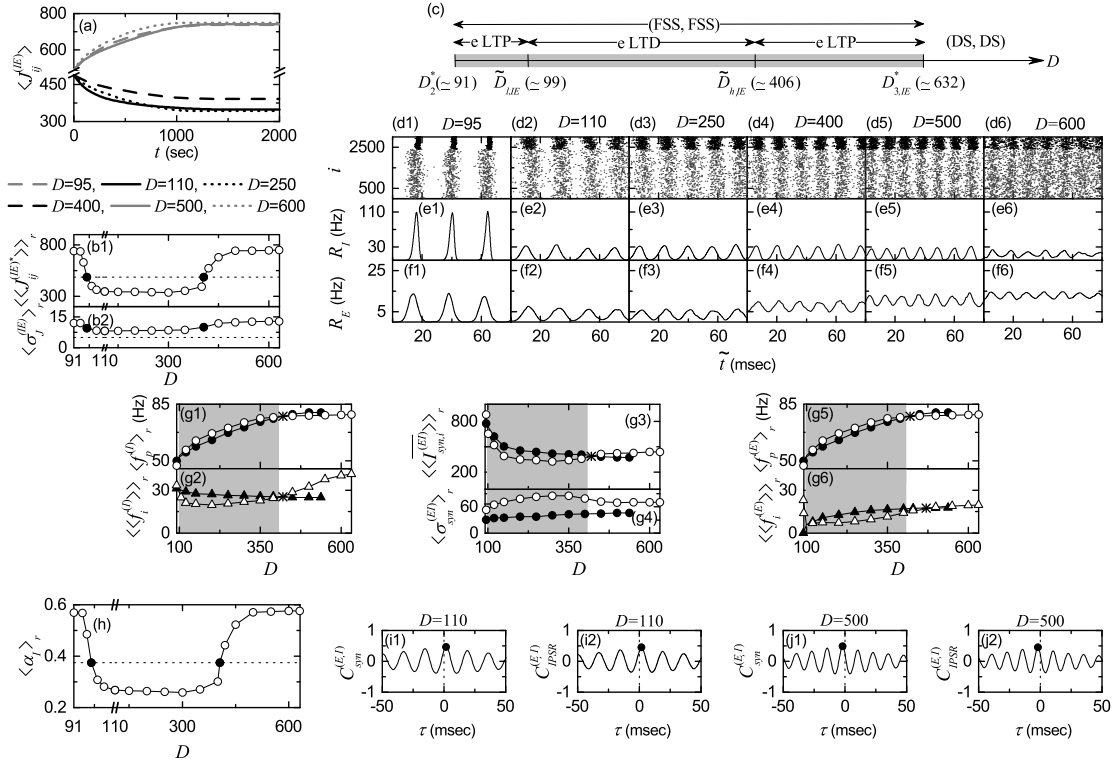


FIG. 12: Effects of E to I eSTDP on population states. (a) Time-evolutions of population-averaged synaptic strengths $\langle J_{ij}^{(IE)} \rangle$ for various values of D . (b1) Plots of population-averaged limit values $\langle \langle J_{ij}^{(IE)*} \rangle_r \rangle$ of synaptic strengths versus D . (b2) Plots of standard deviations $\langle \sigma_J^{(IE)} \rangle_r$ versus D . (c) Bar diagram for the population states (I, E) in the I- and the E-populations. Raster plots of spikes in (d1)-(d6) and IPSRs $R_I(t)$ in (e1)-(e6) and $R_E(t)$ in (f1)-(f6) for various values of D after the saturation time, where $t = t^*$ (saturation time = 1500 sec) + \tilde{t} . Plots of (g1) the population frequency $\langle f_p^{(I)} \rangle$ (open circles) and (g2) the population-averaged MFR of FS interneurons $\langle \langle f_i^{(I)} \rangle_r \rangle$ (open triangles) versus D in the I-populations; those in the absence of STDP are denoted by solid circles and triangles, respectively. Plots of (g3) population average $\langle \langle I_{syn,i}^{(EI)} \rangle_r \rangle$ (open circles) and (g4) standard deviation $\langle \sigma_{syn,i}^{(EI)} \rangle_r$ (open circles) for time-averaged strengths $\{I_{syn,i}^{(EI)}\}$ of individual I to E synaptic currents; those in the absence of STDP are represented by solid circles. Plots of (g5) the population frequency $\langle f_p^{(E)} \rangle$ (open circles) and (g6) the population-averaged MFR of RS pyramidal cells $\langle \langle f_i^{(E)} \rangle_r \rangle$ (open triangles) versus D in the E-populations; those in the absence of STDP are denoted by solid circles and triangles. Break-up of E-I ratio balance in the presence of E to I eSTDP. (h) Plot of the E-I ratio $\langle \alpha_I \rangle_r = (\langle J_{ij}^{(IE)} \rangle_r / J_0^{(II)})$ versus D . Cross-correlation functions between total synaptic input currents $I_{syn}^{(E)}(t)$ and $I_{syn}^{(I)}(t)$ for $D =$ (i1) 110 (eLTD) and (j1) 500 (eLTP). Cross-correlation functions between IPSRs $R_E(t)$ and $R_I(t)$ for $D =$ (i2) 110 (eLTD) and (j2) 500 (eLTP).

Figs. 3 and 12]. These effects of E to I eSTDP on population states for $D = 95, 110, 250, 400$, and 500 are similar to the effects of I to E iSTDP (see the corresponding figures in Fig. 7), although the roles of LTP and LTD are reversed, and the degrees of (FSS, FSS) in the case of E to I eSTDP seem to be nearly the same as those in the case of I to E iSTDP.

We also note that a desynchronized state for $D = 600$ in the absence of STDP [see Figs. 3(b8), 3(c8), and 3(d8)] is transformed into (FSS, FSS) [see Figs. 12(d6), 12(e6), and 12(f6)] via eLTP, as in the case of I to E iSTDP (see the case of $D = 600$ in Fig. 7). However, the degree of (FSS, FSS) for $D = 600$ is smaller than those for other smaller values of D (i.e., the amplitudes of $R_I(t)$ and $R_E(t)$ in the case of $D = 600$ are decreased), be-

cause the value of $D = 600$ is close to the 3rd threshold $D_{3,IE}^*$ ($\simeq 632$) where a transition to desynchronization occurs. In contrast, in the case of I to E iSTDP, the amplitudes of $R_I(t)$ and $R_E(t)$ for $D = 600$ are just a little decreased, because the value of $D = 600$ is far away from its 3rd threshold $D_{3,EI}^*$ ($\simeq 656$). Here, we note that the degree of FSS in the I-(E-)population (i.e., the amplitudes of $R_I(t)$ [$R_E(t)$]) tends to be nearly the same in a wide range of $\tilde{D}_{l,IE} < D < D_{3,IE}^*$, except for the narrow small- D region ($D_2^* < D < \tilde{D}_{l,IE}$). Hence, as in the case of I to E iSTDP, an equalization effect in the E to I synaptic plasticity occurs in a wide range of D . However, the equalization effect in the E to I eSTDP is weaker than that in the I to E iSTDP, because the I-population

is a dominant one in our coupled two-population system. Hence, the region (where the equalization effect occurs) is narrower than that in the case of I to E iSTDP. Quantitative analysis for the degree of (FSS, FSS) and the equalization effect in the case of E to I eSTDP will be done intensively in Fig. 13.

We now study the effect of eLTD and eLTP on the population-averaged MFR $\langle\langle f_i^{(I)} \rangle\rangle_r$ and the population frequency $\langle f_p^{(I)} \rangle_r$ in the (target) I-population. Here, we note that the source and target populations for the E to I eSTDP are opposite to those for the I to E iSTDP. Figures 12(g1) and 12(g2) show plots of $\langle f_p^{(I)} \rangle_r$ and $\langle\langle f_i^{(I)} \rangle\rangle_r$ versus D , respectively. In the gray region of eLTD ($\tilde{D}_{l,IE} < D < \tilde{D}_{h,IE}$), the population-averaged MFR $\langle\langle f_i^{(I)} \rangle\rangle_r$ (open triangles) are lower than those (solid triangles) in the absence of STDP, because of decreased synaptic excitation $\langle\langle J_{ij}^{(IE)*} \rangle\rangle_r$. Due to decrease in $\langle\langle f_i^{(I)} \rangle\rangle_r$, the population frequency $\langle f_p^{(I)} \rangle_r$ (open circles) becomes higher than that (solid circles) in the absence of STDP. On the other hand, in most cases of eLTP for large D except for a narrow region near the higher threshold $\tilde{D}_{h,IE}$, the population-averaged MFRs $\langle\langle f_i^{(I)} \rangle\rangle_r$ (open triangles) are higher than those (solid triangles) in the absence of STDP, due to increased synaptic excitation $\langle\langle J_{ij}^{(IE)*} \rangle\rangle_r$. Because of increase in $\langle\langle f_i^{(I)} \rangle\rangle_r$, the population frequency $\langle f_p^{(I)} \rangle_r$ (open circles) becomes lower than that (solid circles) in the absence of STDP.

In the (exceptional) narrow region of eLTP near the higher threshold [$\tilde{D}_{h,IE} \leq D < D_{cr}^*$ ($\simeq 420$) (D_{cr}^* : denoted by a star)], the overall effect of standard deviation $\langle\sigma_J^{(IE)}\rangle_r$ (decreasing $\langle\langle f_i^{(I)} \rangle\rangle_r$) is found to be dominant in comparison with the effect of eLTP (increasing $\langle\langle f_i^{(I)} \rangle\rangle_r$), and hence values of $\langle\langle f_i^{(I)} \rangle\rangle_r$ (open triangles) become lower than those (solid triangles) in the absence of STDP, like the case of eLTD (in the gray region of intermediate D). We note that the value of D_{cr}^* is smaller than that ($\simeq 430$) in the case of I to E iSTDP [see Fig. 7(g2)]. Hence, the effect of $\langle\sigma_J^{(IE)}\rangle_r$ seems to be weaker than the effect of $\langle\sigma_J^{(EI)}\rangle_r$ in the case of I to E iSTDP. Due to decrease in $\langle\langle f_i^{(I)} \rangle\rangle_r$, in this region of D , the population frequency $\langle f_p^{(I)} \rangle_r$ (open circle) becomes higher than that (solid circles) in the absence of STDP. After passing the crossing point D_{cr}^* (denoted by the star), the effect of eLTP (increasing the population-averaged MFR) becomes dominant, as in the usual case of eLTP.

Figures 12(g3) and 12(g4) show plots of population average $\langle\langle I_{syn,i}^{(EI)} \rangle\rangle_r$ (open circles) and standard deviation $\langle\sigma_{syn}^{(EI)}\rangle_r$ (from the population average) (open circles) for time-averaged strengths $\{I_{syn,i}^{(EI)}\}$ of individual I to E synaptic currents, respectively; for comparison, those in the absence of STDP are represented by solid circles. MFRs of FS interneurons in the I-population affect indi-

vidual I to E synaptic current $I_{syn,i}^{(EI)}$ so much [see Eqs. (9) and (10)]. Hence, the population average $\langle\langle I_{syn,i}^{(EI)} \rangle\rangle_r$ has a strong correlation with the population-averaged MFR $\langle\langle f_i^{(I)} \rangle\rangle_r$ of FS interneurons (Pearson's correlation coefficient $r \simeq 0.75$), as in the case of I to E iSTDP where $\langle\langle I_{syn,i}^{(IE)} \rangle\rangle_r$ has a strong correlation with $\langle\langle f_i^{(E)} \rangle\rangle_r$ (Pearson's correlation coefficient $r \simeq 0.92$). Thus, in the gray region of eLTD ($\tilde{D}_{l,IE} < D < \tilde{D}_{h,IE}$), the population-average values of $\langle\langle I_{syn,i}^{(EI)} \rangle\rangle_r$ (open circles) are lower than those (solid circles) in the absence of STDP, mainly because of decrease in $\langle\langle f_i^{(I)} \rangle\rangle_r$. In contrast, in most cases of eLTP for large D (except for a narrow region near the higher threshold $\tilde{D}_{h,IE}$), the population averages $\langle\langle I_{syn,i}^{(EI)} \rangle\rangle_r$ (open circles) are higher than those (solid circles) in the absence of STDP, mainly due to increase in $\langle\langle f_i^{(I)} \rangle\rangle_r$. In the (exceptional) narrow region of eLTP near the higher threshold [$\tilde{D}_{h,IE} \leq D < D_{cr}^*$ ($\simeq 420$) (D_{cr}^* : denoted by a star)], the population-average values of $\langle\langle I_{syn,i}^{(EI)} \rangle\rangle_r$ (open circles) are lower than those (solid circles) in the absence of STDP, mainly due to decrease in $\langle\langle f_i^{(I)} \rangle\rangle_r$, as in the gray region of eLTP. In addition to population averages $\langle\langle I_{syn,i}^{(EI)} \rangle\rangle_r$, standard deviations $\langle\sigma_{syn}^{(EI)}\rangle_r$ are also shown in Fig. 12(g4). Unlike the case of $\langle\langle I_{syn,i}^{(EI)} \rangle\rangle_r$, all the values of $\langle\sigma_{syn}^{(EI)}\rangle_r$ (open circles) are larger than those (solid circles) in the absence of STDP, independently of D .

Figure 12(g6) shows a plot of $\langle\langle f_i^{(E)} \rangle\rangle_r$ versus D . We study the effects of both the population average $\langle\langle I_{syn,i}^{(EI)} \rangle\rangle_r$ and the standard deviation $\langle\sigma_{syn}^{(EI)}\rangle_r$ for time-averaged strengths of individual I to E synaptic currents on the population-averaged MFR $\langle\langle f_i^{(E)} \rangle\rangle_r$ in the E-population. In most cases, the effect of $\langle\sigma_{syn}^{(EI)}\rangle_r$ is dominant when compared with the effect of $\langle\langle I_{syn,i}^{(EI)} \rangle\rangle_r$, in contrast to the case of I to E iSTDP [see Figs. 7(g3) and 7(g4)] where the effect of the standard deviation $\langle\sigma_{syn}^{(IE)}\rangle_r$ is negligibly small in comparison with the effect of the population average $\langle\langle I_{syn,i}^{(IE)} \rangle\rangle_r$. As shown in Fig. 12(g3), for $\tilde{D}_{l,IE} (\simeq 99) < D < D_{cr,l}^* (\simeq 420)$ ($D_{cr,l}^*$: denoted by a star), values of $\langle\langle I_{syn,i}^{(EI)} \rangle\rangle_r$ (open circles) are lower than those (solid circles) in the absence of STDP, while in the other two separate regions for $D_{cr,l}^* < D < D_{3,IE}^*$ and $D_2^* (\simeq 91) < D < \tilde{D}_{l,IE}$, they are higher than those (solid circles). Hence, in the range of $\tilde{D}_{l,IE} < D < D_{cr,l}^*$, $\langle\langle I_{syn,i}^{(EI)} \rangle\rangle_r$ has a tendency of increasing $\langle\langle f_i^{(E)} \rangle\rangle_r$, due to decreased I to E synaptic inhibition. On the other hand, because of increase in I to E synaptic inhibition, $\langle\langle I_{syn,i}^{(EI)} \rangle\rangle_r$ has a tendency of decreasing $\langle\langle f_i^{(E)} \rangle\rangle_r$ in the other two ranges of $D_{cr,l}^* < D < D_{3,IE}^*$

and $D_2^* < D < \tilde{D}_{l,IE}$.

However, the behaviors of $\langle\langle f_i^{(E)} \rangle\rangle_r$ are completely opposite to effects of $\langle\langle I_{syn,i}^{(EI)} \rangle\rangle_r$. For $\tilde{D}_{l,IE} < D < D_{cr,h}^*$ ($\simeq 470$) ($D_{cr,h}^*$: denoted by a star), values of $\langle\langle f_i^{(E)} \rangle\rangle_r$ (open triangles) are lower than those (solid triangles) in the absence of STDP, while they (open triangles) are higher than those (solid triangles) in the other two separate regions for $D_{cr,h}^* < D < D_{3,IE}^*$ and $D_2^* < D < \tilde{D}_{l,IE}$. These behaviors of $\langle\langle f_i^{(E)} \rangle\rangle_r$ result from significant contributions of the standard deviation $\langle\sigma_{syn}^{(EI)}\rangle_r$. For $\tilde{D}_{l,IE} < D < D_{cr,m}^*$ ($\simeq 450$), $\langle\sigma_{syn}^{(EI)}\rangle_r$ has a tendency of decreasing $\langle\langle f_i^{(E)} \rangle\rangle_r$, while it has a tendency of increasing $\langle\langle f_i^{(E)} \rangle\rangle_r$ in the other two ranges of $D_{cr,m}^* < D < D_{3,IE}^*$ and $D_2^* < D < \tilde{D}_{l,IE}$. We note that these tendencies of $\langle\sigma_{syn}^{(EI)}\rangle_r$ are opposite to those of $\langle\langle I_{syn,i}^{(EI)} \rangle\rangle_r$. In most cases for competitions between the opposite tendencies between $\langle\langle I_{syn,i}^{(EI)} \rangle\rangle_r$ and $\langle\sigma_{syn}^{(EI)}\rangle_r$, the effects of $\langle\sigma_{syn}^{(EI)}\rangle_r$ become dominant, which leads to behaviors of $\langle\langle f_i^{(E)} \rangle\rangle_r$ (which differ distinctly from effects of $\langle\langle I_{syn,i}^{(EI)} \rangle\rangle_r$).

Moreover, the E-population is dynamically more susceptible than the I-population with respect to variations in stimulations ($I_{syn,i}^{(EI)}$ or $J_{ij}^{(IE)*}$), as shown in Figs. 12(g2) and 12(g6) where the values of D_{cr}^* (denoted by stars) for $\langle\langle f_i^{(I)} \rangle\rangle_r$ and $\langle\langle f_i^{(E)} \rangle\rangle_r$ are 420 and 470, respectively. Due to its high dynamical susceptibility, the value of D_{cr}^* ($\simeq 470$) in the E-population is larger than that ($\simeq 420$) in the I-population. In addition to $\langle\langle f_i^{(E)} \rangle\rangle_r$, $\langle f_p^{(E)} \rangle_r$ is also shown in Fig. 12(g5). The I-population is a dominant one in our coupled two-population system, and hence the population frequency is determined by the dominant I-population. Thus, $\langle f_p^{(E)} \rangle_r$ becomes the same as $\langle f_p^{(I)} \rangle_r$ in Fig. 12(g1), as in the case of I to E iSTDP [see Figs. 7 (g1) and 7(g5)].

In a broad range of $\tilde{D}_{l,IE} < D < D_{3,IE}^*$ (including the regions of both intermediate and large D), a weak equalization effect is found to appear in the population frequency $\langle f_p^{(I)} \rangle_r$ ($= \langle f_p^{(E)} \rangle_r$), like the case of I to E iSTDP, because the standard deviation in the distribution of $\langle f_p^{(X)} \rangle_r$ ($X = I$ or E) (open circles) in the presence of E to I eSTDP becomes decreased, in comparison to that (solid circles) in the absence of STDP [see Figs. 12(g1) and 12(g5)]. Particularly, the values of $\langle f_p^{(X)} \rangle_r$ for $D > 350$ seem to be nearly the same. This weak equalization effect in $\langle f_p^{(X)} \rangle_r$ is nearly the same as that in the case of I to E iSTDP, because the values of standard deviations in both cases are nearly the same. However, this kind of weak equalization effect is in contrast to strong equalization effect (with much smaller standard deviation) in the synchronization degrees [represented by the amplitudes of IPSRs $R_I(t)$ and $R_E(t)$] in

the I- and the E-populations. On the other hand, non-equalization effects are found to occur in the population-averaged MFRs $\langle\langle f_i^{(I)} \rangle\rangle_r$ and $\langle\langle f_i^{(E)} \rangle\rangle_r$ and in the population average $\langle\langle I_{syn,i}^{(EI)} \rangle\rangle_r$ for time-averaged strengths of I to E synaptic currents, as in the case of I to E iSTDP, because their distributions (open triangles or open circles) have increased standard deviations, in comparison with those (solid triangles or solid circles) in the absence of STDP [see Figs. 12(g2), 12(g6), and 12(g3)]. However, this non-equalization effect in $\langle\langle f_i^{(X)} \rangle\rangle_r$ ($X = I$ or E) is weaker than that in the case of I to E iSTDP, because the value of standard deviation in the case of I to E iSTDP is larger than that in the case of E to I eSTDP.

As in the case of I to E iSTDP, we study the effect of E to I eSTDP on the E-I ratio and the phase shift between fast synchronized rhythms in the I- and the E-populations, and then comparison with those in the case of I to E iSTDP is made. In the absence of STDP, the two fast sparsely synchronized rhythms in both the E- and the I-populations are in-phase [see Fig. 3], due to the E-I ratio balance [i.e., $\alpha_E = \alpha_I (= 0.375)$]. In the presence of E to I eSTDP, α_I in the (target) I-population changes, while no change in α_E in the (source) E-population occurs. In this way, break-up of the E-I ratio balance occurs in an opposite way, in comparison with the case of I to E iSTDP where α_E in the (target) E-population varies. Figure 12(h) shows a well-shaped plot of the E-I ratio $\langle\alpha_I\rangle_r (= \langle\langle J_{ij}^{(IE)} \rangle\rangle_r / J_0^{(II)})$ versus D in the presence of E to I eSTDP. This well-shaped graph for $\langle\alpha_I\rangle_r$ is similar to that for $\langle\alpha_E\rangle_r$ in the case of I to E iSTDP [see Fig. 8(a)]. In the region of intermediate D [$\tilde{D}_{l,IE} (\simeq 99) < D < \tilde{D}_{h,IE} (\simeq 406)$] where eLTD takes place, $\langle\alpha_I\rangle_r$ is decreased below the value ($= 0.375$) in the absence of STDP, represented by the horizontal dotted line, because of decrease in E to I synaptic excitation. Hence, in this region, the values of $\langle\alpha_I\rangle_r$ become smaller than those of $\langle\alpha_E\rangle_r (= 0.375)$. In contrast, in the other two separate regions of small and large D [$D_2^* (\simeq 91) < D < \tilde{D}_{l,IE}$ and $\tilde{D}_{h,IE} < D < D_{3,IE}^* (\simeq 632)$] where eLTP occurs, $\langle\alpha_I\rangle_r$ is increased above the value ($= 0.375$) in the absence of STDP, due to increase in E to I synaptic excitation. In these two regions, the values of $\langle\alpha_I\rangle_r$ are larger than those of $\langle\alpha_E\rangle_r$.

Break-up of the E-I ratio balance in the case of E to I eSTDP is opposite to that in the case of I to E iSTDP. In the region of intermediate D , $\langle\alpha_I\rangle_r < \langle\alpha_E\rangle_r$ ($\langle\alpha_E\rangle_r < \langle\alpha_I\rangle_r$ in the case of E to I eSTDP (I to E iSTDP), while in the other two regions of small and large D , $\langle\alpha_I\rangle_r > \langle\alpha_E\rangle_r$ ($\langle\alpha_E\rangle_r > \langle\alpha_I\rangle_r$ in the case of E to I eSTDP (I to E iSTDP). Hence, phase shifts between fast sparsely synchronized rhythms in the E- and the I-populations also occur in an opposite way. As an example of intermediate D , we consider the case of $D = 110$ with $\langle\alpha_I\rangle_r = 0.268$ where eLTD occurs. Figure 12(i1) shows the cross-correlation function $C_{syn}^{(E,I)}(\tau)$ of Eq. (19) between the population-averaged total synaptic

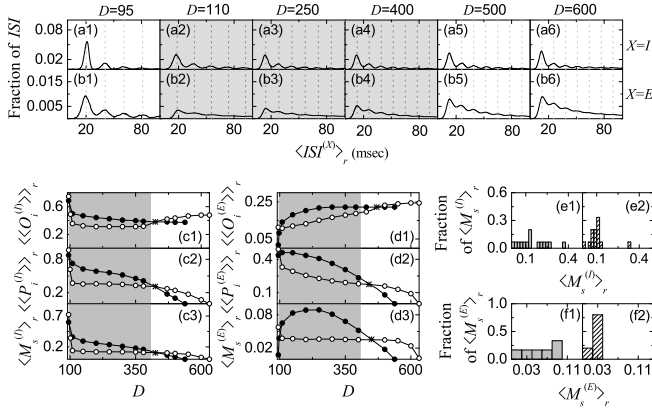


FIG. 13: Characterization of individual and population behaviors for (FSS, FSS) after the saturation time ($t^* = 1500$ sec) in the presence of E to I eSTDP. ISI histograms for various values of D in the (a1)-(a6) I- and (b1)-(b6) E-populations. Vertical dotted lines represent multiples of the global period $T_G^{(X)}$ of the IPSR $R_X(t)$ ($X = I$ and E). Plots of (c1) the average occupation degree $\langle\langle O_i^{(I)} \rangle\rangle_r$ (open circles), (c2) the average pacing degree $\langle\langle P_i^{(I)} \rangle\rangle_r$ (open circles), and (c3) the statistical-mechanical spiking measure $\langle M_s^{(I)} \rangle_r$ (open circles) versus D in the I-population. Plots of (d1) the average occupation degree $\langle\langle O_i^{(E)} \rangle\rangle_r$ (open circles), (d2) the average pacing degree $\langle\langle P_i^{(E)} \rangle\rangle_r$ (open circles), and (d3) the statistical-mechanical spiking measure $\langle M_s^{(E)} \rangle_r$ (open circles) versus D in the E-population. For comparison, $\langle\langle O_i^{(X)} \rangle\rangle_r$, $\langle\langle P_i^{(X)} \rangle\rangle_r$, and $\langle M_s^{(X)} \rangle_r$ ($X = I$ and E) in the absence of STDP are also denoted by solid circles. In (a2)-(a4), (b2)-(b4), (c1)-(c3) and (d1)-(d3), eLTD occurs in the intermediate gray-shaded regions. Histograms for distribution of statistical-mechanical spiking measures $\langle M_s^{(I)} \rangle_r$ in the I-population in the (e1) absence and the (e2) presence of E to I eSTDP. Histograms for distribution of statistical-mechanical spiking measures $\langle M_s^{(E)} \rangle_r$ in the E-population in the (f1) absence and the (f2) presence of E to I eSTDP.

input currents $I_{syn}^{(E)}(t)$ and $I_{syn}^{(I)}(t)$ into the E- and the I-populations. The main peak (denoted by a solid circle) appears at $\tau^* = 1.6$ msec, in contrast to the case of I to E iSTDP where without STDP where $\tau^* = -1.7$ msec [see Fig. 8(b1)]. Hence, $I_{syn}^{(E)}(t)$ shows a phase lag of -40.3° behind $I_{syn}^{(I)}(t)$. As a result, the cross-correlation function $C_{IPSR}^{(E,I)}(\tau)$ of Eq. (21) between the IPSR outputs $R_E(t)$ and $R_I(t)$ also has the main peak at $\tau = 1.6$ msec, as shown in Fig. 12(i2). This phase lag of the E-population rhythm may be well seen in Figs. 12(d2), 12(e2), and 12(f2). The gray E-stripes in the raster plot of spikes are phase-delayed with respect to the black I-stripes, and $R_E(t)$ also makes phase-delayed oscillations with respect to $R_I(t)$. These phase-delayed behaviors for $D = 110$ where $\langle\alpha_I\rangle_r < \langle\alpha_E\rangle_r$ are in contrast to the phase-advanced behaviors for $D = 110$ in the case of I to E iSTDP where $\langle\alpha_E\rangle_r < \langle\alpha_I\rangle_r$ [see Figs. 7(d2), 7(e2), and 7(f2)].

As another example of large D , we consider the case of $D = 500$ with $\langle\alpha_E\rangle_r = 0.571$ where eLTP occurs. In this case, Figure 12(j1) shows the cross-correlation function $C_{syn}^{(E,I)}(\tau)$ between $I_{syn}^{(E)}(t)$ and $I_{syn}^{(I)}(t)$. The main peak (represented by a solid circle) appears at $\tau^* = -2.0$ msec, in contrast to the above case of eLTD. Hence, $I_{syn}^{(E)}(t)$ shows a phase advance of 55.4° ahead of $I_{syn}^{(I)}(t)$. Consequently, the cross-correlation function $C_{IPSR}^{(E,I)}(\tau)$ between $R_E(t)$ and $R_I(t)$ also has the main peak at $\tau = -2.0$ msec [see Fig. 12(j2)]. This phase advance of the E-population rhythm may be well seen in Figs. 12(d5), 7(e5), and 7(f5). The gray E-stripes in the raster plot of spikes are phase-advanced with respect to the black I-stripes, and $R_E(t)$ also makes phase-advanced oscillations with respect to $R_I(t)$. These phase-advanced behaviors for $\langle\alpha_I\rangle_r > \langle\alpha_E\rangle_r$ are in contrast to the phase-delayed behaviors for $D = 500$ in the case of I to E iSTDP where $\langle\alpha_E\rangle_r > \langle\alpha_I\rangle_r$ [see Figs. 7(d5), 7(e5), and 7(f5)].

In the range of $D_2^* (\simeq 91) < D < D_{3,IE}^* (\simeq 632)$, we characterize individual and population behaviors for (FSS, FSS) in both the I- and the E-populations, and make comparison with those in the case of I to E iSTDP. It is thus found that overall behaviors in the case of E to I eSTDP are similar to those in the case of I to E iSTDP, except for the case of large D (cf., $D_{3,IE}^* \simeq 656$ in the case of I to E iSTDP). First, we characterize individual spiking behaviors of FS interneurons and RS pyramidal cells in terms of ISIs. Figures 13(a1)-13(a6) [Figures 13(b1)-13(b6)] show ISI histograms for various values of D in the I-(E)-population. Due to stochastic spike skipings, multiple peaks appear at integer multiples of the global period $T_G^{(X)}$ of $R_X(t)$ ($X = I$ or E), like the case of I to E iSTDP (see Fig. 9). In the case of intermediate D ($=110, 250$, and 400) where eLTD occurs, ISI histograms are shaded in gray color. In these gray-shaded histograms, as in the case of I to E iSTDP, the 1st-order main peaks become lowered and widened, higher-order peaks also become broader, and thus tendencies for merging between multiple peaks are more enhanced, in comparison with those in the absence of STDP (see the corresponding figures in Fig. 5). Hence, when compared with those in the case without STDP, the average ISIs $\langle\langle ISI^{(X)} \rangle\rangle_r$ ($X = I$ or E) are increased [i.e., $\langle\langle f_i^{(X)} \rangle\rangle_r$ is decreased, as shown in Figs. 12(g2) and 12(g6)] due to the developed tail part. Also, because of the enhanced merging between peaks, spiking stripes in the raster plots in Fig. 12 become more smeared (i.e., the average pacing degrees $\langle\langle P_i^{(X)} \rangle\rangle_r$ of spikes in the stripes are decreased [see Figs. 13(c2) and 13(d2)]).

On the other hand, ISI histograms in the case of eLTP for $D = 95, 500$, and 600 have much more clear peaks when compared with those in the absence of STDP, as in the case of I to E iSTDP. Particularly, for $D = 600$, single-peaked ISI histograms in the case without STDP are transformed into multiple-peaked histograms because desynchronization in the absence of STDP is developed into FSS in the case of E to I eSTDP. Thus, in com-

parison with those in the absence of STDP, the average ISI $\langle \langle ISI^{(X)} \rangle \rangle_r$ ($X = I$ or E) are decreased because of enhanced lower-order peaks [i.e., $\langle \langle f_i^{(X)} \rangle \rangle_r$ is increased, as shown in Figs. 12(g2) and 12(g6)]. As a result of appearance of clear peaks, spiking stripes in the raster plots in Fig. 12 become less smeared (i.e., the average pacing degrees $\langle \langle P_i^{(X)} \rangle \rangle_r$ of spikes in the stripes are increased [see Figs. 13(c2) and 13(d2)]). However, for large $D = 600$, peaks in the histograms seem to be a little less clear (due to a little more mergings between peaks), in comparison with the case of I to E iSTDP [see Figs. 9(a6) and 9(b6)], and thus the average pacing degrees of spikes ($\langle \langle P_i^{(I)} \rangle \rangle_r = 0.084$ and $\langle \langle P_i^{(E)} \rangle \rangle_r = 0.077$) for $D = 600$ become lower than those ($\langle \langle P_i^{(I)} \rangle \rangle_r = 0.13$ and $\langle \langle P_i^{(E)} \rangle \rangle_r = 0.107$) in the case of I to E iSTDP. As explained in the above, the value of $D = 600$ is close to the 3rd threshold $D_{3,IE}^*$ ($\simeq 632$) for the transition to desynchronization, while it is somewhat far from $D_{3,EI}^*$ ($\simeq 656$). Hence, in comparison with the case of I to E iSTDP, for $D = 600$ more merging between peaks in the histograms and more smearing of spikes in the raster plots of spikes occur in the case of E to I eSTDP. This also shows that the effect of E to I eSTDP is weaker than that of I to E iSTDP, mainly because the I population is a dominant one in our coupled two-population system.

We now characterize population behaviors for FSS in each X -population ($X = I$ or E) by employing the average occupation degree $\langle \langle O_i^{(X)} \rangle \rangle_r$ of Eq. (26), the average pacing degrees $\langle \langle P_i^{(X)} \rangle \rangle_r$ of Eq. (27), and the statistical-mechanical spiking measure $\langle M_s^{(X)} \rangle_r$ ($X = I$ or E) of Eq. (28). Here, $\langle \langle O_i^{(X)} \rangle \rangle_r$ denotes average density of spikes in the stripes in the raster plot, $\langle \langle P_i^{(X)} \rangle \rangle_r$ represents average phase coherence of spikes in the stripes, and $\langle M_s^{(X)} \rangle_r$ (given by a product of occupation and pacing degrees) represents overall degree of population synchronization. We also note that the average occupation degree $\langle \langle O_i^{(X)} \rangle \rangle_r$ is mainly determined by population-averaged MFRs $\langle \langle f_i^{(X)} \rangle \rangle_r$, and hence they have strong correlations with the Pearson's correlation coefficient $r \simeq 1.0$.

We first consider the case of (target) I-population for the E to I eSTDP. Figures 13(c1)-13(c3) show plots of $\langle \langle O_i^{(I)} \rangle \rangle_r$, $\langle \langle P_i^{(I)} \rangle \rangle_r$, and $\langle M_s^{(I)} \rangle_r$ in the I-population, respectively. In the gray region of eLTD ($\tilde{D}_{h,IE} < D < \tilde{D}_{h,IE}$), the average occupation degrees $\langle \langle O_i^{(I)} \rangle \rangle_r$ and the average pacing degrees $\langle \langle P_i^{(I)} \rangle \rangle_r$ (open circles) are lower than those (solid circles) in the absence of STDP, mainly because of decreased E to I synaptic excitation $\langle \langle J_{ij}^{(IE)*} \rangle \rangle_r$. In contrast, in most cases of eLTP for large D (except for a narrow region near the higher threshold $\tilde{D}_{h,IE}$), $\langle \langle O_i^{(I)} \rangle \rangle_r$ and $\langle \langle P_i^{(I)} \rangle \rangle_r$ (open circles) are higher than those (solid circles) in the absence of STDP, mainly due to increased E to I synaptic excitation $\langle \langle J_{ij}^{(IE)*} \rangle \rangle_r$.

In the (exceptional) narrow region of eLTP near the higher threshold $[\tilde{D}_{h,IE} \leq D < D_{cr}^*]$ [D_{cr}^* (denoted by stars) $\simeq 420$], the overall effect of (increased) standard deviation $\langle \sigma_J^{(IE)} \rangle_r$ (decreasing $\langle \langle O_i^{(I)} \rangle \rangle_r$ and $\langle \langle P_i^{(I)} \rangle \rangle_r$) is found to be dominant in comparison with the effect of eLTP (increasing $\langle \langle O_i^{(I)} \rangle \rangle_r$ and $\langle \langle P_i^{(I)} \rangle \rangle_r$), and hence $\langle \langle O_i^{(I)} \rangle \rangle_r$ and $\langle \langle P_i^{(I)} \rangle \rangle_r$ (open circles) become lower than those (solid circles) in the absence of STDP, like the case of eLTD (in the gray region of intermediate D).

We are concerned about a wide region of $\tilde{D}_{l,EI}$ ($\simeq 99$) $< D < D_{3,IE}^*$ ($\simeq 632$) (including the regions of both intermediate and large D). In the gray region of eLTD, the values of $\langle \langle O_i^{(I)} \rangle \rangle_r$ (open circles) are lower than those (solid circles) in the absence of STDP and their variations are small, while in the region of eLTP for large D $\langle \langle O_i^{(I)} \rangle \rangle_r$ increases with D in a relatively fast way. Thus, the standard deviation in the distribution of $\langle \langle O_i^{(I)} \rangle \rangle_r$ is increased in comparison to that in the absence of STDP, and $\langle \langle O_i^{(I)} \rangle \rangle_r$ exhibits a non-equalization effect, as in the case of $\langle \langle f_i^{(I)} \rangle \rangle_r$. The values of $\langle \langle P_i^{(I)} \rangle \rangle_r$ (open circles) in the gray region of eLTD are also lower than those (solid circles) in the absence of STDP and their variations are small. On the other hand, in the region of eLTP for large D $\langle \langle P_i^{(I)} \rangle \rangle_r$ is a relatively slowly-decreasing function of D , in contrast to the case without STDP. Thus, the standard deviation in the distribution of $\langle \langle P_i^{(I)} \rangle \rangle_r$ is decreased in comparison with that in the absence of STDP, and $\langle \langle P_i^{(I)} \rangle \rangle_r$ shows a weak equalization effect, like the case of $\langle f_p^{(I)} \rangle_r$.

We note that the statistical-mechanical spiking measure $\langle M_s^{(I)} \rangle_r$ is given by a product of the occupation and the pacing degrees. In the region of intermediate D (eLTD), the degrees of good synchronization (solid circles) in the absence of STDP become decreased to lower ones (open circles), while in most cases of large D (eLTP) the degrees of bad synchronization (solid circles) in the absence of STDP get increased to higher values (open circles). Through the effects of eLTP, even desynchronized states in the absence of STDP become transformed into sparsely synchronized states in the range of D_3^* ($\simeq 537$) $< D < D_{3,IE}^*$ ($\simeq 632$), and hence the region of FSS is so much extended in the presence of E to I eSTDP. However, this extended region is narrow when compared with the case of I to E iSTDP where $D_{3,EI}^*$ ($\simeq 656$), because the effects of I to E iSTDP are stronger than those of E to I eSTDP (i.e., the I-population is a dominant one in our coupled system). In this way, via cooperative interplay between the weak equalization effect in (decreasing) $\langle \langle P_i^{(I)} \rangle \rangle_r$ and the non-equalization effect in (increasing) $\langle \langle O_i^{(I)} \rangle \rangle_r$, strong equalization effect in the spiking measure $\langle M_s^{(I)} \rangle_r$ with much smaller standard deviation is found to occur [i.e., the values of $\langle M_s^{(I)} \rangle_r$ in Fig. 13(c3) are nearly the same], which is distinctly in contrast to the Matthew (bipolar-

ization) effect in the intrapopulation (I to I and E to E) STDPs where good (bad) synchronization gets better (worse) [61, 64].

This kind of equalization effect (occurring in a wide range of intermediate and large D) in the I-population may be well seen in the histograms for the distribution of $\langle M_s^{(I)} \rangle_r$. The gray histogram in the absence of STDP is shown in Fig. 13(e1), and the hatched histogram in the presence of E to I eSTDP is given in Fig. 13(e2). The standard deviation ($\simeq 0.081$) in the hatched histogram is decreased in comparison with that ($\simeq 0.112$) in the gray histogram, and thus strong equalization effect occurs. Furthermore, the mean value ($\simeq 0.113$) in the hatched histogram is also decreased in comparison with that ($\simeq 0.162$) in the gray histogram, and hence a dumbing-down effect also occurs. However, those standard deviation and the mean for the E to I eSTDP are larger than the standard deviation ($\simeq 0.067$) and the mean ($\simeq 0.111$) in the case of I to E iSTDP. Hence, the effect of E to I eSTDP is weaker than that of I to E iSTDP because the I-population is a dominant one in our coupled two-population system.

In addition to the (target) I-population, we also characterize population behaviors of FSS in the (source) E-population for the E to I eSTDP. Figures 13(d1)-13(d3) show plots of $\langle \langle O_i^{(E)} \rangle_r \rangle$, $\langle \langle P_i^{(E)} \rangle_r \rangle$, and $\langle M_s^{(E)} \rangle_r$ in the E-population, respectively. As explained in details in the above part of $\langle \langle f_i^{(E)} \rangle_r \rangle$ [see Fig. 12(g6)], both the population average $\langle \langle I_{syn,i}^{(EI)} \rangle_r \rangle$ and the standard deviation $\langle \sigma_{syn}^{(EI)} \rangle_r$ for time-averaged strengths of individual I to E synaptic currents [see Figs. 12(g3) and 12(g4)] also affect $\langle \langle O_i^{(E)} \rangle_r \rangle$ and $\langle \langle P_i^{(E)} \rangle_r \rangle$ so much. In most cases, the effect of $\langle \sigma_{syn}^{(EI)} \rangle_r$ is dominant in comparison with the effect of $\langle \langle I_{syn,i}^{(EI)} \rangle_r \rangle$, in contrast to the case of I to E iSTDP where the effect of the standard deviation $\langle \sigma_{syn}^{(IE)} \rangle_r$ is negligibly small when compared with the effect of the population average $\langle \langle I_{syn,i}^{(IE)} \rangle_r \rangle$ [see Figs. 7(g3) and 7(g4)].

In the range of $\tilde{D}_{l,IE} < D < D_{cr,l}^*$ ($\simeq 420$), $\langle \langle I_{syn,i}^{(EI)} \rangle_r \rangle$ has a tendency of increasing $\langle \langle O_i^{(E)} \rangle_r \rangle$ and $\langle \langle P_i^{(E)} \rangle_r \rangle$, because of decreased I to E synaptic inhibition. On the other hand, due to increase in I to E synaptic inhibition, $\langle \langle I_{syn,i}^{(EI)} \rangle_r \rangle$ has a tendency of decreasing $\langle \langle O_i^{(E)} \rangle_r \rangle$ and $\langle \langle P_i^{(E)} \rangle_r \rangle$ in the other two ranges of $D_{cr,l}^* < D < D_{3,IE}^*$ and $D_2^* < D < \tilde{D}_{l,IE}$. In contrast to the case of $\langle \langle I_{syn,i}^{(EI)} \rangle_r \rangle$, for $\tilde{D}_{l,IE} < D < D_{cr,m}^*$ [$D_{cr,m}^* \simeq 450$ (427) in the case of $\langle \langle O_i^{(E)} \rangle_r \rangle$ ($\langle \langle P_i^{(E)} \rangle_r \rangle$)], $\langle \sigma_{syn}^{(EI)} \rangle_r$ has a tendency of decreasing $\langle \langle O_i^{(E)} \rangle_r \rangle$ and $\langle \langle P_i^{(E)} \rangle_r \rangle$, while it has a tendency of increasing $\langle \langle O_i^{(E)} \rangle_r \rangle$ and $\langle \langle P_i^{(E)} \rangle_r \rangle$ in the other two ranges of $D_{cr,m}^* < D < D_{3,IE}^*$ and $D_2^* < D < \tilde{D}_{l,IE}$. These tendencies of $\langle \sigma_{syn}^{(EI)} \rangle_r$ are opposite to those of $\langle \langle I_{syn,i}^{(EI)} \rangle_r \rangle$. In most cases for competi-

tions between the opposite tendencies between $\langle \langle I_{syn,i}^{(EI)} \rangle_r \rangle$ and $\langle \sigma_{syn}^{(EI)} \rangle_r$, the effects of $\langle \sigma_{syn}^{(EI)} \rangle_r$ become dominant. Hence, in the region of $\tilde{D}_{l,IE} < D < D_{cr,h}^*$ [$D_{cr,h}^*$ (denoted by stars) $\simeq 470$ (432) in the case of $\langle \langle O_i^{(E)} \rangle_r \rangle$ ($\langle \langle P_i^{(E)} \rangle_r \rangle$)], the average occupation degrees $\langle \langle O_i^{(E)} \rangle_r \rangle$ and the average pacing degrees $\langle \langle P_i^{(E)} \rangle_r \rangle$ (open circles) are lower than those (solid circles) in the absence of STDP, while they are higher than those (solid circles) in the absence of STDP in the other two separate regions ($D_2^* < D < \tilde{D}_{l,IE}$ and $D_{cr,h}^* < D < D_{3,IE}^*$).

Like the case of I-population, we are also concerned about population behaviors in a wide region of $\tilde{D}_{l,IE} < D < D_{3,IE}^*$. $\langle \langle O_i^{(E)} \rangle_r \rangle$ is a relatively fast-increasing function of D (composed of open circles), and exhibits a non-equalization effect, because the standard deviation in the distribution of $\langle \langle O_i^{(E)} \rangle_r \rangle$ is increased in comparison to that in the absence of STDP. On the other hand, $\langle \langle P_i^{(E)} \rangle_r \rangle$ is a relatively slowly-decreasing function of D (composed of open circles) and shows a weak equalization effect, because the standard deviation in the distribution of $\langle \langle P_i^{(E)} \rangle_r \rangle$ is decreased in comparison with that in the absence of STDP.

We note that the statistical-mechanical spiking measure $\langle M_s^{(E)} \rangle_r$ is given by a product of the occupation and pacing degrees which exhibit increasing and decreasing behaviors with increasing D , respectively. In the region of intermediate D (eLTD), the degrees of good synchronization (solid circles) in the absence of STDP become decreased to lower ones (open circles), while in most cases of large D (eLTP) the degrees of bad synchronization (solid circles) in the absence of STDP get increased to higher values (open circles). Through the effects of eLTP, even desynchronized states in the absence of STDP become transformed into sparsely synchronized states in the range of D_3^* ($\simeq 537$) $< D < D_{3,IE}^*$ ($\simeq 632$). Hence the region of FSS is much extended in the presence of E to I eSTDP, although the extended region for FSS is narrower than that in the case of I to E iSTDP where $D_{3,EI}^*$ ($\simeq 656$). In this way, via cooperative interplay between the weak equalization effect in (decreasing) $\langle \langle P_i^{(E)} \rangle_r \rangle$ and the non-equalization effect in (increasing) $\langle \langle O_i^{(E)} \rangle_r \rangle$, strong equalization effect in the spiking measure $\langle M_s^{(E)} \rangle_r$ with much smaller standard deviation is found to occur [i.e., the values of $\langle M_s^{(E)} \rangle_r$ in Fig. 13(d3) are nearly the same], which is distinctly in contrast to the Matthew (bipolarization) effect in the intrapopulation (I to I and E to E) STDPs where good (bad) synchronization gets better (worse) [61, 64]. Thus, a bell-shaped curve (composed of solid circles) for $\langle M_s^{(E)} \rangle_r$ in the absence of STDP is transformed into a nearly flat curve (consisting of open circles) in the presence of E to I eSTDP.

This kind of equalization effect may be well seen in the histograms for the distribution of $\langle M_s^{(E)} \rangle_r$. The gray

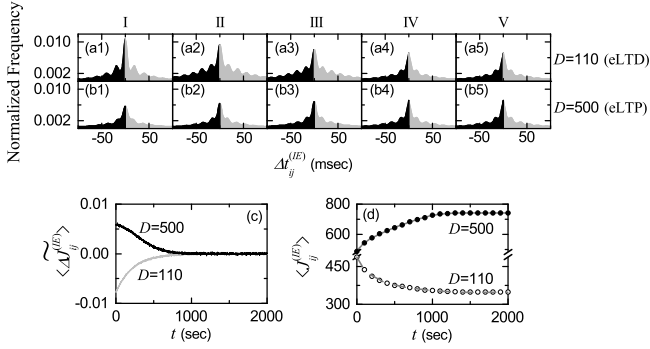


FIG. 14: Microscopic investigations on emergences of eLTD and eLTP in the presence of E to I eSTDP. Time-evolutions of the normalized histogram $H(\Delta t_{ij}^{(IE)})$ for the distributions of time delays $\{\Delta t_{ij}^{(IE)}\}$ between the pre- and the post-synaptic spike times for $D = 110$ in (a1)-(a5) and for $D = 500$ in (b1)-(b5); 5 stages are shown in I (starting from 0 sec), II (starting from 100 sec), III (starting from 400 sec), IV (starting from 800 sec), and V (starting from 1300 sec). (c) Time-evolutions of multiplicative synaptic modification $\langle \Delta J_{ij}^{(IE)} \rangle$ for $D = 110$ (gray line) and $D = 500$ (black line). (d) Time-evolutions of population-averaged synaptic strength $\langle J_{ij}^{(IE)} \rangle$ (obtained by an approximate method) for $D = 110$ (open circle) and $D = 500$ (solid circle); gray dashed and solid lines represent ones (obtained by direct calculations) for $D = 110$ and 500 in Fig. 12(a), respectively.

histogram in the absence of STDP is shown in Fig. 13(f1) and the hatched histogram in the presence of E to I eSTDP is given in Fig. 13(f2). The standard deviation ($\simeq 0.014$) in the hatched histogram is much smaller than that ($\simeq 0.028$) in the gray histogram, and hence strong equalization emerges. Moreover, a dumping-down effect also occurs because the mean value ($\simeq 0.031$) in the hatched histogram is smaller than that ($\simeq 0.056$) in the gray histogram. However, those standard deviation and the mean for the E to I eSTDP are larger than the standard deviation ($\simeq 0.009$) and the mean ($\simeq 0.029$) in the case of I to E iSTDP. Hence, the effect of I to E iSTDP is stronger than that of E to I eSTDP because the I-population is a dominant one in our coupled two-population system.

As in the case of I to E iSTDP, we now study emergences of eLTD and eLTP of E to I synaptic strengths via a microscopic method based on the distributions of time delays $\{\Delta t_{ij}^{(IE)}\}$ ($= t_i^{(post,I)} - t_j^{(pre,E)}$) between the nearest spike times of the post-synaptic FS interneuron i and the pre-synaptic RS pyramidal cell j . Figures 14(a1)-14(a5) and 14(b1)-14(b5) show time-evolutions of normalized histograms $H(\Delta t_{ij}^{(IE)})$ for the distributions of time delays $\{\Delta t_{ij}^{(IE)}\}$ for $D = 110$ and 500, respectively; the bin size in each histogram is 0.5 msec. Here, we consider 5 stages, represented by I (starting from 0 sec), II (starting from 100 sec), III (starting from 400 sec), IV (starting from 800 sec), and V (starting from 1300 sec). At each stage,

we get the distribution of $\{\Delta t_{ij}^{(IE)}\}$ for all synaptic pairs during 0.2 sec and obtain the normalized histogram by dividing the distribution with the total average number of synapses ($=96000$).

As an example of eLTD in the intermediate D , we consider the case of $D = 110$. Due to stochastic spike skipings for the FSS, multiple peaks appear in each histogram, as in the multi-peaked histograms in Fig. 13. In the stage I, along with the sharp main central (1st-order) peak, higher k th-order ($k = 2, \dots, 5$) left and right minor peaks also are well seen. Because of the anti-Hebbian time window for the E to I eSTDP, eLTD and eLTP occur in the gray ($\Delta t^{(IE)} > 0$) and the black ($\Delta t^{(IE)} < 0$) parts, respectively, which is in contrast to the case of I to E iSTDP with a time-delayed Hebbian time window where iLTP and iLTD occur in the black ($\Delta t^{(IE)} > 0$) and the gray ($\Delta t^{(IE)} < 0$) parts, respectively [see Fig. 6(a)]. With increasing the level of stage, the 1st-order main peak becomes lowered and broadened, higher-order peaks also become widened, and thus mergings between multiple peaks occur. Thus, at the final stage V, the histogram consists of lowered and widened 1st-order peak and merged higher-order minor peaks. In the stage I, the effect in the right gray part (eLTD) is dominant, in comparison to the effect in the left black part (eLTP), and hence the overall net eLTD begins to appear. As the level of stage is increased, the effect of eLTD in the gray part tends to nearly cancel out the effect of eLTP in the black part at the stage V.

We consider another case of $D = 500$ where eLTP occurs. In the initial stage I, the histogram is composed of much lowered and broadened 1st-order main peak and higher-order merged peaks, in contrast to the case of $D = 110$. For this initial stage, the effect in the left black part (eLTP) is dominant, when compared with the effect in the right gray part (eLTD), and hence the overall net eLTP begins to occur. However, as the level of stage is increased, the heights of peaks become increased, their widths tend to be narrowed, and thus peaks become more clear, in contrast to the progress in the case of $D = 110$. Furthermore, the effect of eLTP in the black part tends to nearly cancel out the effect of eLTD in the gray part at the stage V. We also note that the two initially-different histograms in the cases of $D = 110$ and 500 are developed into similar ones at the final stage V [see Figs. 14(a5) and 14(b5)], which shows the equalization effect occurring in the case of E to I eSTDP.

As in the case of I to E iSTDP, we consider successive time intervals $I_k \equiv (t_k, t_{k+1})$, where $t_k = 0.2 \cdot (k - 1)$ sec ($k = 1, 2, 3, \dots$). As the time t is increased, in each k th time interval I_k , we obtain the k th normalized histogram $H_k(\Delta t_{ij}^{(IE)})$ ($k = 1, 2, 3, \dots$) through the distribution of $\{\Delta t_{ij}^{(IE)}\}$ for all synaptic pairs during 0.2 sec. Then, using Eqs. (29), (31), and (32), we obtain approximate values of multiplicative synaptic modification $\langle \Delta J_{ij}^{(IE)} \rangle_k$ and population-averaged synaptic strength $\langle J_{ij}^{(IE)} \rangle_k$ in

a recursive way. Figure 14(c) shows time-evolutions of $\langle \Delta J_{ij}^{(IE)} \rangle$ for $D = 110$ (gray curve) and $D = 500$ (black curve). $\langle \Delta J_{ij}^{(IE)} \rangle$ for $D = 110$ is negative, while $\langle \Delta J_{ij}^{(IE)} \rangle$ for $D = 500$ is positive. For both cases they converge toward nearly zero at the stage V (starting from 1300 sec) because the effects of eLTP and eLTD in the normalized histograms are nearly cancelled out. The time-evolutions of $\langle J_{ij}^{(IE)} \rangle$ for $D = 110$ (open circles) and $D = 500$ (solid circles) are also shown in Fig. 14(d). We note that the approximately-obtained values for $\langle J_{ij}^{(IE)} \rangle$ agree well with directly-obtained ones [represented by the gray dashed (solid) line for $D = 110$ (500)] in Fig. 12(a). Consequently, eLTD (eLTP) emerge for $D = 110$ (500), in contrast to the case of I to E iSTDP where iLTP (iLTD) occurs for $D = 110$ (500).

D. Effect of Combined I to E and E to I STDPs on Population States in The I- and The E-Populations

In this subsection, we consider a combined case including both I to E iSTDP and E to I eSTDP, together with the same initial synaptic strengths which are normally distributed with the mean $J_0^{(XY)}$ and the standard deviation σ_0 ($= 5$) ($J_0^{(II)} = 1300$, $J_0^{(EE)} = 300$, $J_0^{(EI)} = 800$, and $J_0^{(IE)} = 487.5$). We note that the initial case satisfies the E-I ratio balance [i.e., $\alpha_E (= J_0^{(EE)}/J_0^{(EI)}) = \alpha_I (= J_0^{(IE)}/J_0^{(II)} = 0.375)$]. In each case of individual (I to E or E to I) interpopulation STDP, equalization effect in the interpopulation synaptic plasticity occurs, and the E-I ratio is broken up, which results in phase shifts between the fast sparsely synchronized rhythms in the I- and the E-populations. In the present case of combined interpopulation STDPs, both synaptic strengths $J_{ij}^{(EI)}$ and $J_{ij}^{(IE)}$ are updated according to the nearest-spike pair-based STDP rule in Eq. (12), while intrapopulation (I to I and E to E) synaptic strengths are static. By increasing D from D_2^* ($\simeq 91$), we investigate the effects of combined interpopulation STDPs on population states (I, E) in the I- and the E-populations, and make comparison with those of individual (I to E or E to I) interpopulation STDP (studied in the above subsections). Due to cooperative interplay between the two individual interpopulation STDPs, the equalization effect in interpopulation synaptic plasticity is found to be much enhanced in an extended region for FSS. Moreover, the E-I ratio balance is found to be recovered, and hence the fast sparsely synchronized rhythms in both the I- and the E-populations are in-phase, in contrast to the case of individual (I to E or E to I) STDP.

Figures 15(a1) and 15(a2) show time-evolutions of population-averaged I to E synaptic strengths $\langle J_{ij}^{(EI)} \rangle$ and E to I synaptic strengths $\langle J_{ij}^{(IE)} \rangle$ for various values of D , respectively. These time evolutions are similar

to those in each case of individual (I to E or E to I) STDP, except for quantitative differences in the case of small and large D . We first consider the case of $\langle J_{ij}^{(EI)} \rangle$ whose time evolutions are governed by the time-delayed Hebbian time window. In each case of intermediate values of $D = 110$, 250, and 400 (shown in black color), $\langle J_{ij}^{(EI)} \rangle$ increases monotonically above its initial value $J_0^{(EI)}$ ($= 800$), and eventually it approaches a saturated limit value $\langle J_{ij}^{(EI)*} \rangle$ nearly at $t = 1500$ sec. Consequently, iLTP occurs for these values of D . On the other hand, for small and large values of $D = 95$, 500, and 600 (shown in gray color), $\langle J_{ij}^{(EI)} \rangle$ decreases monotonically below $J_0^{(EI)}$, and approaches a saturated limit value $\langle J_{ij}^{(EI)*} \rangle$. As a result, iLTD occurs in the cases of $D = 95$, 500 and 600.

Next, we consider the case of $\langle J_{ij}^{(IE)} \rangle$. Due to the effect of anti-Hebbian time window, its time evolutions are in contrast to those of $\langle J_{ij}^{(EI)} \rangle$. For intermediate values of $D = 110$, 250, and 400 (shown in black color), $\langle J_{ij}^{(IE)} \rangle$ decreases monotonically below its initial value $J_0^{(IE)}$ ($= 487.5$), and eventually it converges toward a saturated limit value $\langle J_{ij}^{(IE)*} \rangle$ nearly at $t = 1500$ sec. As a result, eLTD occurs for these values of D . In contrast, for small and large values of $D = 95$, 500, and 600 (shown in gray color), $\langle J_{ij}^{(IE)} \rangle$ increases monotonically above $J_0^{(IE)}$, and converges toward a saturated limit value $\langle J_{ij}^{(IE)*} \rangle$. Consequently, eLTP occurs for $D = 95$, 500 and 600.

Figure 15(b1) shows a bell-shaped plot of population-averaged limit values $\langle \langle J_{ij}^{(EI)*} \rangle \rangle_r$ (open circles) of I to E synaptic strengths versus D . Here, the horizontal dotted line represents the initial average value $J_0^{(EI)}$ ($= 800$) of I to E synaptic strengths. In contrast, the plot for population-averaged limit values $\langle \langle J_{ij}^{(IE)*} \rangle \rangle_r$ (open circles) of E to I synaptic strengths versus D forms a well-shaped graph, as shown in Fig. 15(b3), where the horizontal dotted line denotes the initial average value of E to I synaptic strengths $J_0^{(IE)}$ ($= 487.5$). The lower and the higher thresholds, $\tilde{D}_{l,COM}$ ($\simeq 99$) and $\tilde{D}_{h,COM}$ ($\simeq 408$), for LTP/LTD (where $\langle \langle J_{ij}^{(EI)*} \rangle \rangle_r$ and $\langle \langle J_{ij}^{(IE)*} \rangle \rangle_r$ lie on their horizontal lines) are denoted by solid circles. In the case of a bell-shaped graph for $\langle \langle J_{ij}^{(EI)*} \rangle \rangle_r$, iLTP occurs in a broad region of intermediate D ($\tilde{D}_{l,COM} < D < \tilde{D}_{h,COM}$), while iLTD takes place in the other two (separate) regions of small and large D [$D_2^* < D < \tilde{D}_{l,COM}$ and $\tilde{D}_{h,COM} < D < D_{3,COM}^*$ ($\simeq 672$)]. On the other hand, in the case of a well-shaped graph for $\langle \langle J_{ij}^{(IE)*} \rangle \rangle_r$, eLTD takes place in a broad region of intermediate D ($\tilde{D}_{l,COM} < D < \tilde{D}_{h,COM}$), while eLTP occurs in the other two (separate) regions of small and large D [$D_2^* < D < \tilde{D}_{l,COM}$ and $\tilde{D}_{h,COM} < D < D_{3,COM}^*$]. For comparison, saturated limit values in each case of individual (I to E or E to I) STDP are also represented by

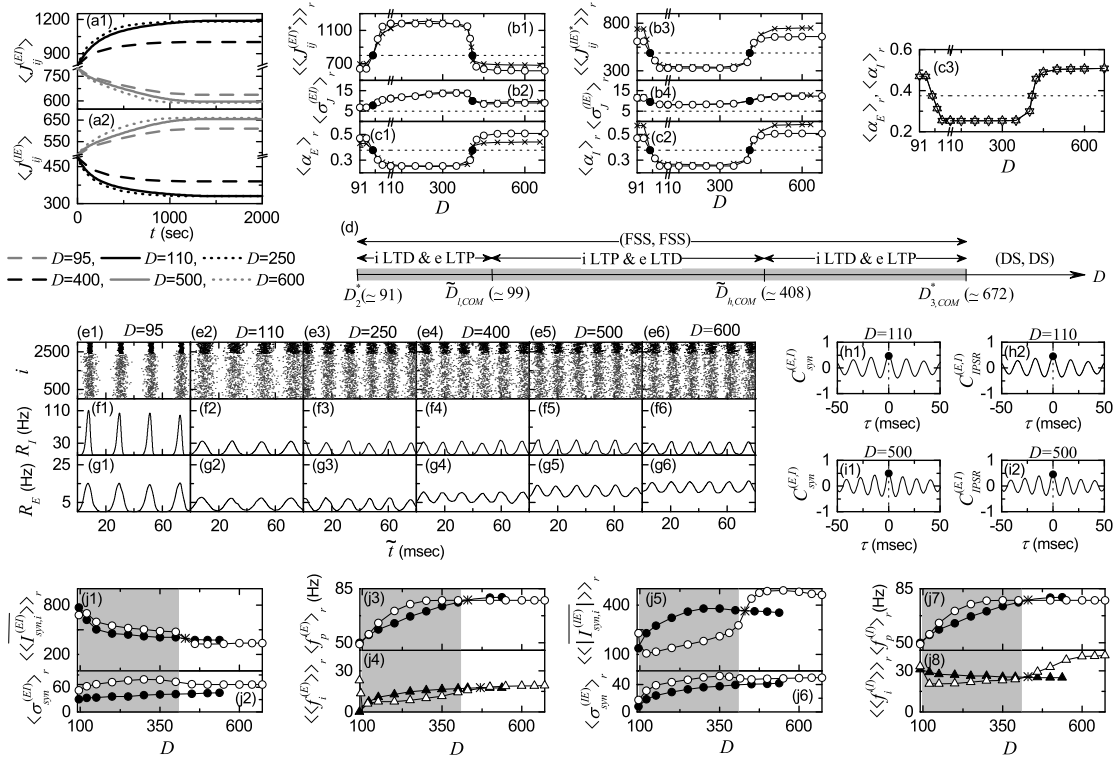


FIG. 15: Effect of combined I to E and E to I STDPs on population states. Time-evolutions of population-averaged synaptic strengths (a1) $\langle J_{ij}^{(EI)} \rangle$ and (a2) $\langle J_{ij}^{(IE)} \rangle$ for various values of D . Plots of population-averaged saturated limit values of synaptic strengths (b1) $\langle \langle J_{ij}^{(EI)*} \rangle \rangle_r$ and (b3) $\langle \langle J_{ij}^{(IE)*} \rangle \rangle_r$ (open circles) versus D ; those in the individual I to E and E to I STDPs are denoted by crosses. Plots of standard deviations (b2) $\langle \sigma_J^{(EI)} \rangle_r$ and (b4) $\langle \sigma_J^{(IE)} \rangle_r$ versus D . Plots of the E-I ratio (c1) $\langle \alpha_E \rangle_r$ and (c2) $\langle \alpha_I \rangle_r$ (open circles) versus D ; those in the individual I to E and E to I STDPs are denoted by crosses. (c3) Plots of the E-I ratios $\langle \alpha_E \rangle_r$ (up-triangles) and (c2) $\langle \alpha_I \rangle_r$ (down-triangles) versus D . (d) Bar diagram for the population states (I, E) in the I- and the E-populations. Raster plots of spikes in (e1)-(e6) and IPSPs $R_I(t)$ in (f1)-(f6) and $R_E(t)$ in (g1)-(g6) for various values of D after the saturation time, where $t = t^* + \tilde{t}$ (saturation time = 1500 sec) + \tilde{t} . Cross-correlation functions between total synaptic input currents $I_{syn}^{(E)}(t)$ and $I_{syn}^{(I)}(t)$ for $D =$ (h1) 110 (iLTP and eLTD) and (i1) 500 (iLTD and eLTP). Cross-correlation functions between IPSPs $R_E(t)$ and $R_I(t)$ for $D =$ (h2) 110 and (i2) 500. Plots of (j1) population average $\langle \langle I_{syn,i}^{(EI)} \rangle \rangle_r$ (open circles) and (j2) standard deviation $\langle \sigma_{syn,i}^{(EI)} \rangle_r$ (open circles) for time-averaged strengths $\{I_{syn,i}^{(EI)}\}$ of individual I to E synaptic currents; those in the absence of STDP are represented by solid circles. Plots of (j3) the population frequency $\langle f_i^{(E)} \rangle$ (open circles) and (j4) the population-averaged MFR of RS pyramidal cells $\langle \langle f_i^{(E)} \rangle \rangle_r$ (open triangles) versus D in the E-populations; those in the absence of STDP are denoted by solid circles and triangles, respectively. Plots of (j5) population average $\langle \langle I_{syn,i}^{(IE)} \rangle \rangle_r$ (open circles) and (j6) standard deviation $\langle \sigma_{syn,i}^{(IE)} \rangle_r$ (open circles) for time-averaged strengths $\{I_{syn,i}^{(IE)}\}$ of individual E to I synaptic currents; those in the absence of STDP are represented by solid circles. Plots of (j7) the population frequency $\langle f_p^{(I)} \rangle$ (open circles) and (j8) the population-averaged MFR of FS interneurons $\langle \langle f_i^{(I)} \rangle \rangle_r$ (open triangles) versus D in the I-populations; those in the absence of STDP are denoted by solid circles and triangles, respectively.

crosses in Figs. 15(b1) and 15(b3).

In the case of intermediate D , values in the combined (open circles) and the individual (crosses) cases are nearly the same (i.e., they nearly overlap), while for small and large D ($D_2^* < D < \tilde{D}_{l,COM}$ and $\tilde{D}_{h,COM} < D < D_{3,COM}^*$), they become distinctly different. In the case of $\langle \langle J_{ij}^{(EI)*} \rangle \rangle_r$, their values (open circles) in the combined case are more decreased in comparison with those (crosses) in the case of individual I to E iSTDP. Thus, iLTD becomes strengthened. On the other hand, in the case of $\langle \langle J_{ij}^{(IE)*} \rangle \rangle_r$, their values (open circles) in

the combined case are lower than those (crosses) in the case of individual E to I eSTDP. Thus, eLTP becomes weakened. We next consider standard deviations (from the population-averaged limit values) in the distribution of saturated limit values of interpopulation synaptic strengths. Figures 15(b2) and 15(b4) show plots of standard deviations $\langle \sigma_J^{(EI)} \rangle_r$ and $\langle \sigma_J^{(IE)} \rangle_r$ versus D , respectively. Here, the horizontal dotted lines represent the initial value $\sigma_0 (= 5)$ of the standard deviations. We note that all the values of $\langle \sigma_J^{(EI)} \rangle_r$ and $\langle \sigma_J^{(IE)} \rangle_r$ are larger than $\sigma_0 (= 5.0)$, independently of D .

We study the effect of combined interpopulation STDPs on the E-I ratios, α_E and α_I (given by the ratio of average excitatory to inhibitory synaptic strengths), in the E- and the I-populations; $\alpha_E (= \langle J_{ij}^{(EE)} \rangle / \langle J_{ij}^{(EI)} \rangle)$ and $\alpha_I (= \langle J_{ij}^{(IE)} \rangle / \langle J_{ij}^{(II)} \rangle)$. In the absence of STDP, there exists an E-I ratio balance between the E- and the I-populations (i.e., $\alpha_E = \alpha_I = 0.375$), and then the two fast sparsely synchronized rhythms in the I- and the E-populations are in-phase. In the individual case of I to E iSTDP, the values of α_E in the (target) E-population are changed depending on D , while α_I in the (source) I-population is static. On the other hand, in the individual case of E to I eSTDP, the values of α_I in the (target) I-population are varied depending on D , while α_E in the (source) E-population is static. Thus, in both individual cases, the E-I ratio balance in the absence of STDP becomes broken up, and then phase shifts between the two fast sparsely synchronized rhythms in the I- and the E-populations occur. The phase shifts in the case of individual I to E STDP are opposite those in the case of E to I eSTDP.

Figures 15(c1) and 15(c2) show plots of $\langle \alpha_E \rangle_r$ and $\langle \alpha_I \rangle_r$ (open circles) versus D in the case of combined (I to E and E to I) STDP, respectively. For comparison, $\langle \alpha_E \rangle_r$ and $\langle \alpha_I \rangle_r$ (crosses) in the case of individual (I to E or E to I) STDP are also given. In the case of $\langle \alpha_E \rangle_r$, for intermediated values of D their values (open circles) in the combined case are nearly the same as those (crosses) in the individual case, while for small and large values of D their values (open circles) are higher than those (crosses) in the individual case due to decrease in $\langle \langle J_{ij}^{(EI)*} \rangle \rangle_r$. On the other hand, in the case of $\langle \alpha_I \rangle_r$, for intermediated values of D their values (open circles) in the combined case are nearly the same as those (crosses) in the individual case, while in the small and large values of D their values (open circles) are lower than those (crosses) in the individual case because of decrease in $\langle \langle J_{ij}^{(IE)*} \rangle \rangle_r$. Figures 15(c3) shows plots of $\langle \alpha_E \rangle_r$ (up-triangles) and $\langle \alpha_I \rangle_r$ (down-triangles) in the combined case. We note that, via constructive interplay between the I to E iSTDP and the E to I eSTDP, the E-I ratio balance is recovered (i.e., $\langle \alpha_E \rangle_r = \langle \alpha_I \rangle_r$) in the whole range of D . Thus, in the combined case, states in our coupled two-population system are evolved into ones with the E-I ratio balance, in contrast to the individual case where the E-I ratio is broken up.

A bar diagram for the population states (I, E) in the I- and the E-populations is shown in Fig. 15(d). We note that (FSS, FSS) occurs in a broadened range of D [$D_2^* (\simeq 91) < D < D_{3,COM}^* (\simeq 672)$], in comparison with the case without STDP where (FSS, FSS) appears for $D_2^* < D < D_3^* (\simeq 537)$ [see Fig. 3(a)]. Desynchronized states for $D_3^* < D < D_{3,COM}^*$ in the absence of STDP are transformed into (FSS, FSS) in the presence of combined (I to E and E to I) STDPs, and thus the region of (FSS, FSS) is broadened. When compared with thresholds for transition to desynchronization in the case of individual

(I to E or E to I) STDP, $D_{3,COM}^* > D_{3,EI}^* (\simeq 656) > D_{3,IE}^* (\simeq 632)$. Hence, the region for (FSS, FSS) in the combined case is the widest one between the 3 cases, due to cooperative combined effect. The region in the individual I to E iSTDP case corresponds to a 2nd widest one, because the effect of I to E iSTDP is stronger than that of E to I eSTDP.

The effects of LTP and LTD at inhibitory and excitatory synapses on population states after the saturation time ($t^* = 1500$ sec) may be well seen in the raster plot of spikes and the corresponding IPSRs $R_I(t)$ and $R_E(t)$. Figures 15(e1)-15(e6), Figures 15(f1)-15(f6), and Figures 15(g1)-15(g6) show raster plots of spikes, the IPSRs $R_I(t)$, and the IPSRs $R_E(t)$ for various values of D , respectively. In comparison with the case without STDP [see Figs. 3(b4)-3(b6), Figs. 3(c4)-3(c6), and Figs. 3(d4)-3(d6)], the degrees of (FSS, FSS) for intermediate values of D ($D = 110, 250$, and 400) are decreased (i.e., the amplitudes of $R_I(t)$ and $R_E(t)$ are decreased) due to increased I to E synaptic inhibition (i.e., increase in iLTP) and decreased E to I synaptic excitation (decrease in eLTD). In contrast, for small and large values of D ($D = 95$ and 500), the degrees of (FSS, FSS) are increased (i.e., the amplitudes of $R_I(t)$ and $R_E(t)$ are increased) because of decreased I to E synaptic inhibition (i.e., decrease in iLTD) and increased E to I synaptic excitation (increase in eLTP) (see the corresponding raster plots, $R_I(t)$, and $R_E(t)$ for $D = 95$ and 500 in Fig. 3).

The effects of combined (I to E and E to I) STDPs on population states for $D = 95, 110, 250, 400$, and 500 are similar to those of individual (I to E or E to I) STDP (see the corresponding figures in Figs. 7 and 12). Hence, for these values of D the degrees of (FSS, FSS) in the case of combined STDPs are nearly the same as those in the case of individual interpopulation STDP. We note that a desynchronized state for $D = 600$ in the absence of STDP [see Figs. 3(b8), 3(c8), and 3(d8)] is transformed into (FSS, FSS) [see Figs. 15(e6), 15(f6), and 15(g6)] via iLTD and eLTP, as in the case of individual interpopulation STDP (see the case of $D = 600$ in Figs. 7 and 12). The degree of (FSS, FSS) for $D = 600$ is also nearly the same as those for other smaller values of D , because the value of $D = 600$ is much far away from its 3rd threshold $D_{3,COM}^* (\simeq 672)$, which is in contrast to the case of individual (I to E or E to I) STDP where the degree of (FSS, FSS) for $D = 600$ is lower in comparison with those for the other smaller values of D . Here, we also note that the degree of FSS in the I-(E-)population (i.e., the amplitude of $R_I(t)$ [$R_E(t)$]) tends to be nearly the same in an “extended” wide range of $\tilde{D}_{l,COM} < D < D_{3,COM}^*$, except for the narrow small- D region ($D_2^* < D < \tilde{D}_{l,COM}$). Hence, an equalization effect in the combined interpopulation synaptic plasticity occurs in such an extended wide range of D . Quantitative analysis for the degree of (FSS, FSS) and the equalization effect in the case of combined STDP will be done intensively in Fig. 16. An enhanced equalization effect is thus found to occur, in comparison

with the case of individual (I to E or E to I) STDP.

As explained in Fig. 15(c3), the E-I ratio balance is recovered (i.e., $\alpha_E = \alpha_I$) in the whole range of D , in contrast to the individual (I to E or E to I) STDP where the E-I ratio balance is broken up. Consequently, the fast sparsely synchronized rhythms in both the I- and the E-populations become in-phase, unlike the case of individual (I to E or E to I) STDP where phase shifts between the two population rhythms occur. As an example of intermediate D , we consider the case of $D = 110$ with $\langle \alpha_E \rangle_r = \langle \alpha_I \rangle_r = 0.254$ where iLTP and eLTD occur. Figure 15(h1) shows the cross-correlation function $C_{syn}^{(E,I)}(\tau)$ of Eq. (19) between the population-averaged total synaptic input currents $I_{syn}^{(E)}(t)$ and $I_{syn}^{(I)}(t)$ into the E- and the I-populations. The main peak (denoted by a solid circle) appears at $\tau^* = 0$. Hence, no phase shift between $I_{syn}^{(E)}(t)$ and $I_{syn}^{(I)}(t)$ occurs. As a result, the cross-correlation function $C_{IPSR}^{(E,I)}(\tau)$ of Eq. (21) between the IPSR outputs $R_E(t)$ and $R_I(t)$ also has the main peak at $\tau = 0$, as shown in Fig. 15(h2). We note that the black I-stripes and the gray E-stripes in the raster plot of spikes are in-phase, as shown in in Figs. 15(e2). Hence, both $R_I(t)$ and $R_E(t)$ make in-phase oscillations with the same population frequency [see Figs. 15(f2) and 15(g2)], as in the case without STDP (see Fig. 3).

As another example of large D , we consider the case of $D = 500$ with $\langle \alpha_E \rangle_r = \langle \alpha_I \rangle_r = 0.504$ where iLTP and eLTP occur. In this case, Figure 15(i1) shows the cross-correlation function $C_{syn}^{(E,I)}(\tau)$ between $I_{syn}^{(E)}(t)$ and $I_{syn}^{(I)}(t)$. The main peak (represented by a solid circle) appears at $\tau^* = 0$, as in the above case of $D = 110$. Hence, both $I_{syn}^{(E)}(t)$ and $I_{syn}^{(I)}(t)$ are in-phase. Consequently, the cross-correlation function $C_{IPSR}^{(E,I)}(\tau)$ between $R_E(t)$ and $R_I(t)$ also has the main peak at $\tau = 0$ [see Fig. 15(i2)]. Thus, the black I-stripes and the gray E-stripes in the raster plot of spikes are in-phase, as shown in in Figs. 15(e5). Hence, both $R_I(t)$ and $R_E(t)$ make in-phase oscillations with the same population frequency [see Figs. 15(f5) and 15(g5)], as in the above case of $D = 110$. When compared with the case without STDP, the degrees of (FSS, FSS) for $D = 110$ and 500 in the case of combined STDPs are changed to become nearly the same, while their the E-I ratio continues to be balanced.

We now study the effect of LTP and LTD at inhibitory and excitatory synapses on the population-averaged MFR $\langle \langle f_i^{(X)} \rangle \rangle_r$ ($X = E$ or I) and the population frequency $\langle f_p^{(X)} \rangle_r$. The synaptic input current $I_{syn,i}^{(XY)}$ of Eq. (9) from the source Y -population into the target X -population makes effects on MFRs $f_i^{(X)}$ of individual target neurons. The main factors in $I_{syn,i}^{(XY)}$ are both synaptic strengths $J_{ij}^{(XY)}$ and synaptic gate functions $s_j^{(XY)}$ of Eq. (10) (representing the fraction of open channels from the source Y -population to the tar-

get X -population). Here, $s_j^{(XY)}$ is determined by spikings of individual neurons in the source Y -population. Hence, both the population-averaged synaptic strengths $\langle \langle J_{ij}^{(XY)*} \rangle \rangle_r$ and the population-averaged MFR $\langle \langle f_i^{(Y)} \rangle \rangle_r$ in the source Y -population make effects on $I_{syn,i}^{(XY)}$ which then affects population-averaged MFR $\langle \langle f_i^{(X)} \rangle \rangle_r$ in the target X -population. We also note that, in the present case of combined (I to E and E to I) STDPs, both $\langle \langle J_{ij}^{(EI)*} \rangle \rangle_r$ and $\langle \langle J_{ij}^{(IE)*} \rangle \rangle_r$ change, in contrast to the case of individual (I to E or E to I) STDP where only one corresponding interpopulation synaptic strength varies.

We first consider the case of E-population with high dynamical susceptibility with respect to variations in I to E synaptic inputs. Figures 15(j1) and 15(j2) show plots of population average $\langle \langle I_{syn,i}^{(EI)} \rangle \rangle_r$ (open circles) and standard deviation $\langle \sigma_{syn}^{(EI)} \rangle_r$ (from the population average) (open circles) for time-averaged strengths $\{I_{syn,i}^{(EI)}\}$ of individual I to E synaptic currents, respectively; for comparison, those in the absence of STDP are represented by solid circles. In this case, $\langle \langle J_{ij}^{(EI)*} \rangle \rangle_r$ and $\langle \langle f_i^{(I)} \rangle \rangle_r$ in Figs. 15(b1) and 15(j8) make opposite effects on $\langle \langle I_{syn,i}^{(EI)} \rangle \rangle_r$. In the region of iLTP of $\langle \langle J_{ij}^{(EI)*} \rangle \rangle_r$ (increasing $\langle \langle I_{syn,i}^{(EI)} \rangle \rangle_r$), $\langle \langle f_i^{(I)} \rangle \rangle_r$ has a tendency of decreasing $\langle \langle I_{syn,i}^{(EI)} \rangle \rangle_r$, while in the region of iLTD of $\langle \langle J_{ij}^{(EI)*} \rangle \rangle_r$ (decreasing $\langle \langle I_{syn,i}^{(EI)} \rangle \rangle_r$), $\langle \langle f_i^{(I)} \rangle \rangle_r$ has a tendency of increasing $\langle \langle I_{syn,i}^{(EI)} \rangle \rangle_r$. However, the effects of $\langle \langle J_{ij}^{(EI)*} \rangle \rangle_r$ are found to be dominant in comparison with those of $\langle \langle f_i^{(I)} \rangle \rangle_r$. Hence, in the gray region of iLTP ($\tilde{D}_{l,COM} < D < \tilde{D}_{h,COM}$), the population-average values of $\langle \langle I_{syn,i}^{(EI)} \rangle \rangle_r$ (open circles) are higher than those (solid circles) in the absence of STDP, mainly due to increase in $\langle \langle J_{ij}^{(EI)*} \rangle \rangle_r$. On the other hand, in most cases of iLTD for large D for large D (except for a narrow region near the higher threshold $\tilde{D}_{h,COM}$), the population averages $\langle \langle I_{syn,i}^{(EI)} \rangle \rangle_r$ (open circles) are lower than those (solid circles) in the absence of STDP, mainly because of decrease in $\langle \langle J_{ij}^{(EI)*} \rangle \rangle_r$.

In the (exceptional) narrow region of iLTD near the higher threshold [$\tilde{D}_{h,COM} \leq D < D_{cr}^*$ ($\simeq 430$) (D_{cr}^* : denoted by a star)], the overall effect of standard deviation $\langle \sigma_j^{(EI)} \rangle_r$ (increasing $\langle \langle I_{syn,i}^{(EI)} \rangle \rangle_r$) is found to be dominant in comparison with the effect of iLTD (decreasing $\langle \langle I_{syn,i}^{(EI)} \rangle \rangle_r$), and hence the population averages $\langle \langle I_{syn,i}^{(EI)} \rangle \rangle_r$ (open circles) become higher than those (solid circles) in the absence of STDP, like the case of iLTP (in the gray region of intermediate D). In this way, the E-population seems to have high dynamical susceptibility against variations (i.e., $\langle \sigma_j^{(EI)} \rangle_r$) in I to E synaptic strengths. After passing the crossing point D_{cr}^* (denoted by a star), the

effect of iLTD (decreasing $\langle\langle I_{syn,i}^{(EI)} \rangle\rangle_r$) becomes dominant, as in the usual case of iLTD. We also note that the population average $\langle\langle I_{syn,i}^{(EI)} \rangle\rangle_r$ in Fig. 15(j1) has an oppositely-changing tendency in comparison with that in the case of individual E to I eSTDP [see Fig. 12(g3)] where values of $J_{ij}^{(EI)}$ are static and only $\langle\langle f_i^{(I)} \rangle\rangle_r$ affects $\langle\langle I_{syn,i}^{(EI)} \rangle\rangle_r$. In addition to population averages $\langle\langle I_{syn,i}^{(EI)} \rangle\rangle_r$, standard deviations $\langle\sigma_{syn}^{(EI)}\rangle_r$ are also shown in Fig. 15(j2). Unlike the case of $\langle\langle I_{syn,i}^{(EI)} \rangle\rangle_r$, all the values of $\langle\sigma_{syn}^{(EI)}\rangle_r$ (open circles) are higher than those (solid circles) in the absence of STDP, independently of D .

We study the effects of both the population average $\langle\langle I_{syn,i}^{(EI)} \rangle\rangle_r$ and the standard deviation $\langle\sigma_{syn}^{(EI)}\rangle_r$ on the population-averaged MFR $\langle\langle f_i^{(E)} \rangle\rangle_r$ in the E-population. Figure 15(j4) shows a plot of $\langle\langle f_i^{(E)} \rangle\rangle_r$ versus D . In the region where $\langle\langle I_{syn,i}^{(EI)} \rangle\rangle_r$ (open circles) is increased in comparison with those (solid circles) in the absence of STDP [$\tilde{D}_{l,COM} < D < D_{cr,l}^*$ ($\simeq 430$)], the population-averaged MFRs $\langle\langle f_i^{(E)} \rangle\rangle_r$ (open triangles) become lower than those (solid triangles) in the absence of STDP, due to increased I to E synaptic input inhibition. On the other hand, in most other cases where $\langle\langle I_{syn,i}^{(EI)} \rangle\rangle_r$ (open circles) is decreased, [except for a narrow region of $D_{cr,l}^* < D < D_{cr,h}^*$ ($\simeq 470$)] [$D_{cr,h}^*$: denoted by a star in Fig. 15(j4)], the population-averaged MFRs $\langle\langle f_i^{(E)} \rangle\rangle_r$ (open triangles) become higher than those (solid triangles) in the absence of STDP, because of decreased I to E synaptic input inhibition. As mentioned above, the E-population has high dynamical susceptibility with respect to variations in $\{I_{syn,i}^{(EI)}\}$. In the exceptional narrow region of $D_{cr,l}^* < D < D_{cr,h}^*$, the overall effect of standard deviation $\langle\sigma_{syn}^{(EI)}\rangle_r$ (decreasing $\langle\langle f_i^{(E)} \rangle\rangle_r$) is found to be dominant when compared with the effect of $\langle\langle I_{syn,i}^{(EI)} \rangle\rangle_r$ (increasing $\langle\langle f_i^{(E)} \rangle\rangle_r$). Hence, values of $\langle\langle f_i^{(E)} \rangle\rangle_r$ (open circles) are lower than those (solid circles) in the absence of STDP.

We now consider the case of I-population with low dynamical susceptibility with respect to variations in E to I synaptic inputs. Figures 15(j5) and 15(j6) show plots of population average $\langle\langle |I_{syn,i}^{(IE)}| \rangle\rangle_r$ (open circles) and standard deviation $\langle\sigma_{syn}^{(IE)}\rangle_r$ (from the population average) (open circles) for time-averaged strengths $\{|I_{syn,i}^{(IE)}|\}$ of individual E to I synaptic currents, respectively; for comparison, those in the absence of STDP are represented by solid circles. In this case, $\langle\langle J_{ij}^{(IE)*} \rangle\rangle_r$ and $\langle\langle f_i^{(E)} \rangle\rangle_r$ in Figs. 15(b3) and 15(j4) make nearly the same effects on $\langle\langle |I_{syn,i}^{(IE)}| \rangle\rangle_r$, in contrast to the above case in Fig. 15(j1) where $\langle\langle J_{ij}^{(EI)*} \rangle\rangle_r$ and $\langle\langle f_i^{(I)} \rangle\rangle_r$ make opposite effects on $\langle\langle I_{syn,i}^{(EI)} \rangle\rangle_r$. Hence, changing tendencies in $\langle\langle |I_{syn,i}^{(IE)}| \rangle\rangle_r$ are

the same as those in $\langle\langle f_i^{(E)} \rangle\rangle_r$, except for a narrow region of $D_{cr,m}^*$ ($\simeq 440$) $< D < D_{cr,h}^*$ ($\simeq 470$) [$D_{cr,m}^*$: denoted by a star in Fig. 15(j5)]. Due to the effects of $\langle\langle J_{ij}^{(IE)*} \rangle\rangle_r$, such changing tendencies become intensified (i.e., the differences from those in the absence of STDP become much larger), and also $\langle\langle |I_{syn,i}^{(IE)}| \rangle\rangle_r$ becomes increased rapidly by passing a crossing point $D_{cr,m}^*$ (lower than $D_{cr,h}^*$).

Along with population averages $\langle\langle |I_{syn,i}^{(IE)}| \rangle\rangle_r$, standard deviations $\langle\sigma_{syn}^{(IE)}\rangle_r$ are also shown in Fig. 15(j6). Like the case of $\langle\sigma_{syn}^{(EI)}\rangle_r$ in Fig. 15(j2), all the values of $\langle\sigma_{syn}^{(IE)}\rangle_r$ (open circles) are higher than those (solid circles) in the absence of STDP, independently of D .

We study the effects of both the population average $\langle\langle |I_{syn,i}^{(IE)}| \rangle\rangle_r$ and the standard deviation $\langle\sigma_{syn}^{(IE)}\rangle_r$ on the population-averaged MFR $\langle\langle f_i^{(I)} \rangle\rangle_r$ and the population frequency $\langle f_p^{(I)} \rangle_r$ in the I-population. Figures 15(j7) and 15(j8) shows plots of $\langle f_p^{(I)} \rangle_r$ and $\langle\langle f_i^{(I)} \rangle\rangle_r$ versus D , respectively. We note that the I-population is a dominant one in our coupled two-population system, and it has low dynamical susceptibility against variations $\langle\sigma_{syn}^{(IE)}\rangle_r$ in time-averaged strengths in the E to I synaptic currents. Hence, effects of time-averaged strengths of individual E to I synaptic input currents on the I-population are given mainly by their population average $\langle\langle |I_{syn,i}^{(IE)}| \rangle\rangle_r$ (i.e., effects of standard deviation $\langle\sigma_{syn}^{(IE)}\rangle_r$ may be neglected). Thus, population-averaged MFRs $\langle\langle f_i^{(I)} \rangle\rangle_r$ (open circles) are lower than those (solid circles) in the absence of STDP for $\tilde{D}_{l,COM} < D < D_{cr,m}^*$ ($\simeq 440$), because of decrease in $\langle\langle |I_{syn,i}^{(IE)}| \rangle\rangle_r$. As a result of decreased $\langle\langle f_i^{(I)} \rangle\rangle_r$, the population frequency $\langle f_p^{(I)} \rangle_r$ (open circles) becomes higher than that (solid circles) in the absence of STDP. In contrast, in the other two separate regions ($D_2^* < D < \tilde{D}_{l,COM}$ and $D_{cr,m}^* < D < D_{3,COM}^*$), population-averaged MFRs $\langle\langle f_i^{(I)} \rangle\rangle_r$ (open circles) are higher than those (solid circles) in the absence of STDP, due to increase in $\langle\langle |I_{syn,i}^{(IE)}| \rangle\rangle_r$. Because of increased $\langle\langle f_i^{(I)} \rangle\rangle_r$, the population frequency $\langle f_p^{(I)} \rangle_r$ (open circles) become lower than that (solid circles) in the absence of STDP. We also note that the population frequency in our coupled two-population system is determined by the dominant I-population. Hence, the population frequency $\langle f_p^{(E)} \rangle_r$ in Fig. 15(j3) is the same as $\langle f_p^{(I)} \rangle_r$, as in the case of individual (I to E or E to I) STDP.

In a wide range of $\tilde{D}_{l,COM} < D < D_{3,COM}^*$, a weak equalization effect is found to appear in the population frequency $\langle f_p^{(I)} \rangle_r$ ($= \langle f_p^{(E)} \rangle_r$), as in the case of individual (I to E or E to I) STDP, because the standard deviation in the distribution of $\langle f_p^{(X)} \rangle_r$ ($X=I$ or E) in the presence of combined STDPs becomes decreased, in comparison to that in the absence of STDP. Particularly, the flat region for $\langle f_p^{(X)} \rangle_r$ is extended (i.e., for $D > 300$ the val-

ues of $\langle f_p^{(X)} \rangle_r$ are nearly the same), in comparison with the case of individual (I to E or E to I) STDP where the values of $\langle f_p^{(X)} \rangle_r$ are nearly the same for $D > 350$. Hence, the standard deviation in the case of combined STDPs becomes smaller than that in the case of individual STDP, and thus the weak equalization effect becomes enhanced in the combined case. However, this kind of equalization effect in $\langle f_p^{(X)} \rangle_r$ is weak in comparison with strong equalization effect in the synchronization degree [denoted by the amplitudes of $R_I(t)$ and $R_E(t)$] in the I- and the E-populations. In contrast to the case of $\langle f_p^{(X)} \rangle_r$, non-equalization effects are found to occur in the population-averaged MFRs $\langle \langle f_i^{(I)} \rangle \rangle_r$ and $\langle \langle f_i^{(E)} \rangle \rangle_r$ and in the population averages $\langle \langle |I_{syn,i}^{(IE)}| \rangle \rangle_r$ and $\langle \langle |I_{syn,i}^{(EI)}| \rangle \rangle_r$ for time-averaged strengths of interpopulation synaptic currents, like the case of individual (I to E or E to I) STDP, because their distributions have increased standard deviations, in comparison with those in the absence of STDP.

Finally, in the range of $D_2^* (\simeq 91) < D < D_{3,COM}^* (\simeq 672)$, we characterize individual and population behaviors for (FSS, FSS) in both the I- and the E-populations, and make comparison with those in the case of individual (I to E or E to I) STDP. Enhanced equalization effect in the spiking measure $\langle M_s^{(X)} \rangle_r$ ($X=I$ or E) is thus found to occur in an extend wide region of (FSS, FSS).

We first characterize individual spiking behaviors of FS interneurons and RS pyramidal cells in terms of ISIs, and find that the overall spiking behaviors are similar to those in the case of individual STDP. Figures 16(a1)-16(a6) [Figures 16(b1)-16(b6)] show ISI histograms for various values of D in the I-(E-)population. Because of stochastic spike skipings, multiple peaks appear at integer multiples of the global period $T_G^{(X)}$ of $R_X(t)$ ($X=I$ or E), as in the case of individual STDP. For intermediate values of D ($=110, 250$, and 400) where iLTP and eLTD occur, ISI histograms are shaded in gray color. In these gray-shaded histograms, like the case of individual STDP, the 1st-order main peaks become lowered and broadened, higher-order peaks also become wider, and thus mergings between multiple peaks are more developed, when compared with those in the absence of STDP (see the corresponding figures in Fig. 5). Hence, in comparison with those in the case without STDP, the average ISIs $\langle \langle ISI^{(X)} \rangle \rangle_r$ ($X=I$ or E) are increased [i.e., $\langle \langle f_i^{(X)} \rangle \rangle_r$ is decreased, as shown in Figs. 15(j4) and 15(j8)] because of the developed tail part. Moreover, due to the enhanced merging between peaks, spiking stripes in the raster plots in Fig. 15 become more smeared (i.e., the average pacing degrees $\langle \langle P_i^{(X)} \rangle \rangle_r$ of spikes in the stripes are decreased [see Figs. 16(c2) and 16(d2)]).

In contrast, ISI histograms for small and large D ($=95, 500$, and 600) have much more clear peaks in comparison with those in the absence of STDP, like the case of individual (I to E or E to I) STDP. Particularly, for $D = 600$, single-peaked ISI histograms in the absence of STDP are transformed into multi-peaked histograms in the pres-

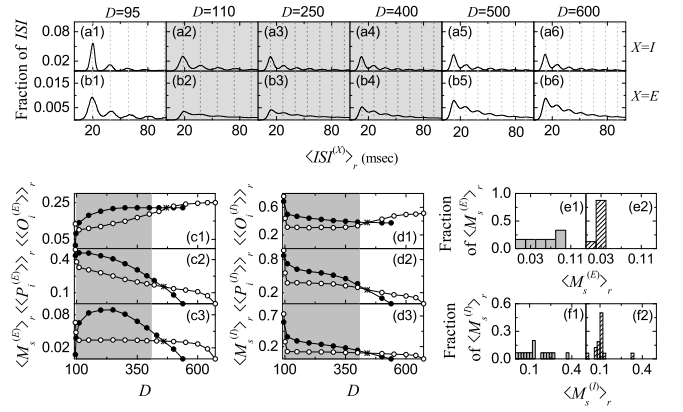


FIG. 16: Characterization of individual and population behaviors for FSS after the saturation time ($t^* = 1500$ sec) in the presence of combined I to E and E to I STDPs. ISI histograms for various values of D in the (a1)-(a6) I- and (b1)-(b6) E-populations. Vertical dotted lines represent multiples of the global period $T_G^{(X)}$ of the IPSR $R_X(t)$ ($X=I$ and E). Plots of (c1) the average occupation degree $\langle \langle O_i^{(E)} \rangle \rangle_r$ (open circles), (c2) the average pacing degree $\langle \langle P_i^{(E)} \rangle \rangle_r$ (open circles), and (c3) the statistical-mechanical spiking measure $\langle M_s^{(E)} \rangle_r$ (open circles) versus D in the E-population. Plots of (d1) the average occupation degree $\langle \langle O_i^{(I)} \rangle \rangle_r$ (open circles), (d2) the average pacing degree $\langle \langle P_i^{(I)} \rangle \rangle_r$ (open circles), and (d3) the statistical-mechanical spiking measure $\langle M_s^{(I)} \rangle_r$ (open circles) versus D in the I-population. For comparison, $\langle \langle O_i^{(X)} \rangle \rangle_r$, $\langle \langle P_i^{(X)} \rangle \rangle_r$, and $\langle M_s^{(X)} \rangle_r$ ($X=E$ and I) in the absence of STDP are also denoted by solid circles. In (a2)-(a4), (b2)-(b4), (c1)-(c3) and (d1)-(d3), iLTP and eLTD occur in the intermediate gray-shaded regions. Histograms for distribution of statistical-mechanical spiking measures $\langle M_s^{(E)} \rangle_r$ in the E-population in the (e1) absence and the (e2) presence of combined I to E and E to I STDPs. Histograms for distribution of statistical-mechanical spiking measures $\langle M_s^{(I)} \rangle_r$ in the I-population in the (f1) absence and the (f2) presence of combined I to E and E to I STDPs.

ence of combined STDPs because desynchronization in the case without STDP is developed into FSS in the case of combined STDPs. When compared with those in the absence of STDP, the average ISIs $\langle \langle ISI^{(X)} \rangle \rangle_r$ ($X=I$ or E) are decreased due to enhanced lower-order peaks [i.e., $\langle \langle f_i^{(X)} \rangle \rangle_r$ is increased, as shown in Figs. 15(j4) and 15(j8)]. Because of appearance of clear peaks, spiking stripes in the raster plots in Fig. 15 become less smeared [i.e., the average pacing degrees $\langle \langle P_i^{(X)} \rangle \rangle_r$ of spikes in the stripes are increased, as shown in Figs. 16(c2) and 16(d2)].

From now on, we characterize population behaviors for FSS in each X -population ($X=E$ or I) by employing the average occupation degree $\langle \langle O_i^{(X)} \rangle \rangle_r$, the average pacing degree $\langle \langle P_i^{(X)} \rangle \rangle_r$, and the statistical-mechanical spiking measure $\langle M_s^{(X)} \rangle_r$ ($X=E$ or I). As explained in the above, $\langle \langle O_i^{(X)} \rangle \rangle_r$ represents average density of spikes

in the stripes in the raster plot, $\langle\langle P_i^{(X)} \rangle\rangle_r$ denotes average phase coherence of spikes in the stripes, and $\langle M_s^{(X)} \rangle_r$ (given by a product of occupation and pacing degrees) represents overall degree of population synchronization. Here, the average occupation degree $\langle\langle O_i^{(X)} \rangle\rangle_r$ is mainly determined by population-averaged MFRs $\langle\langle f_i^{(X)} \rangle\rangle_r$, and thus they have strong correlations with the Pearson's correlation coefficient $r \simeq 1.0$.

We first consider the case of E-population which has high dynamical susceptibility with respect to variations $\langle\sigma_{syn}^{(EI)} \rangle_r$ in I to E synaptic input currents. Figures 16(c1)-16(c3) show plots of $\langle\langle O_i^{(E)} \rangle\rangle_r$, $\langle\langle P_i^{(E)} \rangle\rangle_r$, and $\langle M_s^{(E)} \rangle_r$ in the E-population, respectively. In the gray region of iLTP ($\tilde{D}_{l,COM} < D < \tilde{D}_{h,COM}$), the average occupation degrees $\langle\langle O_i^{(E)} \rangle\rangle_r$ and the average pacing degrees $\langle\langle P_i^{(E)} \rangle\rangle_r$ (open circles) are lower than those (solid circles) in the absence of STDP, mainly due to increased I to E synaptic input current $\langle\langle I_{syn,i}^{(EI)} \rangle\rangle_r$. On the other hand, in most cases of iLTD for large D (except for a narrow region near the higher threshold $\tilde{D}_{h,COM}$), $\langle\langle O_i^{(E)} \rangle\rangle_r$ and $\langle\langle P_i^{(E)} \rangle\rangle_r$ (open circles) are higher than those (solid circles) in the absence of STDP, mainly because of decreased I to E synaptic input current $\langle\langle I_{syn,i}^{(EI)} \rangle\rangle_r$. In the (exceptional) narrow region of iLTD near the higher threshold [$\tilde{D}_{h,COM} \leq D < D_{cr}^*$] [D_{cr}^* (denoted by stars) $\simeq 470$ (450) in the case of $\langle\langle O_i^{(E)} \rangle\rangle_r$ ($\langle\langle P_i^{(E)} \rangle\rangle_r$)], the overall effect of (increased) standard deviation $\langle\sigma_{syn}^{(EI)} \rangle_r$ (decreasing $\langle\langle O_i^{(E)} \rangle\rangle_r$ and $\langle\langle P_i^{(E)} \rangle\rangle_r$) is found to be dominant in comparison with the effect of decreased I to E synaptic input current $\langle\langle I_{syn,i}^{(EI)} \rangle\rangle_r$ (increasing $\langle\langle O_i^{(E)} \rangle\rangle_r$ and $\langle\langle P_i^{(E)} \rangle\rangle_r$). Hence, $\langle\langle O_i^{(E)} \rangle\rangle_r$ and $\langle\langle P_i^{(E)} \rangle\rangle_r$ (open circles) become lower than those (solid circles) in the absence of STDP.

We are concerned about a broad region of $\tilde{D}_{l,COM}$ ($\simeq 99$) $< D < D_{3,COM}^*$ ($\simeq 672$) (including the regions of both intermediate and large D). In this region, behaviors of $\langle\langle O_i^{(E)} \rangle\rangle_r$ and $\langle\langle P_i^{(E)} \rangle\rangle_r$ are similar to those in the case of individual (I to E or E to I) STDP. $\langle\langle O_i^{(E)} \rangle\rangle_r$ is a relatively fast-increasing function of D (consisting of open circles), and shows a non-equalization effect, because the standard deviation in the distribution of $\langle\langle O_i^{(E)} \rangle\rangle_r$ is increased in comparison to that in the absence of STDP. In contrast, $\langle\langle P_i^{(E)} \rangle\rangle_r$ is a relatively slowly-decreasing function of D (consisting of open circles) and exhibits a weak equalization effect, because the standard deviation in the distribution of $\langle\langle P_i^{(E)} \rangle\rangle_r$ is decreased in comparison with that in the case without STDP.

The statistical-mechanical spiking measure $\langle M_s^{(E)} \rangle_r$ is given by a product of the occupation and the pacing degrees which exhibit increasing and decreasing behaviors with D , respectively. In the region of intermediate D , the degrees of good synchronization (solid circles) in the

absence of STDP become decreased to lower ones (open circles), while in the region of large D the degrees of bad synchronization (solid circles) in the absence of STDP get increased to higher values (open circles). Via the effects of iLTD, even desynchronized states in the absence of STDP are transformed into sparsely synchronized states in the range of $D_3^* (\simeq 537) < D < D_{3,COM}^* (\simeq 672)$, and hence the region of FSS is so much extended in the presence of combined STDP. In this way, through cooperative interplay between the weak equalization effect in (decreasing) $\langle\langle P_i^{(E)} \rangle\rangle_r$ and the non-equalization effect in (increasing) $\langle\langle O_i^{(E)} \rangle\rangle_r$, strong equalization effect in the spiking measure $\langle M_s^{(E)} \rangle_r$ with much smaller standard deviation is found to occur [i.e., the values of $\langle M_s^{(E)} \rangle_r$ in Fig. 16(c3) are nearly the same], which is markedly in contrast to the Matthew (bipolarization) effect in the intrapopulation (I to I and E to E) STDPs where good (bad) synchronization gets better (worse) [61, 64]. Thus, a bell-shaped curve (consisting of solid circles) for $\langle M_s^{(E)} \rangle_r$ in the absence of STDP is transformed into a nearly flat curve (composed of open circles) in the presence of combined STDPs.

This kind of equalization effect may be well seen in the histograms for the distribution of $\langle M_s^{(E)} \rangle_r$. The gray histogram in the absence of STDP is shown in Fig. 16(e1) and the hatched histogram in the presence of combined STDPs is given in Fig. 16(e2). The standard deviation ($\simeq 0.007$) in the hatched histogram is much smaller than that ($\simeq 0.028$) in the gray histogram, and hence strong equalization emerges, as in the case of individual STDP. Particularly, we note that this standard deviation ($\simeq 0.007$) is smaller than those in the case of individual STDP (their values in the case of I to E and E to I STDPs are 0.009 and 0.014, respectively). Hence, via cooperative interplay between I to E iSTDP and E to I eSTDP in the case of combined STDPs, enhanced equalization effect occurs in the E-population in an extended broad region of $\tilde{D}_{l,COM}$ ($\simeq 99$) $< D < D_{3,COM}^*$ ($\simeq 672$). Furthermore, a dumbing-down effect also occurs because the mean value ($\simeq 0.029$) in the hatched histogram is smaller than that ($\simeq 0.056$) in the gray histogram.

We now consider the case of I-population which has low dynamical susceptibility with respect to variations $\langle\sigma_{syn}^{(IE)} \rangle_r$ in E to I synaptic input currents. Figures 16(d1)-16(d3) show plots of $\langle\langle O_i^{(I)} \rangle\rangle_r$, $\langle\langle P_i^{(I)} \rangle\rangle_r$, and $\langle M_s^{(I)} \rangle_r$ in the I-population, respectively. As explained in the case of $\langle\langle f_i^{(I)} \rangle\rangle_r$, effects of time-averaged strengths of individual E to I synaptic input currents on the I-population are given mainly by their population average $\langle\langle I_{syn,i}^{(IE)} \rangle\rangle_r$; effects of standard deviation $\langle\sigma_{syn}^{(IE)} \rangle_r$ may be neglected. In the region of $\tilde{D}_{l,COM} < D < D_{cr}^*$ ($\simeq 440$) where values of $\langle\langle I_{syn,i}^{(IE)} \rangle\rangle_r$ (open circles) are lower than those in the absence of STDP, the values of $\langle\langle O_i^{(I)} \rangle\rangle_r$ (open circles) are lower than those (solid circles) in the

absence of STDP, due to decreased E to I synaptic input current, and their variations are small in this region. On the other hand, in the other two separate regions (i.e., $D_2^* < D < \tilde{D}_{l,COM}$ and $D_{cr}^* < D < D_{3,COM}^*$ where values of $\langle\langle I_{syn,i}^{(IE)} \rangle\rangle_r$ (open circles) are higher than those in the absence of STDP, the values of $\langle\langle O_i^{(I)} \rangle\rangle_r$ (open circles) are higher than those (solid circles) in the absence of STDP, due to increased E to I synaptic input current, and $\langle\langle O_i^{(I)} \rangle\rangle_r$ increases with D in a relatively fast way. Thus, the standard deviation in the distribution of $\langle\langle O_i^{(I)} \rangle\rangle_r$ is increased in comparison to that in the absence of STDP, and $\langle\langle O_i^{(I)} \rangle\rangle_r$ exhibits a non-equalization effect, as in the case of $\langle\langle f_i^{(I)} \rangle\rangle_r$.

We next consider behaviors of $\langle\langle P_i^{(I)} \rangle\rangle_r$. In the region of $\tilde{D}_{l,COM} < D < D_{cr}^*$ ($\simeq 440$) where the values of $\langle\langle I_{syn,i}^{(IE)} \rangle\rangle_r$ are decreased, the values of $\langle\langle P_i^{(I)} \rangle\rangle_r$ (open circles) are also lower than those (solid circles) in the absence of STDP and their variations are small in this region. In contrast, in the other two separate regions (i.e., $D_2^* < D < \tilde{D}_{l,COM}$ and $D_{cr}^* < D < D_{3,COM}^*$ where the values of $\langle\langle I_{syn,i}^{(IE)} \rangle\rangle_r$ are increased, the values of $\langle\langle P_i^{(I)} \rangle\rangle_r$ (open circles) are also higher than those (solid circles) in the absence of STDP, and $\langle\langle P_i^{(I)} \rangle\rangle_r$ decreases in a relatively slow way, in contrast to the case without STDP. Thus, the standard deviation in the distribution of $\langle\langle P_i^{(I)} \rangle\rangle_r$ is decreased in comparison with that in the absence of STDP, and $\langle\langle P_i^{(I)} \rangle\rangle_r$ shows a weak equalization effect, like the case of $\langle\langle f_p^{(I)} \rangle\rangle_r$.

The statistical-mechanical spiking measure $\langle M_s^{(I)} \rangle_r$ in the I-population is given by a product of the occupation and the pacing degrees which exhibit increasing and decreasing behaviors with D , respectively. In the region of intermediate D , the degrees of good synchronization (solid circles) in the absence of STDP get decreased to lower ones (open circles), while in the region of large D the degrees of bad synchronization (solid circles) in the absence of STDP become increased to higher values (open circles). Through the effects of eLTP, even desynchronized states in the absence of STDP become transformed into sparsely synchronized states in the range of $D_3^* (\simeq 537) < D < D_{3,COM}^* (\simeq 672)$, and hence the region of FSS is so much extended in the presence of combined STDP. As in the case of $\langle M_s^{(E)} \rangle_r$, via cooperative interplay between the weak equalization effect in (decreasing) $\langle\langle P_i^{(I)} \rangle\rangle_r$ and the non-equalization effect in (increasing) $\langle\langle O_i^{(I)} \rangle\rangle_r$, strong equalization effect in the spiking measure $\langle M_s^{(I)} \rangle_r$ with much smaller standard deviation is found to occur [i.e., the values of $\langle M_s^{(I)} \rangle_r$ in Fig. 16(d3) are nearly the same], which is distinctly in contrast to the Matthew (bipolarization) effect in the intrapopulation (I to I and E to E) STDPs where good (bad) synchronization gets better (worse) [61, 64].

This kind of equalization effect may also be well seen in the histograms for the distribution of $\langle M_s^{(I)} \rangle_r$. The gray histogram in the absence of STDP is shown in Fig. 16(f1) and the hatched histogram in the presence of combined STDP is given in Fig. 16(f2). The standard deviation ($\simeq 0.056$) in the hatched histogram is much smaller than that ($\simeq 0.112$) in the gray histogram, and hence strong equalization emerges, as in the case of individual STDP. Particularly, this standard deviation ($\simeq 0.056$) is smaller than those in the case of individual STDP (their values in the case of I to E and E to I STDPs are 0.067 and 0.081, respectively). Thus, through cooperative interplay between I to E iSTDP and E to I eSTDP in the case of combined STDPs, enhanced equalization effect also occurs in the I-population in an extended broad region of $\tilde{D}_{l,COM} (\simeq 99) < D < D_{3,COM}^* (\simeq 672)$, as in the case of E-population. Moreover, a dumbing-down effect also occurs because the mean value ($\simeq 0.111$) in the hatched histogram is smaller than that ($\simeq 0.162$) in the gray histogram.

IV. SUMMARY AND DISCUSSION

We are interested in fast sparsely synchronized brain rhythms, related to diverse cognitive functions. In most cases of previous works, emergence of fast sparsely synchronized rhythms and their properties have been studied for static synaptic strengths (i.e., without considering synaptic plasticity) in single-population networks of purely inhibitory interneurons and in two-population networks composed of inhibitory interneurons and excitatory pyramidal cells [24–29]. Only in one case [64], intrapopulation I to I iSTDP was considered in an inhibitory SWN of FS interneurons. In contrast to these previous works, in the present work, we took into consideration adaptive dynamics of I to E and E to I (interpopulation) synaptic strengths, governed by the I to E iSTDP and the E to I eSTDP, respectively. We considered clustered SWNs with two I- and E-populations. The I-SWN is composed of FS interneurons and the E-SWN consists of RS pyramidal cells. A time-delayed Hebbian time window has been used for the I to E iSTDP update rule, while an anti-Hebbian time window has been employed for the E to I eSTDP update rule.

By varying the noise intensity D , we have investigated the effects of interpopulation STDPs on diverse population and individual properties of fast sparsely synchronized rhythms that emerge in the I- and the E-populations for the 3 cases of I to E iSTDP, E to I eSTDP, and combined I to E and E to I STDPs. In the presence of interpopulation STDPs, the distribution of interpopulation synaptic strengths $\{J_{ij}^{(XY)}\}$ is evolved into a saturated one after a sufficiently long time. Depending on D , the mean $\langle\langle J_{ij}^{(XY)*} \rangle\rangle_r$ for saturated limit interpopulation synaptic strengths has been found to increase or decrease [i.e., occurrence of LTP or LTD]. These LTP and LTD

make effects on the degree of FSS. In the case of I to E iSTDP, increase (decrease) in the mean $\langle\langle J_{ij}^{(EI)*} \rangle\rangle_r$ of the I to E synaptic inhibition disfavors (favors) FSS [i.e. iLTP (iLTD) tends to decrease (increase) of the degree of FSS]. In contrast, the roles of LTP and LTD are reversed in the case of E to I eSTDP. In this case, eLTP (eLTD) in the E to I synaptic excitation favors (disfavors) FSS [i.e., increase (decrease) in the mean $\langle\langle J_{ij}^{(IE)*} \rangle\rangle_r$ tends to increase (decrease) the degree of FSS]. Due to the effects of the mean (LTP or LTD), an equalization effect in interpopulation (I to E or E to I) synaptic plasticity has been found to occur in a wide range of D . In a broad region of intermediate D , the degree of good synchronization in the X -population ($X = \text{I or E}$) (with higher spiking measure $\langle M_s^{(X)} \rangle_r$) gets decreased, while in a region of large D , the degree of bad synchronization (with lower $\langle M_s^{(X)} \rangle_r$) becomes increased. As a result, the degree of FSS in each I- or E-population becomes nearly the same in a wide range of D . This kind of equalization effect in interpopulation synaptic plasticity is markedly in contrast to the Matthew (bipolarization) effect in intrapopulation (I to I and E to E) synaptic plasticity where good (bad) synchronization becomes better (worse) [61, 64].

We note that the spiking measure is given by the product of the occupation (representing density of spiking stripes) and the pacing (denoting phase coherence between spikes) degrees of spikes. Due to interpopulation STDPs, the average pacing degree $\langle\langle P_i^{(X)} \rangle\rangle_r$ has been found to exhibit a kind of weak equalization effect (i.e., $\langle\langle P_i^{(X)} \rangle\rangle_r$ is a relatively slowly-decreasing function of D with a smaller standard deviation, in comparison with $\langle\langle P_i^{(X)} \rangle\rangle_r$ in the absence of STDP). On the other hand, the average occupation degree $\langle\langle O_i^{(X)} \rangle\rangle_r$ has been found to show a type of non-equalization effect (i.e., $\langle\langle O_i^{(X)} \rangle\rangle_r$ is an increasing function of D with a larger standard deviation, when compared with $\langle\langle O_i^{(X)} \rangle\rangle_r$ in the absence of STDP). Through cooperative interplay between the weak equalization effect in (decreasing) $\langle\langle P_i^{(X)} \rangle\rangle_r$ and the non-equalization effect in (increasing) $\langle\langle O_i^{(X)} \rangle\rangle_r$, strong equalization effect in $\langle M_s^{(X)} \rangle_r$ with much smaller standard deviation has been found to emerge (i.e., $\langle M_s^{(X)} \rangle_r$ becomes nearly flat in a wide range of D). We also studied the case of combined (I to E and E to I) STDPs. In this case, the region for (FSS, FSS) in both the I- and the E-populations is extended, in comparison with that in the case of individual (I to E or E to I) STDP. Moreover, in the case of combined STDPs, equalization effect has been found to be much more enhanced in an extended wide range of D through cooperative interplay between I to E iSTDP and E to I eSTDP, in comparison with the case of individual (I to E or E to I) STDP. This kind of equalization effect can be well visualized in the histograms for the spiking measures in the presence and in the absence of interpopulation STDPs. In each I- or E-population, the standard deviation from the mean in the

histogram in the case of interpopulation STDP has been found to be much smaller than that in the case without STDP, which clearly shows emergence of the equalization effect in both the I- and the E-populations. Moreover, a dumbing-down effect in interpopulation synaptic plasticity has also been found to occur in the I- and the E-populations, because the mean in the histogram in the case of interpopulation STDP is smaller than that in the absence of STDPs. Thus, in each I- or E-population, equalization effect occurs together with dumbing-down effect.

Equalization effect has also been found in the population frequency $\langle f_p^{(X)} \rangle_r$ ($X = \text{I or E}$) of fast sparsely synchronized rhythms. The values of $\langle f_p^{(X)} \rangle_r$ are nearly the same in a broad range of large D in the presence of I to E or E to I STDP, and such equalization effect has also been found to be enhanced in the case of combined I to E and E to I STDPs. On the other hand, population-averaged MFR $\langle\langle f_i^{(X)} \rangle\rangle_r$ of individual neurons has been found to exhibit non-equalization effects, like the case of $\langle\langle O_i^{(X)} \rangle\rangle_r$, and they have strong correlation with a large Pearson's correlation coefficient.

We note that the I-population is a dominant one in our coupled two-population system. Hence, the effects of I to E iSTDP are stronger than those of E to I eSTDP. For example, the region for (FSS, FSS) in the case of I to E iSTDP is wider than that in the case of E to I eSTDP. Also, the population frequency of fast sparsely synchronized rhythms in the I- and the E-populations is determined by the dominant I-population, and hence $\langle f_p^{(E)} \rangle_r$ is just the same as $\langle f_p^{(I)} \rangle_r$. Particularly, the I-population has low dynamical susceptibility with respect to variations in E to I synaptic input currents, while the E-population has high dynamical susceptibility with respect to variations I to E synaptic input currents. Hence, the standard deviation $\langle\sigma_{syn}^{(EI)}\rangle_r$ makes much effects on $\langle\langle f_i^{(E)} \rangle\rangle_r$, $\langle\langle O_i^{(E)} \rangle\rangle_r$, $\langle\langle P_i^{(E)} \rangle\rangle_r$, and $\langle M_s^{(E)} \rangle_r$ in the E-population, while the effects of the standard deviation $\langle\sigma_{syn}^{(IE)}\rangle_r$ on the individual and population behaviors in the I-population may be negligible in comparison with the population average $\langle\langle I_{syn,i}^{(IE)} \rangle\rangle_r$.

We have also studied the effect of interpopulation STDP on the E-I ratio [given by the ratio of average excitatory (AMPA) to inhibitory (GABA) synaptic strengths] and the phase shift between fast sparsely synchronized rhythms in the E- and the I-populations. In the absence of STDPs, we considered the case where the E-I ratios $\langle\alpha_E\rangle_r$ and $\langle\alpha_I\rangle_r$ are the same in both RS pyramidal cells and FS interneurons. In this case of E-I ratio balance, the two E- and I-population rhythms are in-phase. However, in the presence of I to E or E to I STDP, the E-I ratio balance is broken up, and thus phase shift between fast sparsely synchronized rhythms in the I- and the E-populations occurs. The phase shifts in the case of I to E iSTDP are opposite to those in the case of E to I eSTDP. However, in the case of combined I to E and E

to I STDPs, E-I ratio balance (i.e., $\langle\alpha_X\rangle_r = \langle\alpha_Y\rangle_r$) has been recovered via cooperative interplay between the two interpopulation STDPs, and then no phase-shift occurs between the E- and the I-population rhythms.

Emergences of LTP and LTD of interpopulation synaptic strengths were investigated via a microscopic method based on the distributions of time delays $\{\Delta t_{ij}^{(XY)}\}$ between the nearest spiking times of the post-synaptic neuron i in the (target) X -population and the pre-synaptic neuron j in the (source) Y -population. Time evolutions of normalized histograms $H(\Delta t_{ij}^{(XY)})$ were followed in both cases of LTP and LTD. We note that, due to the equalization effects, the normalized histograms (in both cases of LTP and LTD) at the final (evolution) stage are nearly the same, which is in contrast to the cases of intrapopulation (I to I and E to E) STDPs where the two normalized histograms are distinctly different because of the Matthew (bipolarization) effect. Employing a recurrence relation, we recursively obtained population-averaged interpopulation synaptic strength $\langle J_{ij}^{(XY)} \rangle$ at successive stages via an approximate calculation of population-averaged multiplicative synaptic modification $\langle \Delta J_{ij}^{(XY)} \rangle$ of Eq. (31), based on the normalized histogram at each stage. These approximate values of $\langle J_{ij}^{(XY)} \rangle$ have been found to agree well with

directly-calculated ones. Consequently, one can understand clearly how microscopic distributions of $\{\Delta t_{ij}^{(XY)}\}$ contribute to $\langle J_{ij}^{(XY)} \rangle$.

Finally, we discuss limitations of our work and future work. In the present work, we have restricted our attention just to interpopulation (I to E and E to I) STDPs and found occurrence of equalization effects. In previous works, intrapopulation (I to I and E to E) STDPs were studied and the Matthew (bipolarization) effects were found to appear [61, 64]. Hence, in future, it would be interesting to study competitive interplay between the equalization effect in interpopulation synaptic plasticity and the Matthew (bipolarization) effect in intrapopulation synaptic plasticity in networks consisting of two E- and I-populations with both intrapopulation and interpopulation STDPs.

Acknowledgments

This research was supported by the Basic Science Research Program through the National Research Foundation of Korea (NRF) funded by the Ministry of Education (Grant No. 20162007688).

-
- [1] G. Buzsáki, *Rhythms of the Brain* (Oxford University Press, New York, 2006).
 - [2] R. D. Traub and M. A. Whittington, *Cortical Oscillations in Health and Diseases* (Oxford University Press, New York, 2010).
 - [3] D. Khodagholy, N. Gelineas, and G. Buzsáki, *Science* **358**, 369 (2017).
 - [4] L. Roux, B. Hu, R. Eichler, E. Stark, and G. Buzsáki, *Nat. Neurosci.* **20**, 845 (2017).
 - [5] A. Oliva, A. Fernández-Ruiz, G. Buzsáki, and A. Berényi, *Neuron* **91**, 1 (2016).
 - [6] J. Taxis, C. A. Anastassiou, K. Diva, and C. Koch, *Neuron* **87**, 590 (2015).
 - [7] G. Buzsáki and X.-J. Wang, *Annu. Rev. Neurosci.* **35**, 203 (2012).
 - [8] A. B. Saleem, A. D. Lien, M. Krumin, B. Haider, M. R. Rosón, A. Ayaz, K. Reinhold, L. Busse, M. Carandini, and K. D. Harris, *Neuron* **93**, 315 (2017).
 - [9] J. Veit, R. Hakim, M. P. Jadi, T. J. Sejnowski, and H. Adesnik, *Nat. Neurosci.* **20**, 951 (2017).
 - [10] G. Michalareas, J. Vezoli, S. van Pelt, J.-M. Schoffelen, H. Kennedy, and P. Fries, *Neuron* **89**, 384 (2016).
 - [11] E. Garcia-Rill, *Waking and the Reticular Activating System in Health and Disease* (Elsevier, London, 2015).
 - [12] P. P. Ujma, R. Bódizs, F. Gombos, J. Stintzing, B. N. Konrad, L. Ginzel, A. Steiger, and M. Dresler, *Sci. Rep.* **5**, 17159 (2015).
 - [13] H. Miyawaki and K. Diva, *Curr. Biol.* **26**, 893 (2016).
 - [14] M. Ploner, C. Sorg, and J. Gross, *Trends Cogn. Sci.* **21**, 100 (2017).
 - [15] N. C. Swann, C. de Hemptinne, S. Miocinovic, S. Qasim, S. S. Wang, N. Ziman, J. L. Ostrem, M. San Luciano, N. B. Galifianakis, and P. A. Starr, *J. Neurosci.* **36**, 6445 (2017).
 - [16] X.-J. Wang, *Physiol. Rev.* **90**, 1195 (2010).
 - [17] E. H. Buhl, G. Tamas, and A. Fisahn, *J. Physiol.* **513**, 117 (1998).
 - [18] A. Fisahn, F. G. Pike, E. H. Buhl, and O. Paulsen, *Nature* **394**, 186 (1998).
 - [19] J. Csicsvari, H. Hirase, A. Czurko, and G. Buzsáki, *Neuron* **21**, 179 (1998).
 - [20] J. Csicsvari, H. Hirase, A. Czurko, A. Mamiya, and G. Buzsáki, *J. Neurosci.* **19**, 274 (1999).
 - [21] J. Fellous and T. J. Sejnowski, *Hippocampus* **10**, 187 (2000).
 - [22] P. Fries, J. H. Reynolds, A. E. Rorie, and R. Desimone, *Science* **291**, 1560 (2001).
 - [23] N. K. Logothetis, J. Pauls, M. A. Augath, T. Trinath, and A. Oeltermann, *Nature* **412**, 150 (2001).
 - [24] N. Brunel and V. Hakim, *Neural Comput.* **11**, 1621 (1999).
 - [25] N. Brunel, *J. Comput. Neurosci.* **8**, 183 (2000).
 - [26] N. Brunel and X.-J. Wang, *J. Neurophysiol.* **90**, 415 (2003).
 - [27] C. Geisler, N. Brunel, and X.-J. Wang, *J. Neurophysiol.* **94**, 4344 (2005).
 - [28] N. Brunel and D. Hansel, *Neural Comput.* **18**, 1066 (2006).
 - [29] N. Brunel and V. Hakim, *Chaos* **18**, 015113 (2008).
 - [30] O. Sporns, *Networks of the Brain* (MIT Press, Cambridge, 2011).
 - [31] D.B. Chklovskii, B.W. Mel, and K. Svoboda, *Nature*

- 431**, 782 (2004).
- [32] S. Song, P.J. Sjöström, M. Reigl, S. Nelson, and D. B. Chklovskii, *PLoS Biol.* **3**, e68 (2005).
- [33] O. Sporns and C.J. Honey, *Proc. Natl. Acad. Sci. USA* **103**, 19219 (2006).
- [34] P. Larimer and B.W. Strowbridge, *J. Neurosci.* **28**, 12212 (2008).
- [35] E. Bullmore and O. Sporns, *Nat. Rev. Neurosci.* **10**, 186 (2009).
- [36] O. Sporns, G. Tononi, and G.M. Edelman, *Cereb. Cortex* **10**, 127 (2000).
- [37] D. S. Bassett and E. Bullmore, *The Neuroscientist* **12**, 512 (2006).
- [38] S.-Y. Kim and W. Lim, *Physica A* **421**, 109 (2015).
- [39] S.-Y. Kim and W. Lim, *Phys. Rev. E* **92**, 022717 (2015).
- [40] S.-Y. Kim and W. Lim, *Phys. Rev. E* **92**, 052716 (2015).
- [41] D. O. Hebb, *The Organization of Behavior; A Neuropsychological Theory* (Wiley & Sons, New York, 1949).
- [42] J. Kornoski, *Conditional Reflexes and Neuron Organization* (Cambridge University Press, Cambridge, 1948).
- [43] C. J. Shatz, *Sci. Am.* **267**, 60 (1992).
- [44] G. S. Stent, *Proc. Natl. Acad. Sci. USA* **70**, 997 (1973).
- [45] C. von der Malsburg, *Kybernetik* **14**, 85 (1973).
- [46] T. J. Sejnowski, *J. Math. Biol.* **4**, 303 (1977).
- [47] E. L. Bienenstock, L. N. Cooper, and P. W. Munro, *J. Neurosci.* **2**, 32 (1982).
- [48] L. F. Abbott and S. B. Nelson, *Nat. Neurosci.* **3**, 1178 (2000).
- [49] S. Song, K. D. Miller, and L. F. Abbott, *Nat. Neurosci.* **3**, 919 (2000).
- [50] G.-Q. Bi and M.-M. Poo, *Annu. Rev. Neurosci.* **24**, 139 (2001).
- [51] A. Kepecs, M. C. W. van Rossum, S. Song, and J. Tegner, *Biol. Cybern.* **87**, 446 (2002).
- [52] Y. Dan and M.-M. Poo, *Neuron* **44**, 23 (2004).
- [53] Y. Dan and M.-M. Poo, *Physiol. Rev.* **86**, 1033 (2006).
- [54] N. Caporale and Y. Dan, *Annu. Rev. Neurosci.* **31**, 25 (2008).
- [55] D. E. Feldman, *Neuron* **75**, 556 (2012).
- [56] H. Markram, W. Gerstner, and P. J. Sjöström, *Front. Synaptic Neurosci.* **4**, 2 (2012).
- [57] O. V. Popovych and P. A. Tass, *Front. Hum. Neurosci.* **6**, 58 (2012).
- [58] O. V. Popovych, S. Yanchuk, and P. A. Tass, *Sci. Rep.* **3**, 2926 (2013).
- [59] R. R. Borges, F. S. Borges, A. M. Batista, E. L. Lameu, R. L. Viana, K. C. Iarosz, I. L. Caldas, M. A. F. Sanjuán, *Commun. Nonlinear Sci. Numer. Simulat.* **34**, 12 (2016).
- [60] R. R. Borges, F. S. Borges, E. L. Lameu, A. M. Batista, K. C. Iarosz, I. L. Caldas, C. G. Antonopoulos, and M. S. Batista, *Neural Netw.* **88**, 58 (2017).
- [61] S.-Y. Kim and W. Lim, *Neural Netw.* **97**, 92 (2018).
- [62] S.-Y. Kim and W. Lim, *Cogn. Neurodyn.* **12**, 315 (2018).
- [63] S.-Y. Kim and W. Lim, *Cogn. Neurodyn.* **13**, 53 (2019).
- [64] S.-Y. Kim and W. Lim, *Neural Netw.* **106**, 50 (2018).
- [65] H. Markram, J. Lübke, M. Frotscher, and B. Sakmann, *Science* **275**, 213 (1997).
- [66] L. I. Zhang, H. W. Tao, C. E. Holt, W. A. Harris, and M. Poo, *Nature* **395**, 37 (1998).
- [67] G.-Q. Bi and M.-M. Poo, *J. Neurosci.* **18**, 10464 (1998).
- [68] D. Debanne, B. H. Gähwiler, and S. M. Thompson, *J. Physiol.* **507.1**, 237 (1998).
- [69] V. Egger, D. Feldmeyer, and B. Sakmann, *Nat. Neurosci.* **2**, 1098 (1999).
- [70] T. Tzounopoulos, Y. Kim, D. Oertel, and L. O. Trussell, *Nat. Neurosci.* **7**, 719 (2004).
- [71] G. M. Wittenberg and S. S. Wang, *J. Neurosci.* **26**, 6610 (2006).
- [72] T. P. Vogels, R. C. Froemke, N. Doyon, M. Gilson, J. S. Haas, R. Liu, A. Maffei, P. Miller, C. J. Wierenga, M. A. Woodin, F. Zenke and H. Sprekeler, *Front. Neural Circuits* **7**, 119 (2013).
- [73] D. M. Kullmann, A. W. Moreau, Y. Bakiri, and E. Nicholson, *Neuron* **75**, 951 (2012).
- [74] K. P. Lamsa, D. M. Kullmann, and M. A. Woodin, *Front. Synaptic Neurosci.* **2**, 8 (2010).
- [75] J.-L. Gaiarsa, O. Caillard, and Y. Ben-Ari, *Trends Neurosci.* **25**, 564 (2002).
- [76] R. C. Froemke, *Annu. Rev. Neurosci.* **38**, 195 (2015).
- [77] K. Deisseroth, G. Feng, A. K. Majewska, G. Miesenböck, A. Ting, and M. J. Schnitzer, *J. Neurosci.* **26**, 10380 (2006).
- [78] J. A. Cardin, *J. Physiol. (Paris)* **106**, 104 (2012).
- [79] T. P. Vogels, H. Sprekeler, F. Zenke, C. Clopath, and W. Gerstner, *Science* **334**, 1569 (2011).
- [80] P. E. Castillo, C. Q. Chiu, and R. C. Carroll, *Curr. Opin. Neurobiol.* **21**, 328 (2011).
- [81] S. S. Talathi, D. U. Hwang, and W. L. Ditto, *J. Comput. Neurosci.* **25**, 262 (2008).
- [82] R. R. Borgers, F. S. Borgers, E. E. Lameu, P. R. Protachevich, K. C. Iarosz, I. L. Caldas, R. L. Viana, E. E. L. Macau, M. S. Baptista, C. Grebogi, A. M. Baptista, *Braz. J. Phys.* **47**, 678 (2017).
- [83] J. Haas, T. Nowotny, H. Abarbanel, B. Zavala, and C. Landisman, *J. Neurophysiol.* **96**, 3305 (2006).
- [84] M. A. Woodin, K. Ganguly, and M.-M. Poo, *Neuron* **39**, 807 (2003).
- [85] C. Soto-Trevino, K. A. Thoroughman, E. Marder, and L. F. Abbott, *Nat. Neurosci.* **4**, 297 (2001).
- [86] G. Buzsáki, C. Geisler, D.A. Henze and X.-J. Wang, *Trends Neurosci.* **27**, 186 (2004).
- [87] D.J. Watts and S.H. Strogatz, *Nature* **393**, 440 (1998).
- [88] S. H. Strogatz, *Nature* **410**, 268 (2001).
- [89] D. J. Watts, *Small Worlds: The Dynamics of Networks Between Order and Randomness* (Princeton University Press, 2003).
- [90] S. Milgram, *Psychol. Today* **1**, 61 (1967).
- [91] J. Guare, *Six Degrees of Separation: A Play* (Random House, New York, 1990).
- [92] E. M. Izhikevich, *IEEE Trans. Neural Netw.* **14**, 1569 (2003).
- [93] E. M. Izhikevich, *IEEE Trans. Neural Netw.* **15**, 1063 (2004).
- [94] E. M. Izhikevich, *Dynamical Systems in Neuroscience* (MIT Press, Cambridge, 2007).
- [95] E. M. Izhikevich, *Pil. Trans. R. Soc. A* **368**, 5061 (2010).
- [96] A. L. Hodgkin, *J. Physiol.* **107**, 165 (1948).
- [97] E. M. Izhikevich, *Int. J. Bifurcat. Chaos* **10**, 1171 (2000).
- [98] J. Rubin, D. D. Lee, and H. Sompolinsky, *Phys. Rev. Lett.* **86**, 364 (2001).
- [99] A. Morrison, A. Aertsen, and M. Diesmann, *Neural Comput.* **19**, 1437 (2007).
- [100] J. S. Haas, T. Nowotny, and H. D. I. Abarbanel, *J. Neurophysiol.* **96**, 3305 (2006).
- [101] S. S. Talathi, D. U. Hwang, and W. L. Ditto, *J. Comput. Neurosci.* **25**, 262 (2008).

- [102] C. C. Bell, V. Z. Han, Y. Sugawara, and K. Grant, *Nature* **387**, 278 (1997).
- [103] N. Caporale and Y. Dan, *Ann. Rev. Neurosci.* **31**, 25 (2008).
- [104] M. San Miguel and R. Toral, in *Instabilities and Nonequilibrium Structures VI*, edited by J. Martinez, R. Tiemann, and E. Tirapegui (Kluwer Academic Publisher, Dordrecht, 2000), p. 35.
- [105] S.-Y. Kim and W. Lim, *J. Neurosci. Methods* **226**, 161 (2014).
- [106] H. Shimazaki and S. Shinomoto, *J. Comput. Neurosci.* **29**, 171 (2010).
- [107] W. Lim and S.-Y. Kim, *J. Korean Phys. Soc.* **52**, 1913 (2008).
- [108] D. Golomb and J. Rinzel, *Physica D* **72**, 259 (1994).
- [109] A. Longtin, *Nuovo Cimento D* **17**, 835 (1995).
- [110] A. Longtin, in *Stochastic Dynamics and Pattern Formation in Biological and Complex Systems*, edited by S. Kim, K. J. Lee, and W. Sung (AIP, New York, 2000), pp. 219-239.
- [111] W. Lim and S.-Y. Kim, *J. Comput. Neurosci.* **31**, 667 (2011).
- [112] D.-G. Hong, S.-Y. Kim, and W. Lim, *J. Korean Phys. Soc.* **59**, 2840 (2011).
- [113] S.-Y. Kim and W. Lim, *J. Korean Phys. Soc.* **63**, 104 (2013).
- [114] K. Pearson, *Proc. Royal Soc. Lond.* **58**, 240 (1895).